Addis Ababa University
College of Technology and Built Environment
School of Mechanical Engineering and Industrial Engineering

Numerical Analysis of Coffee Husk Combustion

A Thesis Submitted to the School of Graduate Studies of Addis Ababa University in Partial Fulfillment of the Requirements for the Award of the Degree of Master of Science in Mechanical Engineering (Thermal Engineering)

Tinsae Geremew Behaga

Advisor: Kamil Dino Adem (PhD)

June 2025

Addis Ababa University
College Of Technology and Built Environment

School of Mechanical and Industrial engineering
School of Graduate Studies

Numerical Analysis of Coffee Husk Combustion

By: Tinsae Geremew Behaga

Submitted in accordance with the requirement for the degree of Masters of Science (M.Sc.)

Approved by board examiners

Kamil D. Adem (Ph.D) Advisor	Date	Signature
Habtamu Tkubet (Ph.D) Internal Examiner	Date	Signature
Wondwosen Bogale (Ph.D) External Examiner	Date	Signature
Abdulkadir Aman (Ph.D) Head, School of Mechanical & Industrial Engineering	Date	Signature
Shegaw Ahmed (Ph.D) Interim Academic Affairs, CTBE	Date	Signature

Declaration

I hereby declare that the work which is being presented in this MSc thesis entitled as "Numerical analysis of coffee husk combustion" is original work of my own and has not been presented for degree of any university and all the resources of materials used for this thesis have been duly acknowledged.

Tinsae Geremew Behaga		
Name	Date	Signature

This is to Certify that the above declaration made by the candidate is correct to the best of my knowledge.

Kamil D. Adem (Ph.D)		
Advisor	Date	Signature

Acknowledgment

First and foremost, I am deeply grateful to Almighty God for giving me the passion strength, patience, and perseverance to complete this journey.

I would like to express my sincere gratitude to my advisor, Dr. Kamil D. Adem, for his invaluable guidance, encouragement, and unwavering support throughout the course of my research and my overall academic journey. His expertise and insightful feedback were instrumental in shaping this thesis, enhancing the quality of my work.

My heartfelt thanks also go to all my teachers who have contributed to my academic and personal growth throughout my Master's program.

Finally, I owe a deep debt of gratitude to my family for their unwavering love, support, and sacrifices.

Abstract

Coffee husk, the primary byproduct generated during coffee processing, presents a promising opportunity as a renewable energy source, particularly in regions with high coffee production like Ethiopia. Despite its abundance and energy potential, coffee husk remains underutilized—especially in direct combustion systems, where its combustion behavior and environmental impacts have not been thoroughly studied. This study focuses on the numerical simulation of coffee husk combustion within a biomass furnace using ANSYS Fluent. The main objectives is to design a combustion chamber geometry, to investigate the influence of excess air on combustion characteristics, to study the effects of the position of the secondary air inlet and to analyze the environmental impact of the combustion process, with a specific focus on carbon monoxide (CO) emissions.

The simulation was carried out by developing a 2D furnace model and applying appropriate boundary conditions, turbulence models and chemical kinetics. Coffee husk properties is defined based on available literature, with an emphasis on gas-phase combustion of volatiles and gas released from char combustion. Results indicate that excess air significantly affects combustion temperature and CO emission levels. The analysis shows that 60% excess air provides a average outlet temperature of 1295 k with nearly zero carbon monoxide emissions. Furthermore, the location of the secondary air inlet played a critical role in enhancing mixing, while both fuel flow rate and excess air had a direct influence on temperature distribution and emission concentration. The numerical model was validated using experimental data from rice husk combustion, chosen due to its similarity to coffee husk. The flue gas temperatures showed good agreement, with only a 2.2% deviation at 35% excess air. Although the variation increased with higher excess air levels, all deviations remained within an acceptable range.

In conclusion, the study demonstrates that coffee husk can be effectively utilized in direct combustion systems with controlled operating parameters. The findings provide valuable insights for sustainable energy production in coffee-producing regions and open doors for further research in this area.

Table of Contents

Nomenclature

ρ_{bed} bed density

$S_{mass,i}$ mass source terms

$C_{p,bed}$ specific heat capacity of the bed

T_{bed} the temperature of the bed

K_{bed} thermal conductivity of the fuel

$S_{heat,i}$ heat source terms

T_1 inlet drying air temperature

T_w the inlet wet-bulb temperature of the drying air

c_p the specific heat capacity of the air

ω_1 the specific humidity of the drying air at the inlet

h_{g1} enthalpy of saturated gas at the inlet temperature of drying air

h_{fw} enthalpy of saturated liquid at the wet bulb temperature

ω_w the specific humidity of the drying air at saturated state

ΔH_w the latent heat of vaporization at the wet bulb temperature (kJ/kg)

P_{gw} saturation pressure of water at wet bulb temperature

P_v partial water vapor pressure

$\emptyset$ relative humidity of the air

m_w is the mass of water evaporated

C_{pv} specific heat of vapor

C_{pw} specific heat of water

C_{ps} specific heat of solid coffee

T_2 the outlet temperature of the air (°C)

T_{m1} the inlet temperature of the material (dry solid and moisture content)

T_{m2} the exit temperature of the material (dry solid and moisture content)

$\dot{Q}$ is the total heat load in the heat exchanger

M_f the mass flow rate of fuel

η_0 is conversion efficiency of the fuel in the furnace

LHV is lower heating value of the fuel

V is the volume of the furnace

q_v is volumetric heat release rate

A_{grate} is area of the grate

q_F is the area heat release rate

List of Figures

List of Tables

Chapter One
Introduction

1.1 Background

The use of biomass as a CO_2-neutral renewable fuel is gaining importance due to the declining availability of fossil fuels and their contribution to global warming. In 2023, traditional biomass accounted for 6.1% of global energy consumption[1]. In Ethiopia, the potential to use biomass as an alternative energy source is also significant. However, of the 15–20 metric tons of available agricultural waste, only about 30% is utilized — and mostly in inefficient ways[2]. Thermochemical conversion of biomass presents a viable pathway for producing gaseous, liquid, and solid fuels, as well as biomass-derived chemicals. Significant efforts have been dedicated to enhancing the efficiency and economic viability of these processes[3].

Table 1. 1 Breakdown of global energy consumption [1]

	Energy source	Energy consumption (TWh)
1	Other renewables	2,428
2	Moder biofuels	1,318
3	Solar	4,264
4	Wind	6,040
5	Hydropower	11,014
6	Nuclear	6,824
7	Natural gas	40,102
8	Oil	54,564
9	Coal	45,565
10	Traditional biomass	11,111
11	Total	183,230

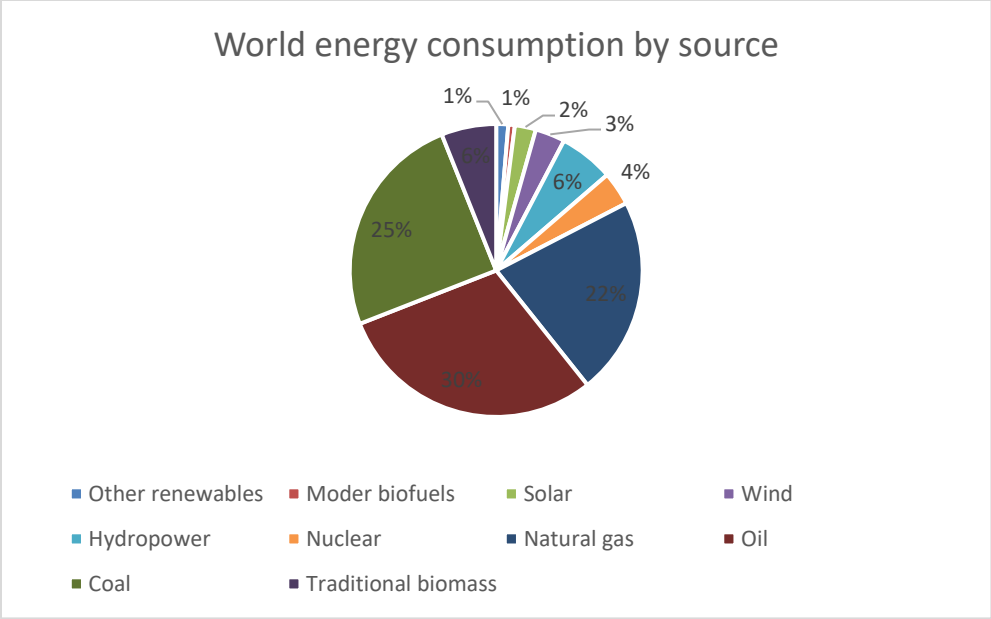

Figure 1. 1 Breakdown of global energy consumption in percentage [1]

Table 1. 2 Energy resources available in Ethiopia and their percentage utilization [2]

	Resource	Unit	Potential	Used in percent
1	Hydropower	GW	45	~10
2	Solar energy	kWh/m2/day	5.5	~1
3	Wind energy	GW	1350	~1
4	Geothermal energy	GW	7	~1
5	Woody biomass	Million tons	1120	50
6	Agricultural residual waste	Million tons	15-20	30
7	Natural gas	Billion m3	113	0
8	Coal	Million tons	300	0

Over the past two decades, a considerable amount of research has been devoted to developing numerical models for thermochemical reactors—such as gasifiers, pyrolizers, combustors,

boilers, and incinerators to support the design and analysis of biomass conversion systems. Advancements in computational power and numerical methods have enabled the practical use of simulation techniques like Computational Fluid Dynamics (CFD). These tools offer a robust virtual framework for examining the physical and chemical behavior of thermochemical processes under varying operational conditions[4].

Accurate CFD simulations contribute to optimizing reactor design and operation, while also enhancing understanding of the complex internal dynamics. As a result, CFD has become increasingly prominent in the study of biomass thermochemical conversion. Researchers utilize it to evaluate and improve the performance of systems including fluidized and fixed beds, combustion furnaces, rotary kilns, firing boilers, and rotating cone reactors. Modern CFD tools can predict not only fluid flow patterns, but also key phenomena such as heat and mass transfer, chemical reactions (e.g., combustion and devolatilization), phase transitions (e.g., drying or slagging), and even mechanical motion within the system. In many cases, CFD predictions show strong alignment with experimental data, offering both qualitative and quantitative insights[5].

1.2 Problem Statement

In Ethiopia, the agro-industrial sector plays a pivotal role in the economy, generating substantial quantities of residues such as vine pruning, bagasse, coffee husks, and forest by-products. Proper treatment of these materials is essential to mitigate environmental impacts and enhance their economic value. Over the past decades, a diverse array of technologies has been developed to address this challenge. Among these, energy recovery methods—particularly combustion and gasification of biomass—have garnered significant attention due to their potential to transform waste into valuable energy resources.

Ethiopia is the world's fifth-largest producer of coffee and the top producer in Africa, with 496,200 metric tons recorded in the 2022/23 season[6]. Although the percentage of residue from coffee processing varies between studies, research conducted on Ethiopian coffee samples indicates an average residue rate of 36.8%[2],[3]. Based on this, the estimated total

coffee husk generated is approximately 288,927 metric tons. This figure highlights the significant potential of coffee husk for various auxiliary applications.

1.3 Research Objective

1.3.1 General Objective

This study aims to establish a numerical model to simulate coffee husk combustion within the furnace of a coffee drying system, enabling detailed analysis of the combustion process

1.3.2 Specific Objective

- ✓ To size the geometry of the combustion chamber
- ✓ To evaluate how variations in primary and secondary air flow rates influence the combustion characteristics within the furnace
- ✓ To assess the impact of positioning of the secondary air inlet on combustion performance
- ✓ To examine and quantify the environmental impact of coffee husk combustion, with particular focus on CO emissions

1.4 Significance of the study

To ensure progress in Ethiopia's national energy security and environmental sustainability, a stable and diversified energy system is essential. The findings of this research will highlight the potential of coffee husk as a fuel source for small-scale heating applications in various drying technologies. Additionally, the results can serve as a foundation for future research aimed at scaling the use of coffee husk for industrial biomass boilers.

This study will also be valuable for researchers seeking to understand the effects of varying primary and secondary air flow rates, fuel feed rates, and the positioning of secondary air inlets on combustion performance.

Chapter Two
Literature review

Combustion is a multifaceted process that combines interrelated heat and mass transfer, chemical reactions, and fluid dynamics[9]. Accurately modeling it for design or control applications depends on a thorough understanding fuel characteristics combustion equipment design, role of operating conditions, and other related factors. So, it is the aim of this section to discuss in detail different properties of biomass fuels including coffee husk, science of thermochemical conversion of solid fuels, design principles of combustion furnace and review of previous studies done on the combustion of biomass fuels.

2.1.Properties and physical structure of biomass fuels

The physical structure and chemical composition of a fuel significantly influence the characteristics and reaction rates of solid fuel combustion. Therefore, understanding these properties is essential for accurate modeling of the combustion process.

2.1.1. Biological composition of biomass fuels

Biomass comprises various polymers, notably cellulose, hemicellulose, and lignin, which collectively form lignocellulose—the primary structural component of plant matter. Additionally, biomass contains other substances such as starch, triglycerides, and fatty acids[10]. The relative concentrations of these components can vary widely depending on the plant species, type of tissue, stage of growth, and environmental growing conditions.

Cellulose is a linear polymer composed of β(1→4)-linked D-glucopyranose units, forming long, unbranched chains with an average molecular weight of approximately 100,000.

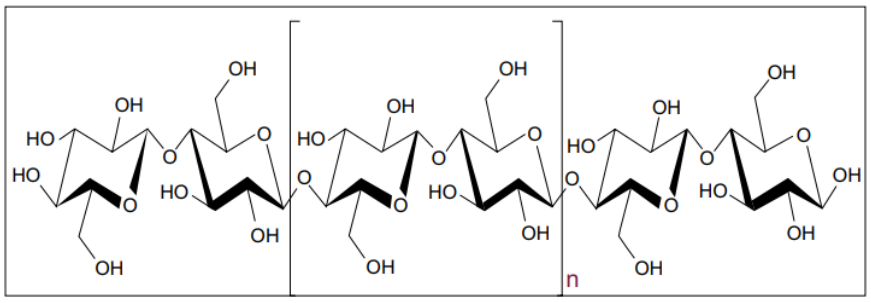

Figure 2. 1 Schematic diagram of the chemical structure of cellulose[11]

Hemicellulose, in contrast, is a heterogeneous and branched polysaccharide with a lower molecular weight (<30,000). It consists of various sugars, including glucose, mannose, xylose, arabinose, and uronic acids. Unlike cellulose, hemicellulose has a more irregular structure and binds tightly (but non-covalently) to cellulose microfibrils. Its composition is dominated by five-carbon sugars, particularly xylose.

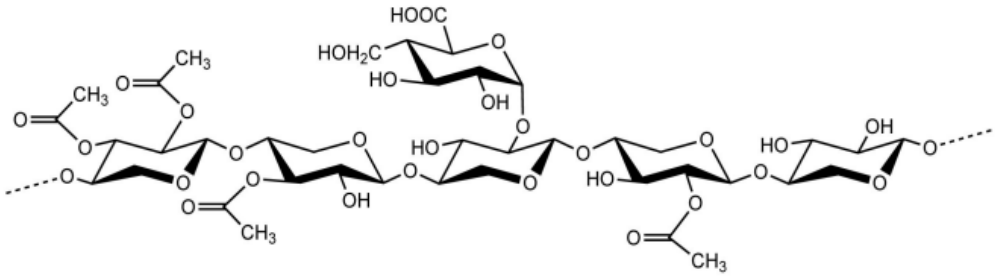

Figure 2. 2 Schematic diagram of the chemical structure of Hemi-cellulose[12]

Lignin is an amorphous, high-molecular-weight polymer made up of phenylpropane units—three-carbon chains attached to aromatic six-carbon rings. Unlike the polysaccharides cellulose and hemicellulose, lignin is a complex, irregular network of phenolic compounds*[13]*.

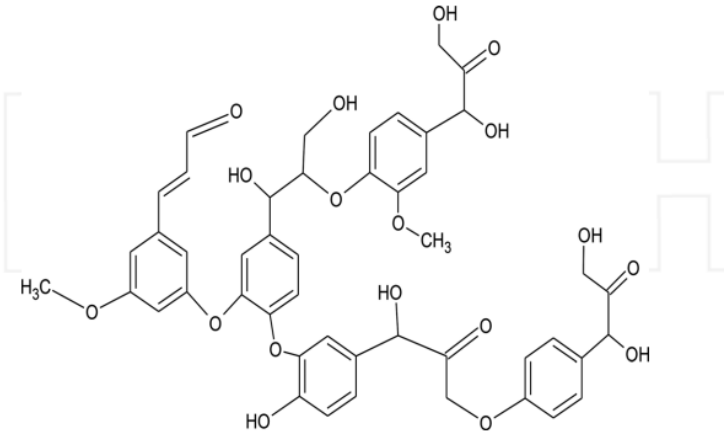

Figure 2. 3 Schematic diagram of the chemical structure of lignin [14]

Cellulose usually forms the largest portion of biomass constituents comprising of about 40-50% of biomass by weight, whereas hemicellulose typically constitutes about 20 to 40% [12]. The proportion of lignin content varies with the type of biomass, but usually falls between the range of 15 to 25% [11]. The pyrolysis process relies on the decomposition of cellulose and hemicellulose within specific temperature ranges, each performing distinct functions, which occurs alongside lignin, while breaking down more slowly within a wider temperature range. Knowing the proportions of these components helps to understand the thermal decomposition, particularly in pyrolysis.

2.1.2. Physical properties of biomass fuels

Physical properties primarily relate to the geometric and mass-related characteristics of biological materials, such as shape, size, surface area, volume, density, and porosity. Among these, key physical properties include moisture content, particle size and its distribution, as well as particle and bulk density[15].

Moisture content is one of the main criteria for the selection of energy conversion process technology. Thermal conversion technology such as direct combustion, gasification etc. requires biomass fuels with low moisture content[16]. On the other hand, moisture in the fuel can be a big limitation because it lowers the heating value. Combustion gives off heat, but water needs a lot of heat to evaporate. So, if the biomass has more than 50–55% moisture, it usually can’t burn on its own. It is either need to dry it first or use an extra fuel like natural gas to keep the fire going[17].

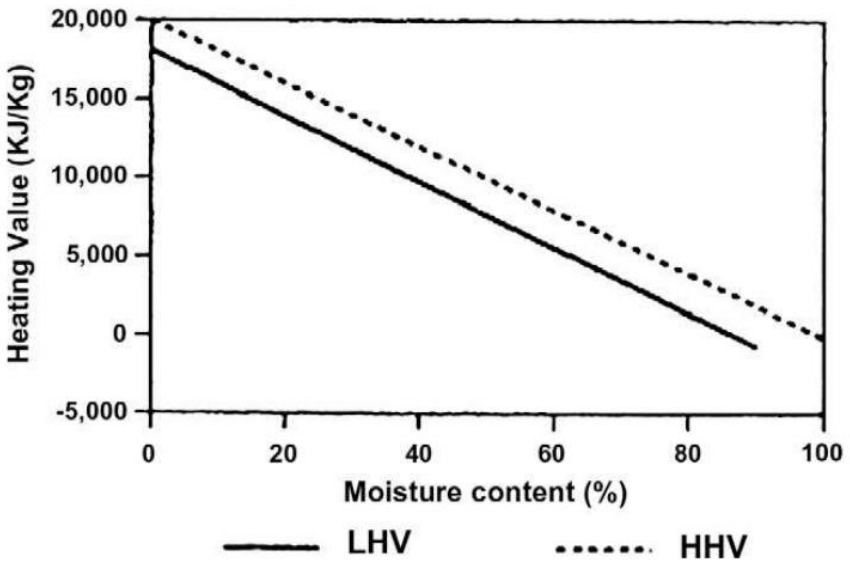

Figure 2. 4 Variation in Biomass Heating Value with Moisture Content [18]

Particle density measures how much mass a single biomass particle has in a given volume, including any closed pores inside it but not the ones open to the outside. Bulk density, on the other hand, takes into account the empty spaces between particles too[12]. It depends a lot on moisture content, shape and how the material is formed. Knowing the bulk density is useful when calculating transport and storage costs and it also helps in designing systems for handling and moving the biomass. Plus, it's a key factor when designing combustion chambers and furnaces[19].

Particle size plays an important role in the combustion and gasification of solid fuels. When solid particles are added to a combustor or gasifier, they come in many different sizes. Smaller particles are usually carried by the gas stream and burn more quickly and easily than larger ones. So, it’s important to know how many particles of each size are present in the fuel [17]. Usually, biomass is ground to particles smaller than 10 mm for use in different conversion processes. The particle size distribution is commonly measured using standard sieves [16].

2.1.3. Thermochemical properties of biomass fuels

The energy content of a fuel is commonly expressed through its heating value, also known as the calorific value or heat of combustion. There are different types of heating values, depending on whether the measurement is based on the enthalpy or internal energy of combustion, and on how water produced from hydrogen combustion is treated—either as vapor or as liquid. The Higher Heating Value (HHV) assumes that all the water produced condenses into liquid form, releasing the maximum possible energy. Lower Heating Value (LHV) assumes that the water remains as vapor, which results in less energy being recovered[20].

This analysis covers key components such as moisture content, volatile matter, fixed carbon, and ash. Moisture is especially important, as it affects both the transportation and conversion efficiency of biomass. Volatile matter contributes to the production of combustible gases during thermal processes. Ash, which is the inorganic residue in biomass, can cause operational issues like fouling, slagging, and agglomeration in reactors, furnaces, and similar systems[21].

Table 2. 1 Proximate analysis of common biomass (w.b.%) [22]

	Moisture* (%)	Volatile matter (%)	Fixed carbon (%)	Ash (%)	LHV (MJ/kg)
Wood	20	82	17	1	18.6
Wheat strew	16	59	21	4	17.3
Barley straw	30	46	18	6	16.1

Ultimate analysis provides the elemental composition of a fuel—specifically its carbon, hydrogen, oxygen, nitrogen, and sulfur content. This analysis is crucial for assessing a fuel's environmental impact and for calculating the theoretical air-to-fuel ratio[20]. Agricultural residues generally have higher hydrogen and oxygen content relative to carbon, which results in a lower calorific value. Fuels with low nitrogen and sulfur levels are more environmentally friendly, as they produce fewer harmful emissions. Because moisture and ash content can

significantly alter the elemental composition, comparisons are typically made on a dry ash-free (daf) basis [23]. The proportions of these elements greatly affect how biomass behaves during pyrolysis and combustion. Specifically, a higher hydrogen-to-carbon ratio—and to a lesser extent, a higher oxygen-to-carbon ratio—leads to greater mass loss from solid fuel particles during the pyrolysis stage[17].

Table 2. 2 Ultimate analysis of different biomass fuels [22]

	Carbon (%)	Hydrogen (%)	Nitrogen (%)	Oxygen (%)	Sulfur (%)	Chlorine (%)
Grass	45.34	5.82	2.04	45.95	0.24	0.62
Straw	48.31	5.85	0.78	44.18	0.18	0.70
Wood chips	51.59	6.14	0.61	41.57	0.07	0.02
Waste wood	49.62	6.34	1.01	42.89	0.07	0.06

Because of its carbohydrate-based structure, biomass contains significantly more oxygen than traditional fossil fuels such as hydrocarbon liquids and coal. On average, oxygen accounts for 30–40% by weight of the dry biomass. Carbon is the main element, typically making up 30–60% of the dry matter, though this can vary depending on the ash content. Hydrogen is the third key element in the organic fraction of biomass, usually comprising around 5–6% of the dry matter [20].

Fuel with more carbon also has more energy—adding 1% carbon by weight increases the energy value by about 0.39 MJ per kg. Biomass usually has less carbon (40-60% dry ash-free) than coal (60-80%), but processes like pyrolysis can increase its carbon content. Oxygen is the second most common element in biomass (30-50%), but it's less in animal faecal biomass (20-30%) and coal (10-30%); bituminous coal has less than 10%. Living biomass has more oxygen because of photosynthesis—oxygen in glucose helps build

cellulose, hemicellulose, and lignin. Hydrogen adds energy too, but it's found in smaller amounts (6-8% in biomass, 3-6% in coal)[10]. The change in atomic ratios H/C and O/C from biomass to peat, lignite, coal and anthracite is shown in Figure 2.5 is presented for comparison [20].

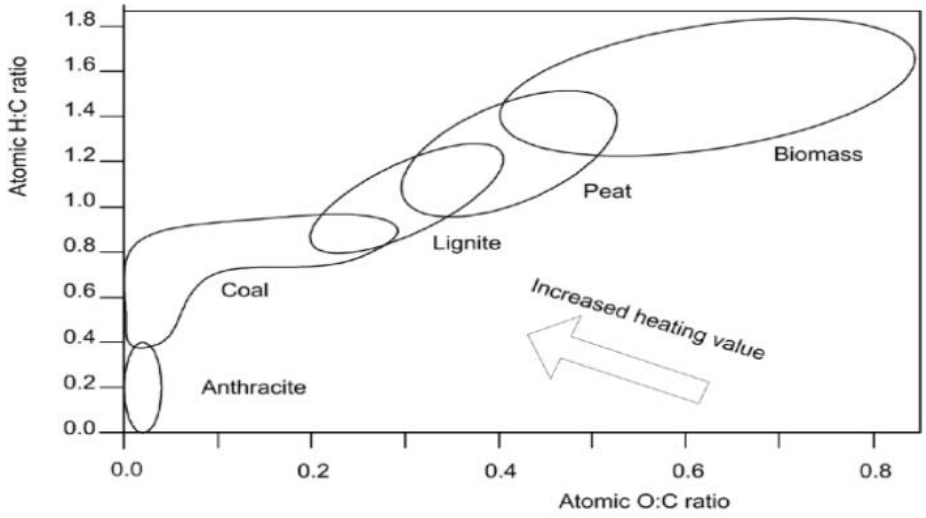

Figure 2. 5 Van Krevelen diagram showing the coalification process of biomass to coal [24]

2.2.Biomass fuel thermochemical conversion processes

Bioenergy can be made from biomass through two main methods: thermo-chemical and bio-chemical (or biological) processes. Thermo-chemical methods are usually more efficient because they work faster, while bio-chemical methods can take days, weeks, or even longer. Also, thermo-chemical processes are better at breaking down most organic materials. For example, lignin is usually hard to break down with biological methods since it's non-fermentable, but thermo-chemical methods can break it down completely[18].

Biomass feedstocks originating from a wide range of sources can be converted in many different types, designs, and scale of plants to provide useful forms of bioenergy carriers. The sources, process and output of different biomass fuels displayed in figure.

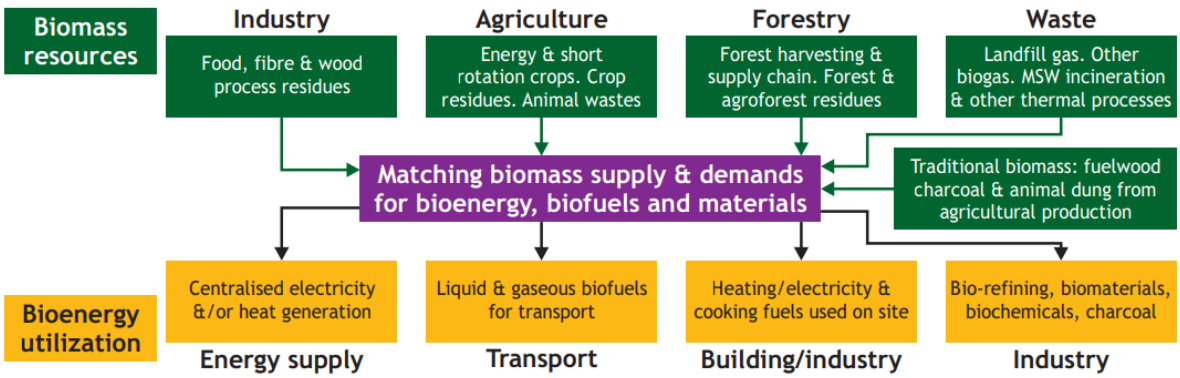

Figure 2. 6 Biomass resources converted to bioenergy carrier [19]

2.2.1. Fundamental types of thermochemical processes

Biomass can be transformed into fuel through various conversion processes. The selection of a specific method depends on factors such as the type and amount of biomass feedstock available, the intended energy carrier (end-use), environmental regulations, economic considerations, and other influencing factors. The primary conversion techniques include direct combustion, pyrolysis, gasification, and liquefaction. As illustrated in Figures 2.7 and 2.8, the energy stored in biomass can be directly extracted as heat through combustion or co-firing. Alternatively, it can be converted into solid fuels (e.g., charcoal), liquid fuels (e.g., bio-oils), or gaseous fuels (e.g., syngas) using pyrolysis, liquefaction, or gasification, each serving different applications[25].

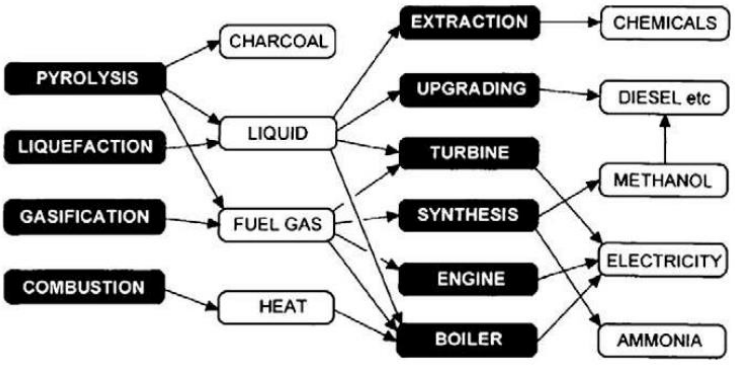

Figure 2. 7 Thermo-chemical processes for bioenergy production and the corresponding products [18]

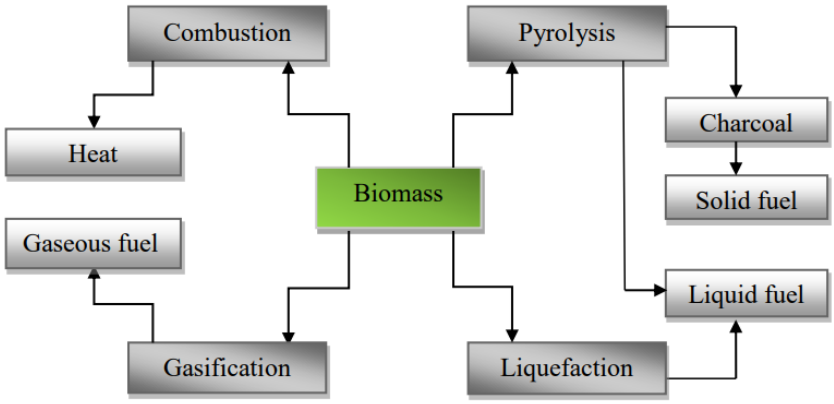

Figure 2. 8 Thermo-chemical process for conversion of biomass into fuels, gases or chemicals[17]

Combustion is a chemical reaction that releases heat, occurring when a fuel reacts with an oxidizer to form combustion products. Usually, air acts as the oxidizer, though pure oxygen (O_2) can also be used. During combustion, the chemical energy stored in biomass is transformed into heat, electricity, or mechanical power. This process is generally applied to biomass with less than 50% moisture content, unless the biomass is dried beforehand [26].

Pyrolysis is the process where biomass breaks down thermally without oxygen. It is a relatively slow reaction that happens at relatively low temperatures, turning biomass into useful gas rich in hydrocarbons and a solid residue high in carbon. The main products from pyrolysis depend on factors like temperature, heating speed, particle size, and any catalysts used. For woody biomass, the gases produced usually include CO, CO_2, CH_4, and H_2, along with other organic compounds. Fast pyrolysis tends to produce more gas and less solid residue[25].

The main pyrolysis reaction is:

Biomass → Charcoal + Volatile matter

Gasification is a partial oxidation process where biomass is converted into gas through controlled heating. It's designed to produce high amounts of gas—mainly CO, H_2, CH_4, and CO_2—known as syngas or producer gas. This gas can be cleaned and used directly as fuel in engines or further processed into liquid fuels or chemical feedstocks using biological or catalytic methods[27].

Direct liquefaction is a thermo-chemical process that breaks down biomass into smaller molecules in water or another solvent at low temperatures and high pressure. These small, unstable fragments then recombine into oily liquids with different molecular sizes. While it's similar to pyrolysis because both aim to produce liquid fuels, the two differ in how they operate. Direct liquefaction works at lower temperatures but needs much higher pressures (5–20 MPa) compared to pyrolysis (0.1–0.5 MPa). Also, liquefaction doesn't require drying the feedstock, unlike pyrolysis where drying is essential. Another key difference is that liquefaction always needs catalysts, while pyrolysis can often run without them [18].

2.2.2. Phases of biomass fuel combustion

Biomass combustion involves four main stages: drying, pyrolysis, gasification, and combustion. The process can be either batch or continuous, with air supplied by natural or forced draught. Batch combustion, often with natural draught, is typical for small units like traditional woodstoves. Larger units use continuous combustion with forced draught. Pyrolysis and gasification together are known as devolatilization [24]. The pyrolysis and gasification phases of a combustion process are commonly called devolatilization.

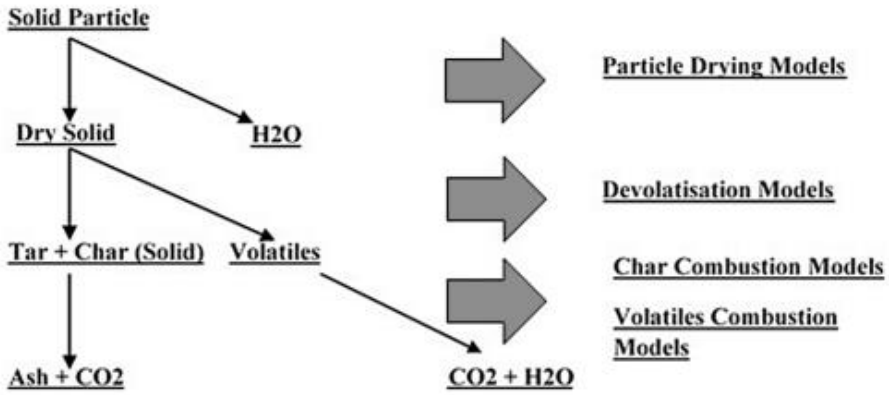

Figure 2. 9 Solid fuel combustion process [28]

Drying and pyrolysis/gasification are always the initial steps in solid fuel combustion. Their significance varies based on the combustion technology, fuel type, and conditions. Sometimes, these stages are separated from gas and char combustion, as seen in staged-air combustion. Figure 2.10 illustrates the distinct stages of a single biomass particle's combustion.

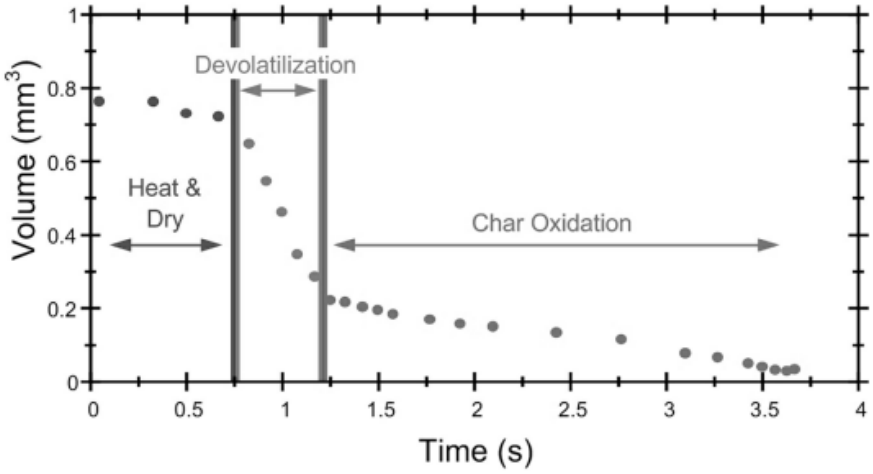

Figure 2. 10 The combustion of a small biomass particle proceeds in distinct stages [24]

2.3.Coffee husk as a biomass fuel

The coffee fruit has a five layer of protective material that needs to be removed to reveal the bean inside. From outside to inside, it is composed by:

- The skin (epicarp or exocarp), a monocellular layer covered with waxy substance
- The pulp(mesocarp), composed by fleshy pulp and, in ripe fruits, a slimy pectinaceous layer of mucilage.
- The parchment (endocarp), a thin polysaccharide covering.
- The silver skin (or chaff), a thin tegument that directly coats the seed
- Two seeds with elliptical form

The first three parts of the coffee fruit are commonly called coffee husk and it is a byproduct of coffee post harvesting process. Figure 2.11 shows the structure of coffee fruit before it is post processed.

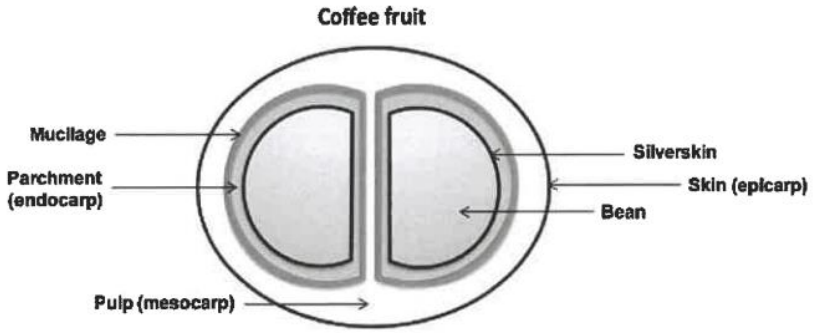

Figure 2. 11 Structure of coffee fruit [29]

Even if it varies by type and origin, coffee husk has potential as an energy source. It can be utilized through direct combustion, gasification, or in a carbonized form.

Coffee husks typically have low moisture (10–11%), high volatile matter (65–72%), low ash (1–4%), and low fixed carbon (17–20%) contents. Nitrogen ranges from 0.6 to 1.6%, while sulfur is about 0.1%. These values vary depending on coffee type and origin. A summary table of these properties is provided below.

Figure 2. 12 Coffee husk sample [30]

Table 2. 3 Physical properties of sample coffee husk fuels

	Average Particle Size (mm)	Bulk density(kg/m^3)	Porosity (%)	Reference
1	3.55	240	71.9	[30]

Table 2. 4 Proximity analysis of sample coffee husk fuels

	Moisture content (%)	Volatile matter (%)	Ash content (%)	Fixed carbon (%)	Reference
1	11.4	64.6	4.1	20	[31]
2	7.92	71.63	3.54	16.9	[7]
3	8.8	78.4	3.9	17.7	[30]
4	8.2	77.0	5.6	17.4	[32]

Table 2. 5 Ultimate analysis of sample coffee husk fuels

	Carbon (%)	Hydrogen (%)	Oxygen (%)	Nitrogen (%)	Sulfur (%)	Reference
1	43.9	4.8	49.6	1.6	0.1	[31]
2	40.1	5.6	49.1	5.2	-	[33]
3	46.8	4.8	47.9	0.4	0.05	[7]
4	47.3	6.4	37.7	2.7	0.3	[32]

2.4.Combustion furnace types and designs

Biomass combustion commonly employs three main furnace designs: fixed bed combustion, fluidized bed combustion and pulverized fuel combustion. These technologies differ primarily in how the fuel is fed into the system, the method of heat transfer, and the combustion process itself [24].

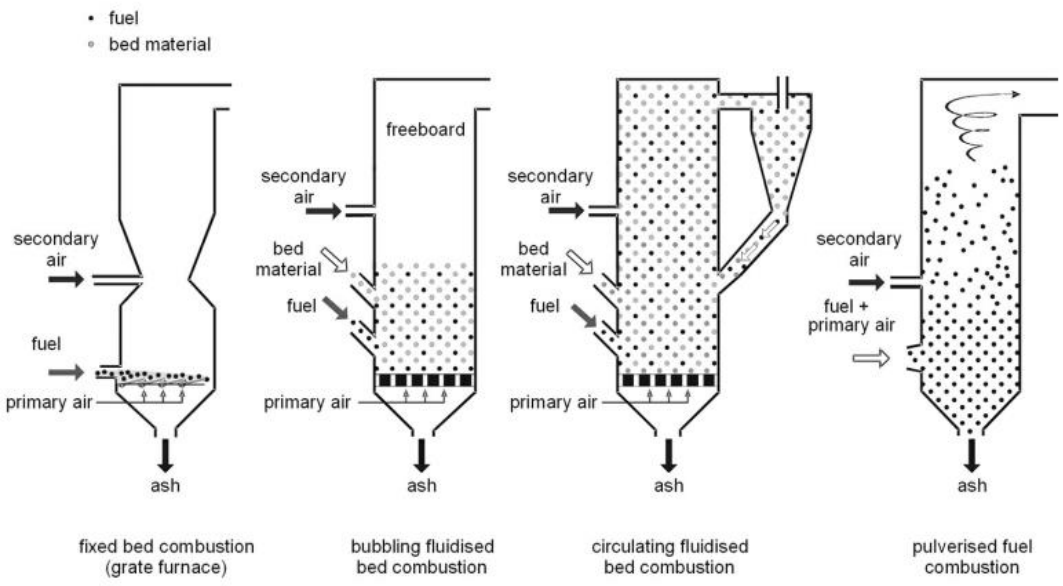

Figure 2. 13 Principal combustion technologies for biomass [24]

2.4.1. Fixed bed (grate) combustion system

Fixed bed combustion, or commonly called grate furnace combustion, is the simplest and most widely used method for converting the chemical energy in biomass into usable energy. [25]. In these systems, primary combustion air is supplied through the fuel bed, enabling drying, devolatilization, and char combustion. The primary air speed is usually around 0.1 m/s, which is too low to lift fuel particles, so they stay on the grate layer. Secondary or tertiary air can be introduced to different position depend on the design of the furnace [17].

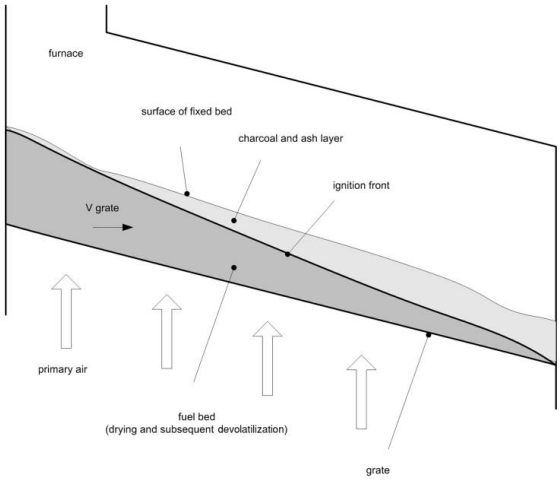

Figure 2. 14 Schematic diagram for combustion process in fixed fuel beds [24]

2.4.2. Fluidized bed combustion system

Fluidized bed combustion system involves a bed of solid particles, typically consisting of sand or limestone, which is fluidized by a high velocity stream of air. The fluidization is achieved by blowing air from the bottom of the bed through a distributor plate or grid. As a result, the solid particles become buoyant and behave like a fluid, exhibiting fluid like properties such as mixing, expansion and high heat transfer rates.

There are two distinct types of FBC:

Bubbling fluidized bed (BFB)

The vertical air speed is high enough to cause fluidization of the fuel bed, but low enough to prevent solid particles from escaping the bed, termed elutriation.

Circulating fluidized beds (CFB)

CFBs have a higher air speed than BFBs. This promotes elutriation of smaller, potentially unburned particles from the fuel bed. A cyclone is required downstream to separate these particles from the flue gas for their return to the fuel bed.

2.4.3. Pulverized bed combustion system

Pulverized combustion also known as pulverized coal combustion, is a method of burning coal or other solid fuels in which the fuel is grounded into a fine powder and then suspended in a stream of air for combustion.

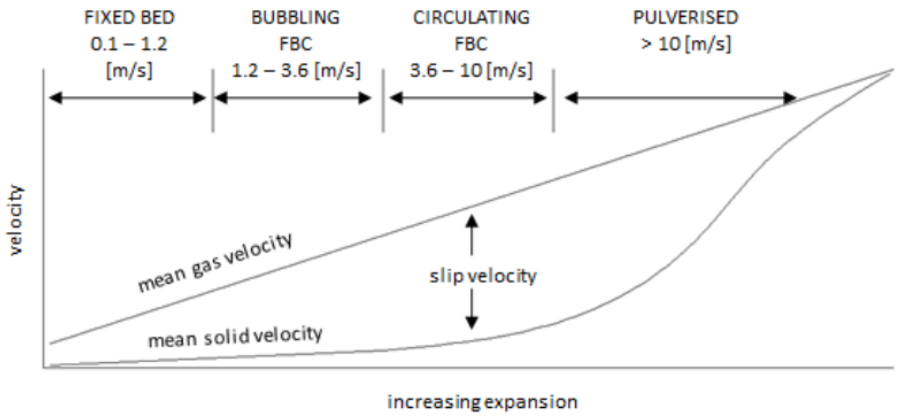

Figure 2. 15 Velocity of air for various combustion bed systems [34]

2.5. Previous numerical and experimental works on biomass fuel combustion

Direct combustion of biomass is one of the most common methods for using biomass energy in industry, and it closely resembles traditional coal combustion technologies[35].

Biomass energy contributes approximately 14% to the global primary energy supply, equating to around 1,000 million tons of oil equivalent annually[36]. In developing nations, biomass plays a more significant role, supplying about 35% of total energy needs[37]. This underscores its importance as a renewable energy source, prompting various experimental and numerical studies on different biomass fuels to explore its potential further.

2.5.1. Numerical and experimental works on wood and other agricultural residuals

Silva et al.[38] conducted a CFD study on an industrial biomass boiler, focusing on the combustion of volatile gases released from the grate. The model provided temperature, velocity, and species concentration data to help analyze and improve combustion efficiency. Their findings indicated that gas and air mixing inside the furnace could be enhanced particularly by optimizing secondary air flow, potentially reducing pollutant emissions [38].

Zhang et al.[39] simulated biomass pellet combustion using a heterogeneous-dimension approach. Intra-pellet processes were modeled with custom MATLAB code (1D), while the surrounding gas-phase reactions were handled using commercial CFD software. Their method proved effective, capturing both internal and external reactions with main errors under 10%. Compared to constant-condition models, the coupled approach reduced average relative error by 5%.

Scharler et al. [40] conducted a case study using CFD modeling to optimize combustion chamber geometry and secondary air nozzle design. Their findings revealed significant potential to improve fuel–air mixing by adjusting furnace geometry and secondary air injection, leading to more efficient combustion.

Kaer[41] used a stand-alone code to generate boundary conditions for CFD analysis of a 33 MW straw-fired boiler. The study highlighted that poor mixing in the freeboard area leads to high levels of fly ash and unburnt carbon during biomass combustion.

Yin et al. [42] developed a reliable baseline CFD model to diagnose and optimize grate boilers and assist in designing new ones. The model's results generally matched experimental data well, although some measurement points showed larger discrepancies.

Porteiro et al. [43] conducted a CFD simulation of a domestic pellet boiler, revealing that particle interactions in the fuel bed and poor gas mixing within the furnace are major contributors to high pollutant emissions.

Rajh et al. [44] conducted CFD modeling of waste wood combustion in a 13 MW grate-fired boiler at a Waste-to-Energy plant, finding the model to be suitably accurate. Their analysis indicated that optimizing the supply of secondary and tertiary air is essential to improve the plant's efficiency.

2.5.2. Numerical and experimental works on coffee husk biomass fuel

Couto et al. [33] developed a computational model to simulate biomass gasification of coffee husks in a fluidized bed reactor using the commercial CFD software FLUENT. The model used an Eulerian-Eulerian approach to represent both gas and solid phases, accounting for mass, energy, and momentum exchange. The predicted syngas composition closely matched experimental data, with minor deviations observed mainly in CO and H_2 concentrations.

Chapter Three
Mathematical modeling

3.1 Governing equations

In combustion modeling, properties like mass, momentum, and energy are conserved, leading to a mathematical framework based on conservation equations. These include the conservation of mass, momentum, energy, and species transport with chemical reactions. These equations are typically derived using the control volume approach, which analyzes a defined region in space to track these quantities [45].

3.1.1 Bed mass and energy conservation

Fuel particles are assumed to be thermally thin, that is, the temperature as well as the composition of individual particles is uniform.

Assuming the grate to be moving continuously at a constant velocity, U_{bed}, a simple relation between the position of the fuel on the grate, x, and its residence time, t, exists[45]

$$t = \frac{x}{U_{bed}} \quad \Leftrightarrow \quad x = U_{bed} t \tag{3. 1}$$

In biomass combustion modeling, it is commonly assumed that the mass transport of solid bed material occurs only along the grate direction[45]. Under this assumption, the continuity (mass conservation) equation for the bed can be expressed as:

$$\frac{\partial(\rho_{bed})}{\partial t} + \frac{\partial(\rho_{bed} U_{bed})}{\partial x} = S_{mass,drying} + S_{mass,devol} + S_{mass,char} \tag{3. 2}$$

The bed density is denoted by ρ_{bed} and $S_{mass,i}$ represents source terms that account for mass changes resulting from conversion processes within the bed. To achieve steady-state conditions in the vertical direction before progressing along the grate, the process is described by a time-dependent, one-dimensional heat conduction equation, which governs heat transfer within the fuel bed.

$$\frac{\partial(\rho_{bed} C_{p,bed} T_{bed})}{\partial t} = \frac{\partial}{\partial y}\left(K_{bed} \frac{\partial(T_{bed})}{\partial y}\right) + S_{heat,exchange} + S_{heat,drying} + S_{heat,char} \tag{3. 3}$$

Where $C_{p,bed}$ represents the specific heat capacity, T_{bed} is the temperature of the bed, and K_{bed}denotes the thermal conductivity of the fuel. The source terms $S_{heat,i}$ capture the heat

generated from the bed's conversion processes and the heat exchanged between the bed and the surrounding gas phase.

3.1.2 Gas phase mass and energy conservation

The gas is considered to flow upward through the bed primarily by convection, driven by the air introduced beneath the grate. Under this assumption, the continuity equation for the gas phase is expressed as follows[41]

$$\frac{\partial(\rho_{gas})}{\partial t} + \frac{\partial(\rho_{gas}U_{gas})}{\partial y} = -S_{mass,drying} - S_{mass,devol} - S_{mass,char} \quad 3.4$$

The gas velocity is predicted from the mean gas density using

$$U_{gas} = \frac{\dot{m}_{gas}}{\rho_{gas}A} \quad 3.5$$

Where, $\dot{m}_{gas}$ denotes the vertical mass flow rate of the gas in the one-dimensional model, and A is the cross-sectional area of the computational cell face. The density of each species i is determined as a function of temperature using the ideal gas law.

$$\rho_{gas,i} = \frac{P}{R_i T_{gas}} \quad 3.6$$

$$R_i = \frac{R_u}{M_i} \quad 3.7$$

where p is pressure, M_i molecular weight, R_i the gas constant, R_u is universal gas constant and T_{gas} the gas temperature. Define the mass fraction of species i, φ_i (dimensionless) by

$$\varphi_i = \frac{\dot{m}_i}{m_{total,gas}} \quad 3.8$$

Where $\dot{m}_i$ being the mass of species i and $m_{total,gas}$the total mass of gas in the cell. The mean density of the gas mixture, ρ_{gas}, is

$$\rho_{gas} = \left(\sum_{i=1}^{i=n} \frac{\varphi_1}{\rho_{gas,i}} \right)^{-1} \quad 3.9$$

Thermal conduction in the gas phase is considered negligible compared to convective heat transfer. The energy equation is given by

$$\frac{\partial(\rho_{gas}c_{p,gas}T_{gas})}{\partial t} + \frac{\partial(\rho_{gas}U_{gas}c_{p,gas}T_{gas})}{\partial y} = -S_{heat,exchange} + S_{heat,vol} + S_{heat,CO} \quad 3.10$$

Where $c_{p,gas}$ is the gas specific heat and $S_{heat,i}$ are source terms accounting for heat exchange with the bed and heat release from reactions in the gas phase.

The convective exchange of heat between the fuel bed and the gas is included through the source terms of the energy equations. h is the mean convective heat transfer coefficient.

$$s_{heat,exchange} = \mathrm{h}A_{p,vol}\left(T_{gas} - T_{bed}\right) \quad 3.\ 11$$

3.2 Chemical kinetics

3.2.1 Evaporation of moisture

The drying process is important as the evaporation of water influences both the temperature fields and the burnout time. Below the boiling point, the evaporation rate is calculated based on a mass transfer correlation. At the boiling point, the evaporation rate is controlled by the heat transfer rate to the fuel. Due to the assumption of thermally thin particles, all the water has to evaporate before the onset of devolatilization. For coffee husk this is a reasonable approximation. For typical wood chips significant internal temperature and concentration gradients may occur due to finite heat and mass transfer rates. The water vapor mass flux leaving the fuel due to mass transfer is given by[45].

$$s_{mass,drying} = \bar{h}_m A_{p,vol}\left(X_{gas} - X_{surface}\right) \quad 3.\ 12$$

Where the mean mass transfer coefficient is approximated from a Sherwood number correlation (dimensionless) for a fuel structure and X is the mass concentration in the gas and at the particle surface. Using the analogy between heat and mass transfer can be used to estimate the mass transfer coefficient.

$$\overline{Sh} = \frac{\bar{h}_m\, d_{cyl}}{D_{AB}} \quad 3.\ 13$$

The diffusivity, D_{AB}, of the vaporizing species in the gas mixture, is approximated by the binary diffusivity of the species in air using the method suggested by Wilke and Lee. The vapor mass concentration at the particle surface is calculated from the vapor pressure at the surface of the fuel particles using a slightly simplified form of the Clausius–Clapeyron equation that neglects the condensed phase volume and expresses the gas phase volume using the perfect gas law

$$\frac{d\ ln(P_{vap})}{dT} = \frac{H_{evap}}{RT^2} \quad 3.\ 14$$

The resulting source term in the bed energy equations is

$$s_{heat,drying} = S_{mass,drying}\, H_{evap} \quad 3.\ 15$$

Where H_{evap} is the heat of evaporation of the evaporating species.

3.2.2 Volatiles release and combustion

The volatiles release rate is modeled by a simple first-order Arrhenius expression [39]

$$k_V = A_V exp\left(-\frac{T_V}{T_{bed}}\right) \quad 3.\ 16$$

The resulting mass source in the gas and bed continuity equations is

$$s_{mass,devol} = -\rho_{bed}\, k_V \left(V_f - V\right) \quad 3.\ 17$$

where V and V_f are the mass of volatiles released from unit mass of raw fuel and the final volatiles yield, respectively.

The combustion of volatiles in the gas phase is modeled as either a full oxidation to CO2 or a partial oxidation to CO. At present, an equal mass of CO2 and CO is assumed to evolve which is based on values measured by Van der Lans et al.

The heat released in the gas phase due to volatiles oxidation is given as

$$s_{heat,vol} = -\frac{dm_{vol\rightarrow CO}}{dt} H_{vol\rightarrow CO} - \frac{dm_{vol\rightarrow CO2}}{dt} H_{vol\rightarrow CO2} - \frac{dm_{vol\rightarrow H2O}}{dt} H_{vol\rightarrow H2O}$$

Where the first-term on the right-hand side expresses the mass of volatiles oxidized to CO per unit volume per second times the heat released from the reaction. The second-term is similar only for the full oxidation of the volatiles. The third term is for heat release from oxidation of H_2 to water.

The main combustible components of devolatilization process are CH_4, H_2 and CO. The homogenous reaction is undergone in these gases is presented in table below.

Table 3. 1 Gas phase homogenous reactions

No	Homogenous reaction of the devolatilized gases
1	$CH_4 + \frac{3}{2}O_2 \rightarrow CO + 2H_2O$
2	$CO + \frac{1}{2}O_2 \rightarrow CO_2$
3	$H_2 + \frac{1}{2}O_2 \rightarrow 2H_2O$

The gas phase reaction is modeled by first-order Arrhenius expression and the parameters affecting the process are the pre-exponential factor, the activation energy and

This based on the assumption that the information we get from detailed mechanisms unnecessary and a much simpler model will suffice. (add citation from the kinetics paper referred).

Overall reaction rate representation for the combustion of the fuels is[46]

$$R = AT^n exp(-Ea\ /\ RT)[Fuel]^a\ [oxidizer]^b \qquad 3.\ 18$$

Where A is the pre-exponential factor, Ea is the activation energy, and b are order of the reaction with respect to the fuel and oxidizer.

Comparisons between computed and experimental combustion rates are required to evaluate the constants A, n, E_a, a, and b. In general, a and b are not related to the stoichiometric coefficients in the global reaction, but are empirical constants determined either from experiment or from detailed kinetics calculations. These constants vary with fuel type, pressure, equivalence ratio, and other parameters as well. In spite of these difficulties, this type of rate expression is probably the most commonly used combustion rate in the literature. In a great majority of cases, it is assumed that the overall reaction is first order with respect to both fuel and oxidizer, so that $a = b = 1$. However, modeling of laminar flame propagation using simplified rate expressions has shown that this choice of reaction order can lead to serious errors. Therefore, actual experimentally determined values for the reaction are recommended to get accurate results[46].

Table 3. 2 Experimentally determined reaction rate constant parameters [38]

No	Gas	A	Ea	a	B
1	CH_4	5.012×10^{11}	2×10^{8}	0.7	0.8
2	CO	2.239×10^{12}	1.702×10^{8}	1	0.25
3	H_2	9.87×10^{8}	3.1×10^{7}	0.7	0.8

Char oxidation

Char is assumed to be either fully or partially oxidized at the particle surface forming CO2 or CO. In comparison with experimental data, the ratio was fixed based on the measurements. In full scale simulation, the temperature dependence of the CO2 to CO ratio, x; was based on an Arrhenius expression[45].

Defining the following ratio: $\varphi = (x + (1/x) + 0.5)$; $1 \leq \varphi \leq 2$ allows the C–O2 reaction to be expressed as

$$C + \frac{1}{\varphi} O_2 \rightarrow \left(2 - \frac{2}{\varphi}\right) CO + \left(\frac{2}{\varphi} - 1\right) CO_2$$

The rate of char oxidation is modeled as a combination of the kinetic reaction rate, kc, and the rate of oxygen diffusion to the surface, kd. The total oxidation rate based on the combined kinetic and diffusion rates is given by

$$s_{mass,char} = -\frac{\varphi}{1K_d^{-1} + k_c^{-1}} p_{02} A_{p,vol} \qquad 3.\ 19$$

At lower temperatures, kinetics control the reaction rate, whereas oxygen diffusion is the limiting term at temperatures exceeding about 800 ^{0}C.

The heat released by oxidation of char to CO is added to the bed energy equation whereas heat released by subsequent oxidation of CO to CO2 in the gas phase is added in the gas energy equation. For the bed this gives

$$s_{heat,char} = -S_{1mass,char} H_{Char \rightarrow CO} \qquad 3.\ 20$$

Where $H_{Char \rightarrow CO}$ is the heat released from oxidation of unit mass of char to CO. For the gas phase the source term is

$$s_{heat,CO} = -s_{mass,char} \frac{w_{CO}}{w_C} \left(\frac{\varphi}{2} - 1 \right) H_{CO \rightarrow CO2} \quad 3.21$$

Where W_{CO} and W_C are the molecular weights of CO and C, respectively. $H_{CO \rightarrow CO2}$ is the heat released from oxidation of unit mass of CO to CO2.

3.3 Turbulence model

Fluid flow can be classified as either laminar or turbulent. Laminar flow is smooth and orderly, with fluid layers moving over one another under the influence of pressure gradients and viscosity. However, in most industrial applications—particularly those involving energy conversion—flows are predominantly turbulent. In such reactive systems, the interaction between turbulence and chemical reactions gives rise to turbulent combustion [47].

Turbulent flows exhibit a broad spectrum of time and length scales, where motion and fluctuations occur. Turbulent eddies form across a wide range of sizes—from the largest structures down to the smallest, known as Kolmogorov scales—and are primarily responsible for transporting turbulent kinetic energy [48]. The comparison between turbulence scales and the thickness of a laminar flame defines the nature of turbulent flames, making the interaction between turbulence and chemical reactions crucial in turbulent combustion. Large eddies, which play a key role in mixing, undergo vortex stretching, a process that transfers motion from larger to smaller scales. As this continues, energy cascades from the larger eddies down to progressively smaller ones, eventually reaching the tiniest eddies where viscosity dominates and energy is converted into heat. This transfer of energy across scales is referred to as the energy cascade[49].

The simulation can be done by direct numerical simulation, Large eddy simulation or Reynolds average Navier stokes equation-based turbulence models. In direct numerical simulation (DNS) simulations, all of the motions contained in the flow are resolved. In order to account for the full nonlinear multi-scale effect of turbulence in a combustion process, the governing equations must be solved resolving the Kolmogrov scale eddies, which makes

such simulations computationally expensive. Thus, DNS is restricted to low-Reynolds number turbulent flows and simple geometries. Instead of directly solving the Navier-Stokes equations for turbulent flows, LES and time-averaging approaches are used. The former approach is still expensive in terms of computational costs, but when compared to DNS, they are much more reasonable. The latter one is solving the RANS equations (Reynolds-Averaged Navier-Stokes). These equations describe the behavior of the time-averaged flow quantities instead of the exact instantaneous values. In this approach, RANS equations arise when the Reynolds decomposition is implemented into the Navier-Stokes equations. Reynolds decomposition refers to the separation of the flow variable into two components: mean component,¯and fluctuating component.

Turbulent flow simulations can be carried out using Direct Numerical Simulation (DNS), Large Eddy Simulation (LES), or turbulence models based on the Reynolds-Averaged Navier-Stokes (RANS) equations. DNS resolves all the flow motions, capturing the complete nonlinear and multi-scale nature of turbulence. This requires solving the governing equations down to the Kolmogorov scales, making DNS highly computationally intensive. As a result, DNS is typically limited to turbulent flows with low Reynolds numbers and simple geometries. To reduce computational demands, alternative approaches like LES and RANS are employed. LES, while still computationally costly, is significantly more practical than DNS and resolves larger turbulent structures while modeling the smaller ones. RANS, on the other hand, focuses on time-averaged flow properties rather than capturing every instantaneous detail. This method is based on Reynolds decomposition, which separates flow variables into a mean part and a fluctuating component, and substitutes them into the Navier-Stokes equations to derive the RANS equations[50].

$$\emptyset = \overline{\emptyset} + \emptyset' \qquad 3.22$$

For the velocity component

$$u = \bar{u}_i + u_i' \qquad 3.23$$

The same decomposition approach is also applied to pressure and other flow variables.

After applying the Favre-averaging method—which is particularly useful for compressible flows—and disregarding gravitational body forces, the resulting Reynolds-Averaged Navier-Stokes (RANS) equations can be expressed as follows:

$$\frac{\partial \rho}{\partial t} + \frac{\partial}{\partial x_j}(u_i) + \frac{\partial}{\partial x_j}(\rho u_i) = 0 \qquad 3.\ 24$$

$$\frac{\partial}{\partial t}(\rho u_i) + \frac{\partial}{\partial x_j}(\rho u_i u_i) = -\frac{\partial p}{\partial x_i} + \frac{\partial}{\partial x_j}\left[\mu\left(\frac{\partial}{\partial x_j}u_i + \frac{\partial}{\partial x_i}u_j - \frac{2}{3}\frac{\partial}{\partial x_k}u_k\delta_{i,j}\right) - \rho\overline{u_i' u_j'}\right] \qquad 3.\ 25$$

An additional unknown term, the Reynolds stress $\rho\overline{u_i' u_j'}$ [N/m2], appears in the RANS equations due to the averaging process. To close the system of equations, this term must be modeled. Several turbulence models have been developed for this purpose, with two-equation models being among the most widely used. Notably, the *k-ε* and *k-ω* models are the most popular due to their ability to deliver reliable results across various turbulent flow conditions. These models are frequently applied in simulations involving gas, coal and biomass combustion [17].

3.4Thermal radiation

In combustion systems, thermal radiation plays a significant role in influencing the overall combustion process. In particular, during biomass combustion and gasification at elevated temperatures, radiation can account for approximately 25–45% of the total heat transfer. Through radiation, energy is emitted from the hot combustion gases and transferred to cooler surroundings, leading to a reduction in the combustion temperature. The radiative heat flux emitted by a blackbody toward isothermal surroundings can be expressed as[51]:

$$Q_r = \sigma\,(T^4 - T_{surr}^4) \qquad 3.\ 26$$

The Stefan-Boltzmann constant, denoted as $\sigma = 5.67 \times 10^{-8}$ W/m²·K⁴, is used in calculating the radiative heat flux, and T_{surr} represents the temperature of the surrounding medium. Since radiative flux is proportional to T^4, it becomes a dominant mode of heat transfer at high temperatures, often surpassing conduction or convection.

In combustion systems, the primary radiating species are carbon dioxide (CO_2) and water vapor (H_2O), which strongly absorb and emit radiation in the infrared region of the spectrum. In contrast, diatomic gases like nitrogen (N_2) and oxygen (O_2) have minimal impact on thermal radiation due to the absence of significant absorption bands[52].

The propagation of thermal radiation is governed by the Radiative Transport Equation (RTE). Accurate modeling of radiative heat transfer is vital in simulations of turbulent combustion, but solving the RTE precisely is computationally expensive. To approximate radiative effects efficiently, various radiation models are employed, including the P-1 model, discrete transfer model, discrete ordinates model, and Rosseland approximation [17].

P-1 model is a first order approximation to the RTE. The radiation intensity is expressed by an orthogonal series of spherical harmonics. Therefore, it is mathematically simple, and its implementation is easy. Additionally, it is computationally robust. The equation of balance of radiative energy transfer in a specified direction through a small differential volume for an absorbing, emitting, and scattering medium can be written as

The P-1 model represents a first-order approximation to the Radiative Transport Equation (RTE). It simplifies the description of radiation intensity by expressing it as a series expansion using spherical harmonics. Due to its mathematical simplicity and ease of implementation, the P-1 model is both computationally efficient and stable.

In an absorbing, emitting, and scattering medium, the radiative energy balance in a given direction, across a small differential volume, is governed by the following form of the RTE:

$$\frac{dI(\vec{r},\vec{s}_{,})}{ds} + (a+\sigma_s)I(\vec{r},\vec{s}_{,}) = an^2\frac{s_b T^4}{\pi} + \frac{\sigma_s}{4\pi}\int_0^{4\pi} I(\vec{r},\vec{s}_{,})\phi\,(\vec{s},\vec{s}_{,})d\Omega \qquad 3.\ 27$$

The P-1 model approximates radiation intensity I by expanding it into an orthogonal series of spherical harmonics. Using this expansion, the radiation flux can be calculated with the following equation:

$$Q_r = -\frac{1}{3(a,+\sigma_s)-C\sigma_s}\nabla G \qquad 3.\ 28$$

where C is the linear-anisotropic phase function coefficient and is the incident radiation. By introducing the parameter $\Gamma = -\frac{1}{3(a,+\sigma_s)-C\sigma_s}$ the above equation is simplified to

$$Q_r = -\Gamma\nabla G \qquad 3.\ 29$$

The transport equation for is given by

$$-\nabla\cdot Q = aG - 4as_b T^4 \qquad 3.\ 30$$

Chapter Four
Combustion Furnace Sizing

Furnace design for heating or power application needs to consider: a furnace Volume, a fuel feeding system, a grate assembly, air supply system (primary and secondary air) and ash discharge system. In this section, we will discuss the design procedure used to determine the above-mentioned systems, the geometric values and process parameters generated from the analysis.

4.1 Process description of the drying unit

Drying is the process where heat and moisture transfer together between a product and the surrounding air. This removes excess water from the product through evaporation until it reaches a stable moisture level, called the equilibrium moisture content. Typically, warm air is used to dry the product gently, helping to preserve its quality during storage[53].

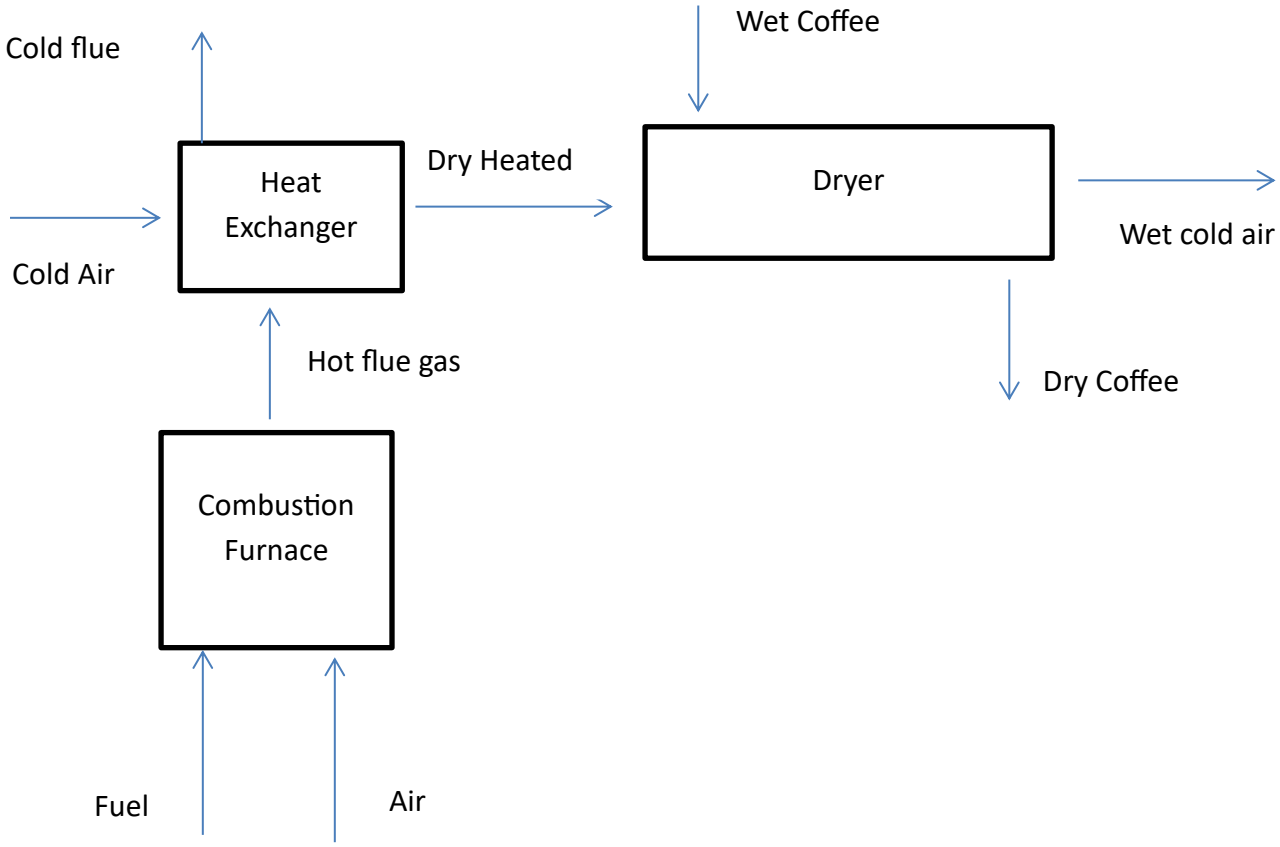

Figure 4. 1 Process flow of coffee drying machine

4.2 Heating load at the dryer

The heat provided by the hot air during the drying process is utilized for five distinct purposes: first, evaporating water from the material; second, heating the evaporated water to the inlet wet-bulb temperature of the air; third, raising the temperature of the vapor from the initial wet-bulb temperature to the exit air temperature; fourth, warming the dry solid from its initial temperature to its final temperature; and fifth, heating the water remaining in the final product from its initial temperature to the product's exit temperature [54].

In process of drying, the driving force for heat transfer comes from the difference in temperature between the air (T_a) and the product surface at the wet bulb temperature (T_w), whereas that for mass transfer comes from the difference in humidity of the air (Ha) and product surface (H_w). The evaporation of water from the material is done at the wet bulb temperature of the drying air. [55].

The wet-bulb temperature of air is commonly used to determine the absolute or relative humidity of an air sample. Achieving the wet-bulb temperature involves an adiabatic saturation process, which is illustrated both schematically and on a temperature-entropy (T–s) diagram below[56].

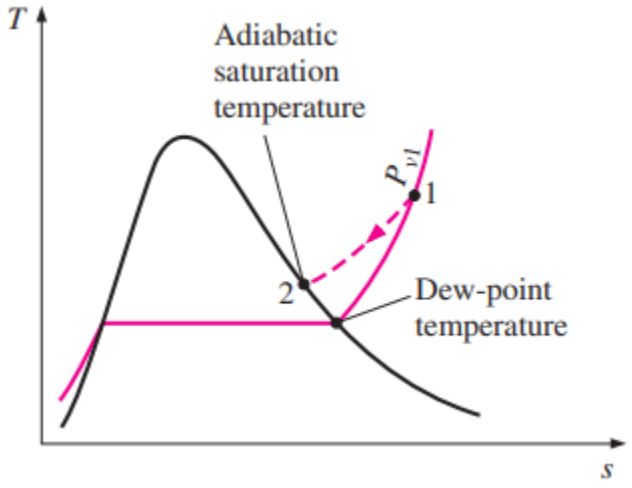

Figure 4. 2 Adiabatic saturation process and its representation on a T-s diagram of water [56].

The below thermodynamic equations are used to determine the wet bulb temperature of the drying air.[57]

$$\omega_1 = \frac{c_p(T_w - T_1) + \omega_w H_w}{h_{g1} - h_{fw}} \quad 4.1$$

$$\omega_w = \frac{0.622 P_{gw}}{P_w - P_{gw}} \quad 4.2$$

$$\omega_1 = \frac{0.622 P_v}{P - P_v} \quad 4.3$$

$$P_v = \emptyset P \quad 4.4$$

Where

T_1 is inlet drying air temperature

T_w is the inlet wet-bulb temperature of the drying air

c_p is the specific heat capacity of the air

ω_1 is the specific humidity of the drying air

h_{g1} is enthalpy of saturated gas at the inlet temperature of drying air

h_{fw} is enthalpy of saturated liquid at the wet bulb temperature

ω_w is the specific humidity of the drying air at saturated state

ΔH_w is the latent heat of vaporization at the wet bulb temperature (kJ/kg)

P_{gw} is saturation pressure of water at wet bulb temperature

P_v is partial water vapor pressure

$\emptyset$ is relative humidity of the air

Table 4. 1 Summary of energy consuming operations in drying process.

	Heat consuming operations	Formula
1	To evaporate the water, that leaves the material	$Q_1 = m_w \Delta H_w$
2	To heat the vapor from the initial wet-bulb temperature of the air to the exit air temperature	$Q_2 = m_w C_{pv}(T_2 - T_w)$
3	To heat the water that evaporates, to the inlet wet bulb temperature of the air, in order to evaporate	$Q_3 = m_w C_{pw}(T_w - T_{m1})$
4	To heat the dry solid from its inlet temperature to its exit temperature	$Q_4 = \mathrm{F} C_{ps}(T_{m2} - T_{m1})$
5	To heat the water that remains in the final product from the inlet to the exit temperature of the material	$Q_5 = \mathrm{F} X C_{pw}(T_{m2} - T_{m1})$

where

m_w is the mass of water evaporated

ΔH_w is the latent heat of vaporization (kJ/kg)

C_{pv}, C_{pw}, C_{ps}, are the specific heat of vapor, water, and solid (kJ/kg °C), respectively

T_2 is the outlet temperature of the air (°C)

T_{m1} , T_{m2} are the inlet and exit temperature (°C) of the material (dry solid and moisture content), respectively

The inlet property of the air into the heat exchanger is referred from the atmospheric property of Teppi zone which is common coffee production area.

Table 4. 2 Atmospheric properties of the drying air

	Atmospheric properties	
1	Elevation(m)	1097
2	Average temperature (^{0}c)	21.5
3	Average relative humidity (%)	60
4	Atmospheric pressure(kpa)	88.8
5	Air density(kg/m3)	1.02

Thermophysical properties of the coffee sample is presented in relation to the moisture it holds in the below equation[58].

$$C_{ps} = 1652.2 + 58.35\frac{Xcoffee}{1+Xcoffee} \quad 4.5$$

The load in the furnace is calculated based on the load on downstream dryer proposed for the design. The dryer capacity selected for the design calculation is 500 kg per batch. Temperature of the drying air is recommended not raise above 80 0c to get the desired quality on the coffee. The calculation is done based on 80 0c for the drying air [58].

The initial moisture content of the wet coffee after harvesting is 60%. Final moisture content of the dried coffee is 12%[7].

Temperature of the drying air recommended not raise above 80 0c to get the desired quality on the coffee. The calculation is done based on 80 0c for the drying air.

The drying air that has a direct contact to the coffee is heat at the heat exchanger. In the side the heat exchanger the hot burned flue gas used to heat the drying air.

The initial moisture content of the wet coffee is 60%

Final moisture content of the dried coffee is 12%

The heat supplied by the hot air is used for five different operations. Detail load calculation done based on the heat requirement for each operation.

1. To evaporate the water that leaves the material

   $$Q_1 = m_w \Delta H_w \quad 4.6$$

   X_o = 60% wb = 1.5kg/kg db

   X_f = 12% wb= 0.14 kg.g db

   The dryer is designed to dry 500kg of wet coffee in 10 hr time period.

   The portion of dry coffee from the initial sample is 40 % of 500kg. which is equal to 200kg.

   M_1 = 1.5 kg/kg dry coffee *200 kg = 300 kg

   M_2 = 0.14 kg/kg dry coffee *200 kg = 28 kg

Where M1 is the moisture found the wet sample in kg and M2 the moisture found in dried sample

The evaporated water from the wet coffee in the drying process

m_w = M1-M2 = 300kg-28kg = 272kg

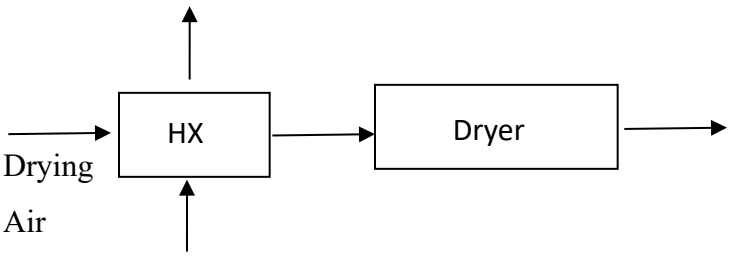

To find the heat of vaporization at wet bulb temperature of the drying air the wet bulb temperature must be determined first.

We use Equation 4.1 and 4.1 to determine the wet bulb temperature.

ω1 can be determined from the relative humidity and temperature of the drying air before getting into the heat exchanger since the specific humidity of the air will not change because of heating up in the heat exchanger.

$$\omega 1 = \frac{0.622\mathrm{Pv}}{\mathrm{P} - \mathrm{Pv}}$$

P_v is the partial vapor pressure of the air sample

P is the total pressure of the air sample

P = 88.8 kpa

$P_{sat@21.5\ 0c}$= 2.59kpa

$P_v = \Phi * P_{sat@21.5\ 0c}$ = 0.6*2.59kpa=1.55 kpa

$\omega 1 = \frac{0.622*1.55}{88.8-1/55}$= 0.0111kg/kg dry air

To determine the wet bulb temperature of the drying air, we have two equations and four unknows. But the four unknowns depend on one variable (wet bulb temperature).

We can iterate to get the value we want. The iteration is done for the temperature of 25, 30 and 35 ^{0c} and the value we get for $\omega 2$ calculated from the two equations is nearly the same at a temperature of 30 ^{0c}.

ΔH_w= hfg@30= 2429.8 kJ/kg

$Q_1 = m_w \Delta H_w$

Q1=272kg*2429.8 kJ/kg

Q1=671.8 MJ

2. To heat the vapor from the initial wet bulb temperature of the air to the exit air temperature

   Cp_v= 1.608 kJ/kg k

   $Q2=m_w\ Cp_v(T_2-T_w)$ 4. 7

   Q2= 272*1.608(40-30)

   Q2=4.37MJ

3. To heat the water that evaporates from its initial temperature, as it enters the dryer to the inlet wet bulb temperature of the air in order to evaporate.

   Cp_w= 4.185 kJ/kg K

   $Q3= m_w Cp_w (T_w-T_1)$ 4. 8

   Q3= 272*4.185(30-21.5)

   Q3=9.33MJ

4. To heat the dry solid from its inlet temperature to its exit temperature

   $C_{ps}=1652.2+58.35\frac{Xcoffee}{1+Xcoffee}$

   C_{ps} calculated based on the average moisture content of the coffee sample.

   $X_{average}= \frac{1.5+0.14}{2}=0.82$

   $C_{ps}=1652.2+58.35\frac{0.82}{1+0.82}=1678.5$ kJ/kg k

   $Q4= F\ C_{ps}\ (T_3-T_1)$ 4. 9

   Q4=200*1678.5(40-21.5)

Q4=6.2 MJ

5. To heat the water that remain in the final product from the inlet to exit temperature of the material.

$$Q5= F\ X_2\ Cp_w(T_3-T_1) \quad (4.10)$$

Q5= 200*0.14*4,185(40-21.5)

Q5=2.2 MJ

Total drying load = Q1+ Q2+ Q3+ Q4+ Q5

=693.5 MJ

Table 4. 3 Summary of drying heat load

	Drying Process	Energy required (MJ)
1	To evaporate the water from the coffee	671.8
2	To raise the vapor to exit temperature	4.37
3	To raise the water to wet bulb temperature	9.3
4	To dry the dry solid	6.2
5	To heat the water remains in the coffee	2.2
	Total	693.5

The efficiency of rotary drier referred from literature is between 55-75 %[54]. The calculation is done assuming a 55% efficient dryer considering conservative approach and a drying time of 10 hr. The effectiveness for cross flow heat exchanger can move up 76 % for air-to-air exchanging mediums[59]. The heat requirement in the hot side of the heat exchanger is calculated assuming a heat exchanger with 70% effectiveness.

Table 4. 4 Summary of energy and heating power requirement

	Energy and heating power requirement	
1	Total heat energy requirement at dryer (MJ)	1261.5
2	Heating power requirement at the dryer (KW)	35
3	Heating power requirement in the hot side of the heat exchanger (KW)	50

4.3 Furnace sizing and combustion parameters setting

A good furnace structural design determines the reasonability of flue gas flow, and it is an important means to increase combustion efficiency and decrease pollutant emission[60]. The structural design and sizing of the furnace directly depends on the fuel flow rate, combustion air flow rate, heat load we want to extract from the furnace and the combustion efficiency. In this section, we will determine the above-mentioned combustion parameters based on our selected fuel and heat load required in downstream of the furnace.

4.3.1 Fuel flow rate and combustion air requirement

To estimate the fuel flow requirement for combustion corresponding to a given furnace load (as presented in Table 4.4), the lower heating value (LHV) of the fuel and the conversion efficiency of the furnace must be known. The LHV of coffee husk is 18.9 MJ/kg, and based on available data, a furnace efficiency of 60% is assumed for coffee husk combustion. This value is derived from various studies: one reference reports conversion efficiencies of 63.7%, 58.6%, and 52.7% for fuel mixtures containing 58%, 63%, and 52% coffee husk blended with wood, respectively [59], while another survey study reports an average efficiency of 65% based on multiple tests [60]. These findings support the assumption of 60% efficiency for further analysis. This assumption, along with the thermophysical properties of the fuel and the total heat load downstream of the combustion furnace, forms the basis for the subsequent calculations to determine the required fuel mass flow rate.

LHV of coffee husk fuel is 18.9 MJ/kg[7]

$$M_f = \frac{\dot{Q}}{\eta_o LHV} \qquad 4.\ 11$$

Where

$\dot{Q}$ is the total heat load in the heat exchanger

M_f is the mass flow rate of fuel

η_0 is conversion efficiency of the fuel in the furnace

LHV is lower heating value of the fuel

Based on a furnace load of 50 kW, a fuel lower heating value (LHV) of 18.9 MJ/kg, and a combustion efficiency of 60%, the fuel mass flow requirement is calculated using Equation 4.6 to be 15.84 kg/hr. This result, along with the corresponding air requirement (to be calculated in the next section), is summarized in Table 4.7.

Table 4. 5 Ultimate analysis of coffee husk fuel [30]

Carbon (%)	Hydrogen (%)	Nitrogen (%)	Sulfur (%)	Oxygen (%)
46.8314	4.8132	0.4454	0.0500	47.86

The ultimate analysis value presented above is in mass basis and it is necessary to convert it into molar basis to do the further calculation needed to determine the quantity of combustion air. To get the molar value of each element you can divide by the molecular weight of each element. As it is seen in the below table, the values then divided by the atomic number of carbons to normalize the molecule. So, for every carbon, you have 1.2 atoms of hydrogen, 0.68 atoms of oxygen. The percentage of nitrogen and sulfur is very small to include it in the calculation.

Where MW is molecular weight of the element

$$CH_{1.2}O_{0.8} + X(O_2 + 3.76N_2) \rightarrow aCO_2 + bH_2O + cO_2 + dN_2$$

Assuming complete combustion of coffee husk, the theoretical air requirement is calculated to be 6.19 kmol of air per 1 kmol of fuel, based on elemental balancing of reactants and products. A molecular weight of 28.96 g/mol is assumed for air. It is important to note that this calculation aims to determine the ideal stoichiometric air requirement and does not imply

that complete combustion occurs under stoichiometric conditions. The stoichiometric air value will be used to define excess air levels, which are then applied in the simulation cases. The actual combustion performance and results will be presented and discussed in the Results and Discussion section.

The actual fuel mass flow rate is calculated using equation 4.6 substituting the heat load calculated, the conversion efficiency assumed and the LHV of coffee husk

$$M_f = \frac{50\text{kW}}{0.6 * 18900\text{kJ/kg}}$$

$M_f = 0.0044\text{kg/s}$ = 15.8 kg/hr

The stoichiometric air flow requirement for the given mass flow rate of the fuel is calculated based on the values obtained from the balanced chemical equation. As previously stated, one kmol of coffee husk fuel requires 6.19 kmol of air. Using this ratio, the stoichiometric air requirement for 15.8 kg of fuel is calculated to be 108.2 kg of air. The corresponding values are summarized in Table 4.7.

Table 4. 6 Summary of the combustion parameters

Combustion Parameter	Values
Fuel flow rate (kg/hr)	15.84
Air flow rate (kg/hr)	108.2
Air fuel ratio (kg of air/kg of fuel	6.86

4.3.2 Geometric sizing of the combustion furnace

From the different types of furnaces discussed in Section 2.4, the grate-type furnace is selected for this application. Using a grate-fired furnace in a rural area is an excellent choice for utilizing coffee husk as a primary fuel. Coffee husks, which are widely available in coffee producing regions in Ethiopia , are fibrous, irregular in shape, and moderately moist making them ideal for grate combustion without the need for extensive fuel preparation like drying, grinding, or pelletizing. In comparison, fluidized bed and pulverized fuel systems require

more uniform, finely sized, and often pre-treated fuels, which can be costly and technically demanding, especially in rural settings. Grate furnaces, on the other hand, offer a mechanically simple and robust design that is easier to operate and maintain with minimal technical expertise. This makes them particularly well-suited for decentralized energy production where low operational complexity and high reliability are essential. Moreover, grate systems can also accommodate other locally available biomass fuels such as wood chips, crop residues, and sawdust, providing flexibility and resilience in fuel supply.

For efficient heat release during combustion, a minimum grate area and combustion volume are necessary. This is directly linked to the residence time required to fully burn the fuel. The grate area and furnace volume must be properly matched to achieve the desired furnace output. If the furnace volume is too small compared to the grate area, combustion won't be completed inside the furnace, and the heat transfer surfaces may get damaged by flames. On the other hand, if the grate area is too small, it won't be possible to reach the rated heat release. Each fuel type has a specific heat release rate, which can be expressed based on either the furnace volume or the cross-sectional area. The volumetric heat release rate refers to the heat produced per unit effective furnace volume, while the area heat release rate is the heat produced per unit effective grate area. These two rates help determine the proper furnace volume and grate area [61].

Volumetric heat release [62]

$$q_v = \frac{M_f * LHV}{V} \quad 4.12$$

Area heat release rate is used to determine the furnace cross sectional area.

$$q_F = \frac{M_f * LHV}{A_{grate}} \quad 4.13$$

where

V is the volume of the furnace

q_v is volumetric heat release rate

A_{grate} is area of the grate

q_F is the area heat release rate

Generally, the volumetric heat release rate for biomass fuel is between 0.1 to 0.12 MW/m^3 and area heat release rate for inclined grate furnace is 970 kw/m^2. Additionally, different volumetric and area heat release are calculated and presented in Table 4.8 to use as a reference for the sizing of the combustion furnace.

Table 4. 7 Reference furnace capacity, heat release rate and dimensional data

Furnace capacity	Dimension (m)	Volume heat release rate (Mw/m^3)	Area heat release rate (Mw/m^2)	Length/Width Ratio	Reference
50 MW	12.15 X 6.52 X 5.8	0.11	1.32	1.12	[63]
31 MW	12 X 9 X 5	0.06	0.67	1.8	[63]
550 MW	17.82 X 98.84 X 17.82	0.02	0.31	5.5	[35]

Taking the smallest value to follow the conservative approach for volume heat release rate and by taking in to account the length to width ratio of the above-mentioned furnaces, the geometric dimension determined iteratively as given below.

Taking the smallest value to follow the conservative approach

q_v =0.1 MW/m^3

V=$\frac{4.4*18.9}{0.1X10\text{^}3}$= 0.83$m^3$

This is the smallest volume required to get necessary resident time to combust the fuel.

Area heat release rate is used to determine the furnace cross sectional area.

$q_F = \frac{Mf * LHV}{A\ grate}$

The area is calculated with area heat release rate as stated in one of the furnaces in table 4.8 which is 310 kW/m^2

$A_{grate} = \frac{4.4 * 18.9}{310} = 0.3$ m2

Increasing the grate area slightly beyond calculated values is a practical decision to enhance combustion stability and accommodate variability in fuel properties such as moisture and density. This extra space helps prevent overloading, reduces the risk of incomplete combustion, and provides greater operational flexibility, which is especially important in rural settings with limited technical support. In this work the grate area is increase by 130% to ensure more reliable and efficient combustion without significantly increasing costs. This also allow as to get a geometrically compatible size with downstream components like dryer.

$A_{grate} = 0.7$ m^2

$H = \frac{0.83}{0.7} = 1.2$ m

By taking length to width ratio 1.2 which is taken from one already found furnaces in practice as presented in Table 4.8 the length and width are approximated to 1.02m and 0.85 m. The sizing of the furnace and heat release rate calculated based on the load of the furnace are summarized on Table 4.9. Both the volumetric and area heat release calculated below the values found in table 4.8 and optimization can be done after the simulation result in the future work.

Table 4. 8 Furnace dimension and heat release rate values

Furnace parameters	
Dimension	1.2m x 1.02m x 0.85m
Volume	1.04 m3
Grate area	0.86 m2
Volumetric heat release rate	48 kw/m3
Area heat release rate	56.7 kw/ m2

The geometric representation of the furnace is as it is seen in the below figure 4.3 and figure 4.4.

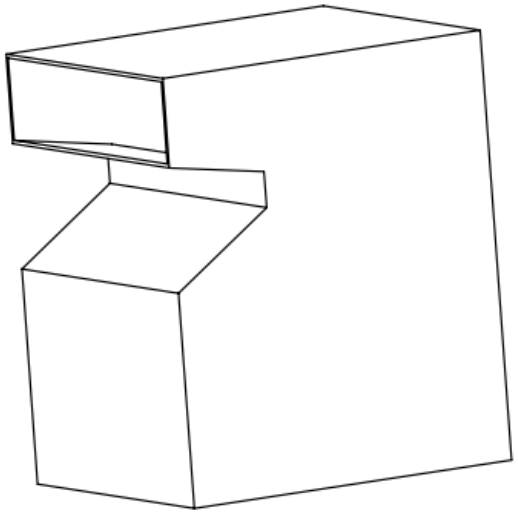

Figure 4. 3 Geometric 3D representation of the furnace

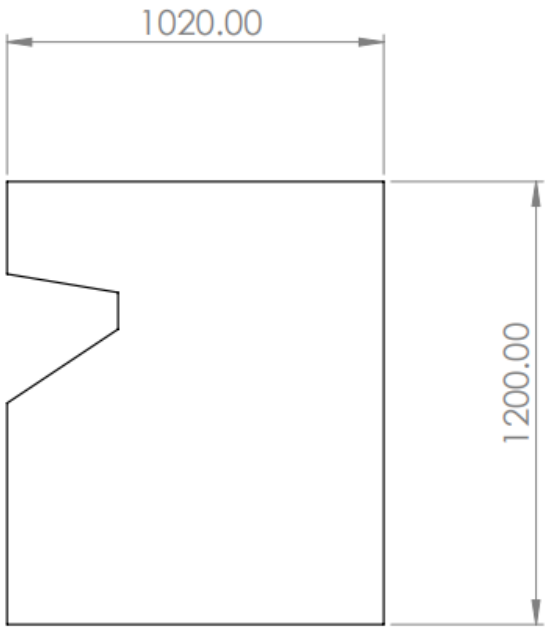

Figure 4. 4 Geometric 2D representation of the furnace

Chapter Five

Result and Discussion

This chapter presents the results obtained from the CFD simulation of coffee husk biomass combustion in small scale furnace. The combustion analysis was conducted in Five main stages to systematically evaluate the performance and behavior of the process. First, a mesh independence test was carried out using different mesh densities to ensure that the simulation results were not influenced by grid resolution. Based on this analysis, an optimal mesh was selected for all subsequent simulations. Before main numerical analysis was started mesh quality was checked to avoid any error that can come with that. Next, the impact of varying excess air levels on the combustion characteristics was investigated, focusing on temperature distribution, CO2 and CO mass fraction. Simulations were then conducted to assess the influence of secondary air injection at various positions within the combustion chamber, aiming to enhance mixing and improve overall combustion performance. Finally, the results were validated using experimental data from rice husk combustion.

5.1. Meshing and Mesh Independent Test

The simulation of the coffee husk was conducted on ANSYS Fluent software based on following standard CFD techniques.

Mesh Independent test

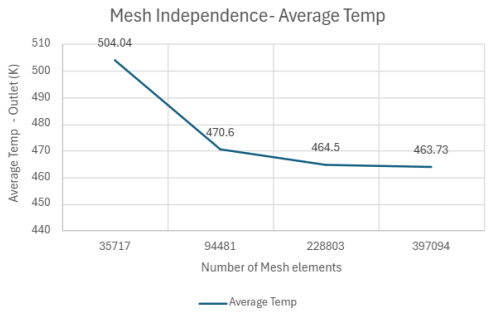

(A)

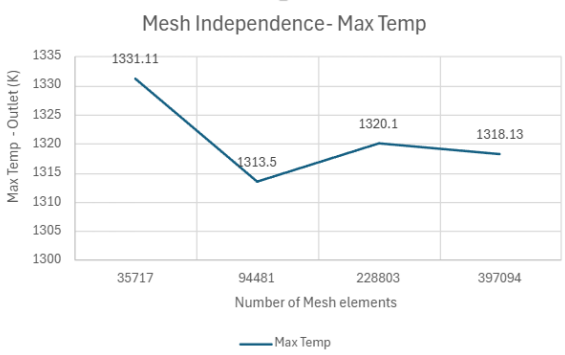

(B)

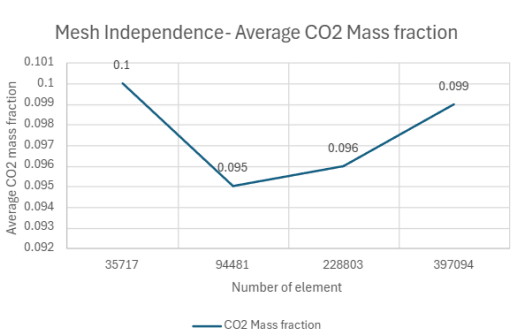

(C)

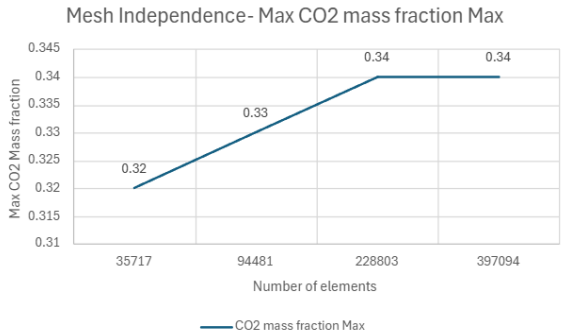

(D)

Figure 5. 1 mesh independent test results (A) Number of elements versus outlet average temperature (B) Number of elements versus outlet maximum temperature (C) Number of elements versus outlet average CO2 mass fraction (D) Number of elements versus outlet maximum

As presented in the above graphs and table below, simulations were conducted using element sizes of 5 mm, 3 mm, 2 mm, and 1.5 mm. Each element size corresponds to a total mesh element count of 35,717; 94,481; 228,803; and 397,094, respectively. A noticeable reduction in the percentage change is observed as the mesh size decreases. Based on this analysis, a mesh size of 2 mm—corresponding to 228,803 elements—was selected for all subsequent simulations.

Table 5. 1 Mesh independent test for average and maximum temperature at the outlet

	Element size	Number of elements	Average Temperature(K)	Percentage reduction (%)	Max Temperature	Percentage reduction (%)
1	5mm	35717	504.1	-	1331.11	-
2	3mm	94481	470.6	6.6	1313.5	1.3
3	2mm	228803	464.5	1.3	1320.1	-0.5
4	1.5mm	397094	463.7	0.2	1318.13	0.1

Table 5. 2 Mesh independent test for average and maximum CO2 mass fraction at the outlet

	Element size	Number of element	Average CO2 mass fraction	Percentage reduction (%)	Max CO2 mass fraction	Percentage reduction (%)
1	5mm	35717	0.1		0.32	
2	3mm	94481	0.095	5	0.33	3.1
3	2mm	228803	0.096	3.1	0.34	3
4	1.5mm	397094	0.099	1.1	0.34	0

Mesh Quality test

After mesh independence study performed, it is essential to evaluate the quality of the generated mesh to ensure numerical stability and solution accuracy. Poor mesh quality can lead to convergence issues, numerical diffusion, or inaccurate representation of gradients, especially in regions with high velocity or temperature variations. In this section, mesh quality is assessed using key parameters such as skewness, orthogonally, and aspect ratio for selected mesh to run the combustion simulation. These metrics were extracted from the mesh quality result of fluent meshing.

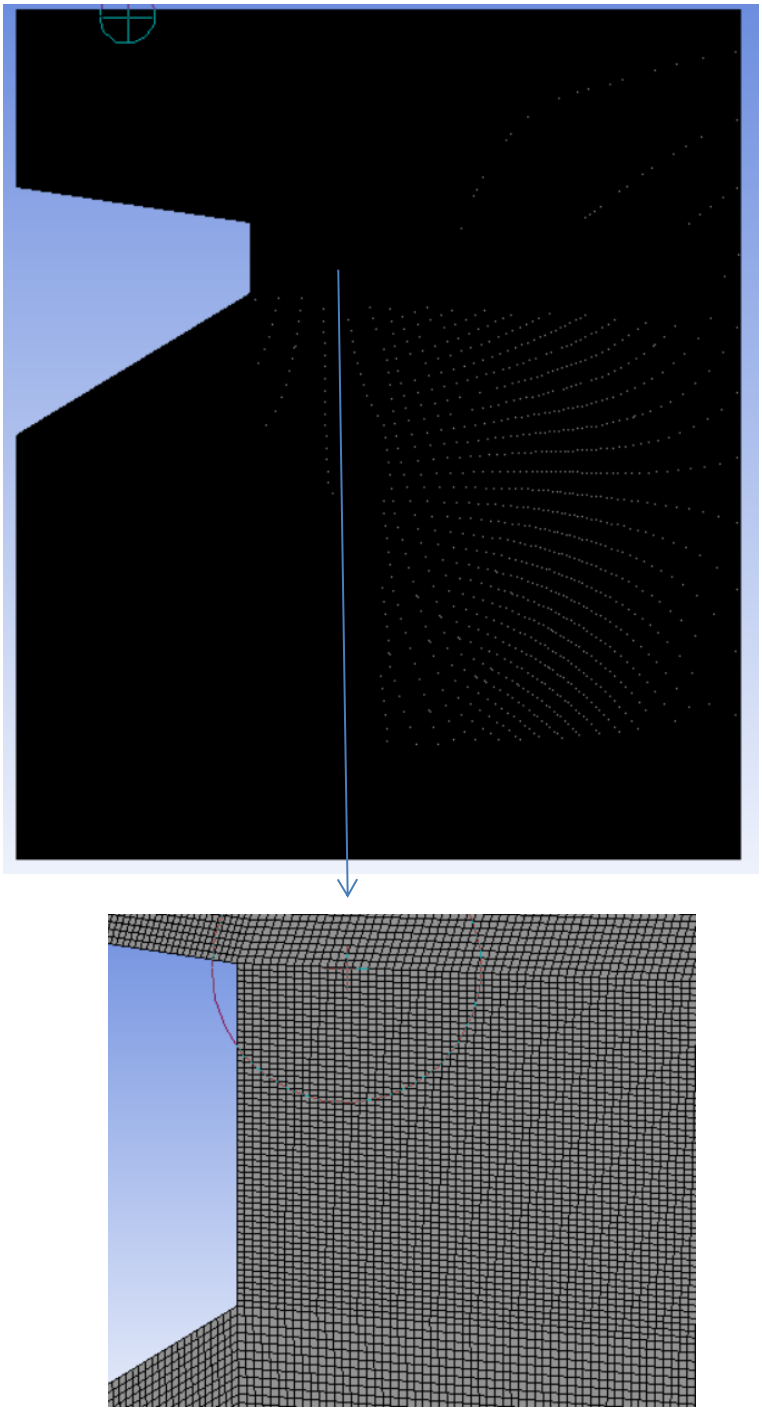

Figure 5. 2 Mesh profile of the combustion furnace

Skewness

Skewness measures how much a cell deviates from the ideal shape (such as a square in 2D or a cube in 3D). For a perfect square or cube, skewness is expected to be zero. High skewness means the cell is distorted, which can degrade solution accuracy and convergence.

Skewness is calculated differently depending on the solver, but one common method is:

$$\text{Skewness} = \frac{\theta_{\max} - \theta_{\text{ideal}}}{180^0 - \theta_{\text{ideal}}}, \frac{\theta_{\min} - \theta_{\text{ideal}}}{180^0 - \theta_{\text{ideal}}}$$

Table 5. 3 Skewness quality guideline for fluent [64]

	Skewness	Quality category
1	< 0.25	Excellent
2	0.25 – 0.5	Very good
3	0.5 – 0.8	Good
4	0.8 – 0.94	Acceptable
5	0.94 – 0.97	Bad
6	0.97 - 1	unacceptable

The minimum skewness calculated is 6.1e-6, which is almost zero. The maximum value is 0.4, which falls into the 'very good' category, and the average value is 8.3e-2, indicating that the overall skewness is in the 'excellent' range. The standard deviation of the skewness is 8.2e-2, suggesting a consistently high-quality mesh.

Table 5. 4 Skewness value for 2D mesh surface

		Skewness	Category
1	Min	6.1 e-6	Excellent
2	Max	0.4	Very Good
3	Average	8.3 e-2	Excellent
4	Standard deviation	8.9 e-2	N/A

The colored display for skewness mesh quality of the surface is presented below. Because of the finer nature of the mesh the display is presented for outlet and inlet section to show them as representative.

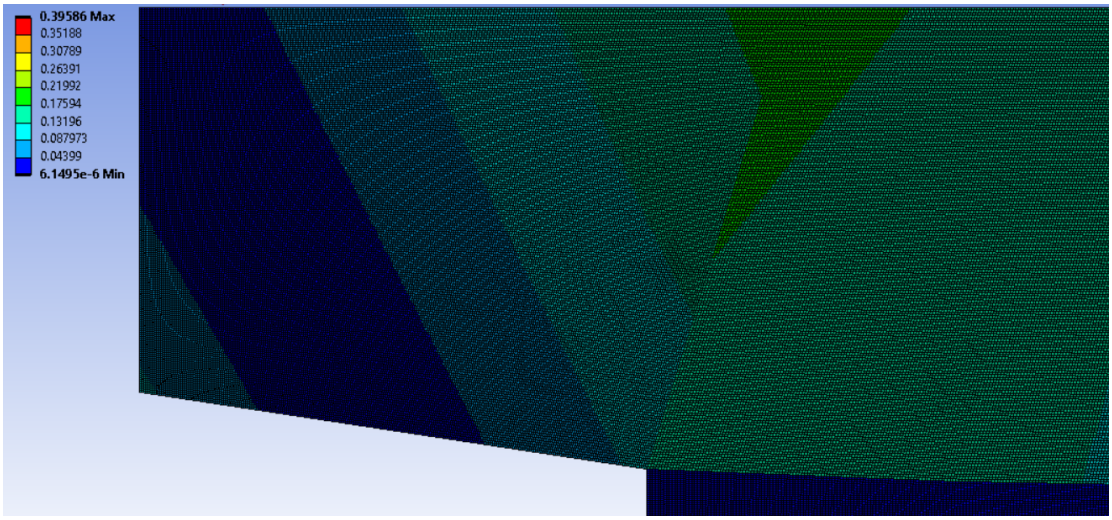

(A)

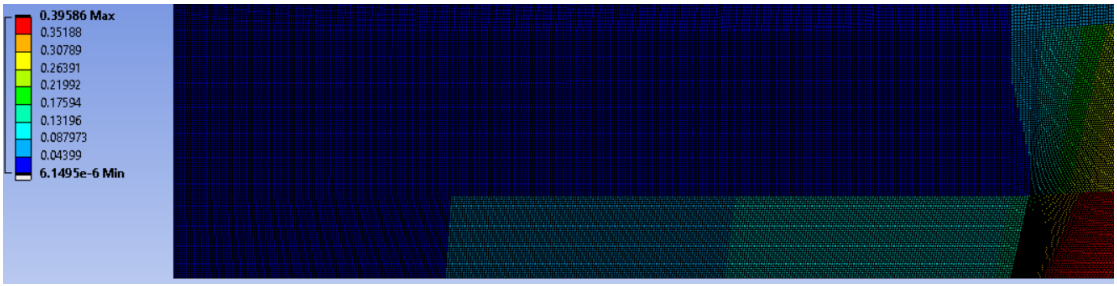

(B)

Figure 5. 3 Skewness graphic display of meshed surface (A) outlet area (B) Inlet area

Orthogonal quality

Orthogonal quality measures the angle between the face normal and the line connecting adjacent cell centers. High orthogonally means the flow direction aligns well with mesh elements. Ideally, face normal are perpendicular to the line connecting cell centers. Poor orthogonally affects the accuracy of gradient and flux calculations.

Orthogonal quality = $\cos(\theta)$ where θ is the angle between face normal and the vector between cell centers

Table 5. 5 Orthogonal quality guideline for fluent [64]

	Orthogonal quality	Quality category
1	0.95 - 1	Excellent
2	0.7 – 0.95	Very good
3	0.2 – 0.7	Good
4	0.15 -0.2	Acceptable
5	0.001 – 0.15	Bad
6	0 – 0.001	Unacceptable

The minimum orthogonal quality calculated is 0.81, which falls within the very good range. The maximum value is 1, which is the ideal for orthogonal quality. The average value is 0.98, placing most of the mesh in the excellent category. The standard deviation is 3.2e-2, indicating that the orthogonal quality is consistently high across the mesh.

Table 5. 6 Orthogonal quality value for 2D mesh surface

		Orthogonal value	Category
1	Min	0.81	Acceptable
2	Max	1	Excellent
3	Average	0.98	Excellent
4	Standard deviation	8.9 e-2	N/A

The colored display for orthogonal mesh quality of the surface is presented below. Because of the finer nature of the mesh the display is presented for outlet and inlet section to show them as representative.

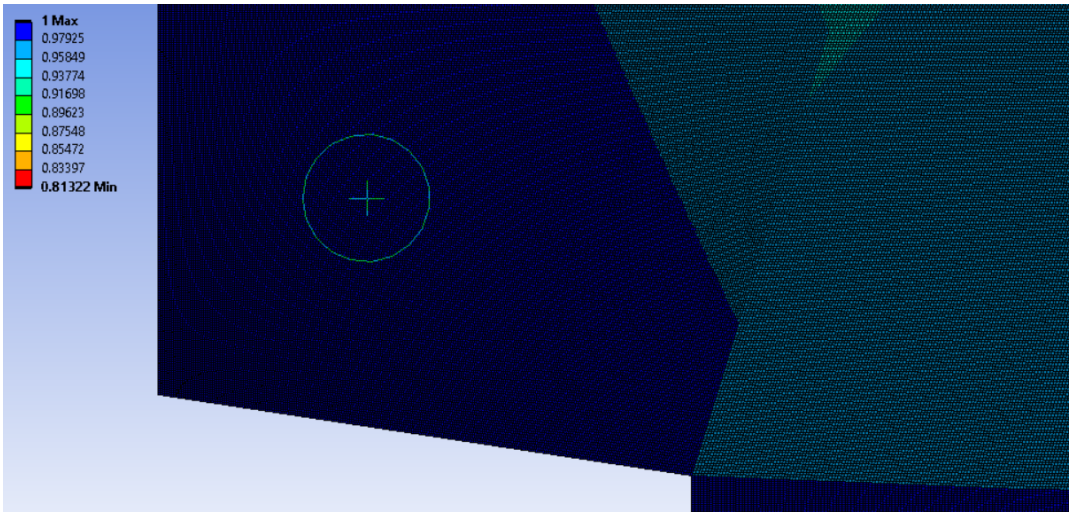

(A)

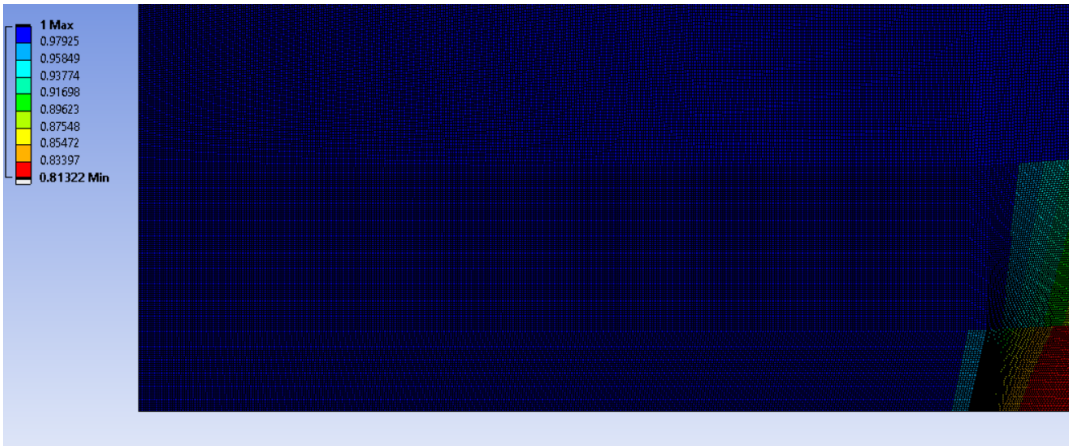

(B)

Figure 5. 4 Orthogonal quality graphic display of meshed surface (A) outlet area (B) Inlet area

Aspect ratio

Aspect ratio is the ratio of the longest edge length to the shortest edge length of a cell (in 2D or 3D). Ideal value is **1** (e.g., square or cube).

$$\text{Aspect ratio} = \frac{\text{Longest edge}}{\text{shortest edge}}$$

Table 5. 7 Aspect ratio quality guideline for fluent [64]

	Aspect ratio	Quality category
1	<3	Excellent
2	3-10	Acceptable
3	>10	Poor

The minimum aspect ratio calculated is 1, which is considered the ideal value. The maximum value is 7.1, which falls within the acceptable range. The average value is 1.2, placing most of the mesh in the excellent category. The standard deviation is 0.3, indicating that the aspect ratio is consistently good across most regions.

Table 5. 8 Aspect ratio value for 2D mesh surface

		Aspect ratio	Category
1	Min	1	Ideal
2	Max	7.1	Acceptable
3	Average	1.2	Excellent
4	Standard deviation	0.3	N/A

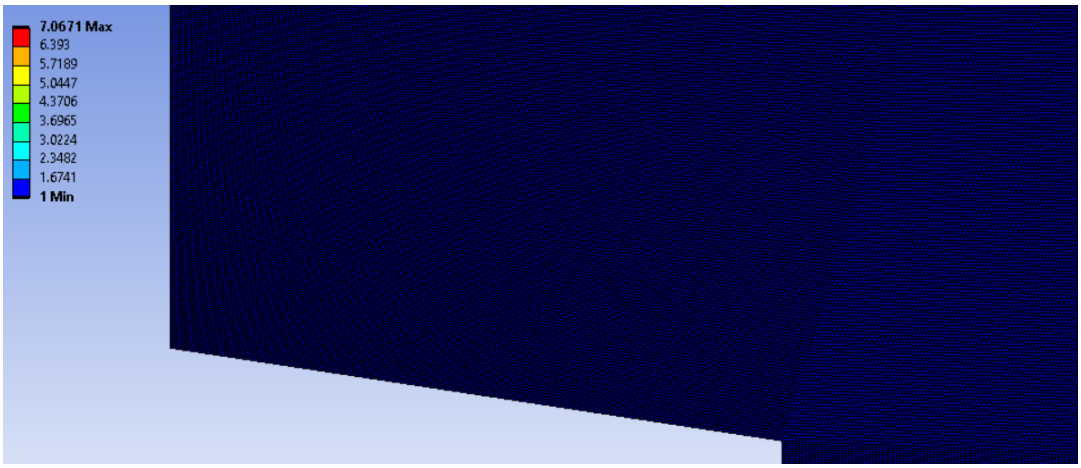

(A)

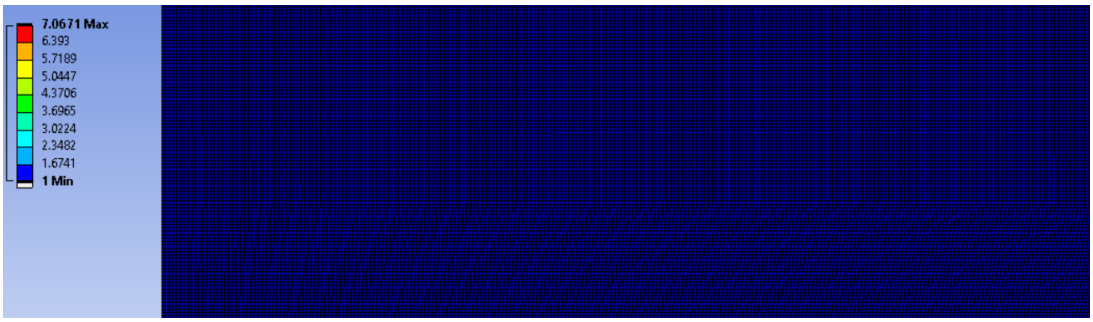

(B)

Figure 5. 5 Aspect ratio graphic display of meshed surface (A) outlet area (B) Inlet area

This simulation, conducted using ANSYS Fluent, focuses on the gas-phase combustion of a fuel mixture containing methane (CH_4), hydrogen (H_2), and carbon monoxide (CO). The residual plot displayed in Figure 5.6 A illustrates the convergence behavior of key equations including continuity, energy, and species transport. The energy residual shows excellent convergence, reaching values below 10^{-6}, indicating stable temperature prediction. The CH_4 and CO_2 species also converge well, with residuals dropping below 10^{-6}. H_2 and CO exhibit slightly slower convergence, stabilizing around 10^{-4} and 10^{-5}, respectively, after initial oscillations. The continuity residual remains higher than the others, settling near 10^{-3} with minor fluctuations, suggesting that while the simulation is generally stable. Overall, the

residual trends confirm that the simulation achieved a sufficiently accurate solution for combustion analysis and post-processing.

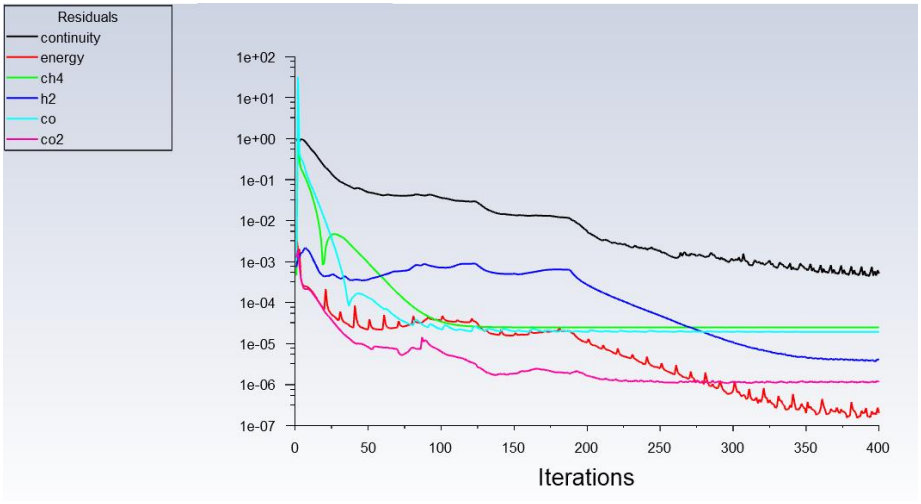

(A)

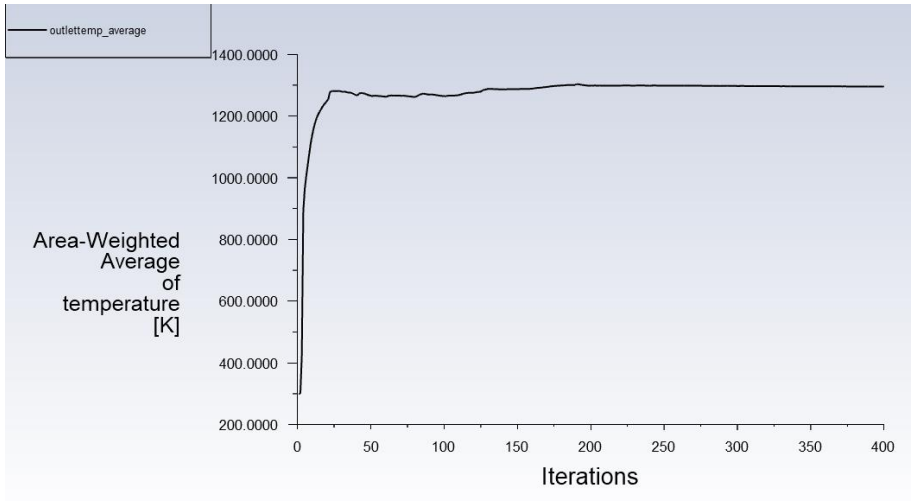

(B)

Figure 5. 6 Convergence graph (A) governing equations and gases (B) temperature

5.2 Ideal combustion analysis and Adiabatic flame temperature

The fuel mass flow rate used in the stochiometric calculation is derived based on the 50kW load on the furnace with 60% conversion efficiency discussed in chapter 4 and the value is presented in Table 4.4.

$$M_f = \frac{\dot{Q}}{\eta_o LHV} \quad 5.1$$

$$M_f = \frac{50kW}{0.6 * 18900kJ/kg}$$

$M_f = 0.0044kg/s$ = 15.8 kg/hr

The percentage of the volatile matter, char and percentage of moisture including the gases released from the pyrolysis are used in generating the mass of each gas used in the combustion process and presented in the below Table 5.9. It is also presented in Appendix I as input for the simulation.

Table 5. 9 Gaseous composition coffee husk fuel

	Gaseous fuels	Mass of gases(kg)
1	H_2	2.65
2	CO	3.65
3	CH_4	4.43
4	CO_2	1.66
5	H_2O	1.20

Mole fraction calculation for each gas

H_2 2.65/2 = 1.31

CO 3.65/28 = 0.13

CO_2 4.43/44 = 0.1

CH_4 1.66/16 = 0.1

H_2O 1.2/18 = 0.07

$$0.1CH_4 + 1.31H_2 + 0.1CO + 0.1CO_2 + 0.07H_2O + X(O_2 + 3.76N_2) \rightarrow aCO_2 + bH_2O + cN_2$$

For balanced chemical equation for complete combustion the unknown values are calculated

C : 0.1 + 0.13 + 0.1 = a → a = 0.33

H : (4 x 0.1) + (1.31 x 2) + (2 x 0.07) = 2 x b → b = 3.16

O : 0.13 + (2 x 0.1) + 0.07 + (2 x X) = (2a+b) → X = 1.91

N : (X x 3.76) = c → c = 7.18

The unknown values x, a, b and c are calculated by balancing the reactant and product side by assuming complete combustion of the fuels. As we see it in the product side there is no CO and H2 and all the gases are completely combusted to CO_2 and H_2O.

The adiabatic flame temperature of the steady flow combustion process is determined by setting there is no heat flow to the outside of the system and no work done

$$\sum N_p \left(\overline{h_f^0} + \bar{h} - \overline{h^0} \right)_p = \sum N_r \left(\overline{h_f^0} + \bar{h} - \overline{h^0} \right)_r \qquad 5.2$$

The reactants are at the reference state, the equation can be reduced to

$$\sum N_p \left(\overline{h_f^0} + \bar{h} + \overline{h^0} \right)_p = \sum N_r \left(\overline{h_f^0} \right)_r \qquad 5.3$$

$\bar{h} - \overline{h^0}$ is the sensible enthalpy relative to the standard reference state

$\bar{h}$ is the sensible enthalpy at the specified state

$\overline{h^0}$ is the sensible enthalpy at the standard reference state of 25 ^{0}c and 1 atm

Table 5. 10 Enthalpy of gaseous components

Substance	$\overline{h_f^0}$ (kJ/kmol)	$\bar{h}_{298}$ (kJ/kmol)
CH_4	-74850	
H_2	-	8468
CO	-110530	8669
CO_2	-393520	9364
H_2O	-241820	9904
O_2	-	8682
N_2	-	8669

Substituting in the above equation gives

[0.33kmol(-393520 + $\bar{h}_{CO2}$ - 9364) kJ/mol] + [3.16kmol(-241820 + $\bar{h}_{H2O}$ - 9904) kJ/mol] +

[7.18kmol(0 + $\bar{h}_{CO2}$ - 8669) kJ/mol] = 0.1 kmol (- 74850 kJ/mol) + 0.13 kmol (- 110530 kJ/mol) +0.1 kmol (- 393520 kJ/mol) +0.07 kmol (- 241820 kJ/mol)

$0.33\bar{h}_{CO2}$ +3.16 $\bar{h}_{H2O}$ + 7.18 $\bar{h}_{N2}$ = 824868.03 kJ

We have one equation with three unknowns but the three unknowns that depend only in one variable which is the temperature of the product.

The first iteration can be done by dividing the total number of moles.

$= \frac{824868.03}{(0.33+3.16+7.18}$

= 77307.21 kJ/kmol

The enthalpy corresponds to 77307.21 kj/mol is 1900 k for H_2O, 1600 for CO_2 and 2350 for N_2. Noting that the majority of the moles are N_2, the temperature of the product can be estimated to 2350 k but somewhat under it.

The next iteration temperature point is taken at 2200 k

$0.33\bar{h}_{CO2}$ +3.16 $\bar{h}_{H2O}$ + 7.18 $\bar{h}_{N2}$ = 0.33(112939) +3.16 (92940) + 7.18 (72040)

The value is higher than 824868.03. Therefore, the actual temperature is slightly under 2200 K

Next iteration point chosen is 2100 K

$0.33\bar{h}_{CO2}$ +3.16 $\bar{h}_{H2O}$ + 7.18 $\bar{h}_{N2}$ = 0.33(106864) +3.16 (87735) + 7.18 (68417)

= 803741.8

The value is lower than 824868.03. Therefore, the actual temperature is slightly higher than 2100 k

Next chosen point is 2150 K

$0.33\bar{h}_{CO2}$ +3.16 $\bar{h}_{H2O}$ + 7.18 $\bar{h}_{N2}$ = 0.33(109898) +3.16 (90330) + 7.18 (70226)

= 825931.8

The value is nearly equal to 824868.03 and the adiabatic flame temperature is approximated to 2150 k.

5.3 Effect of Excess Air on Combustion Performance

With the mesh fixed, simulations were performed at different excess air levels: stoichiometric (0%), 20%, 40%, 60%, 80% and 100 %. The aim was to evaluate how varying air-fuel ratios influence combustion behavior. Mainly, the effect of excess air on the average and maximum temperature, as well as on the average and maximum mass fractions of CO_2 and CO at the furnace outlet is investigated.

The combustion simulation is done for volatile gas released from the solid coffee husk and for the gas releases from char combustion. It based on the assumption that drying and volatile gas release completed in the first half of the furnace and the char combustion release in the second half of the furnace. The percentage of gas's released are derived based on the article on the pyrolysis of coffee husk. The comparison was on the ultimate and proximity of the coffee used in the simulation, which coffee husk from Ethiopian coffee and the paper used for the reference.

It is reasonable to use the reference study values due to the small percentage differences observed in the main components of the proximate and ultimate analyses, as shown in the tables below. The differences in moisture content and char are only 3.4% and 2.9%, respectively. The percentage difference in volatile gases is 7%, which is acceptable for this type of comparison. Although the ash content shows a larger difference of 36.8%, its impact is minimal because ash is not included in the combustion simulation. Additionally, the ash content is relatively low in both fuel samples, so its effect can be neglected.

Table 5. 11 Comparison between sample Ethiopian coffee husk and reference coffee husk – Proximity analysis

		Reference Coffee husk[32]	Ethiopian Coffee husk[7]	Percentage difference (%)
Proximity analysis	Moisture (%)	8.2	7.92	3.4
	Ash (%)	5.6	3.54	36.8
	Volatile matter (%)	77	71.63	7.0
	Fixed Carbon (%)	17.4	16.9	2.9

Table 5. 12 Comparison between sample Ethiopian coffee husk and reference coffee husk – Ultimate analysis

	Element	Reference Coffee husk[32]	Ethiopian Coffee husk[7]	Percentage difference (%)
Ultimate analysis	C (%)	47.3	46.83	1.0
	H (%)	6.4	4.81	24.8
	N (%)	2.7	0.45	83.3
	S (%)	0.3	0.05	83.3
	O (%)	37.7	47.86	-26.9

Similarly, the ultimate analysis shows small percentage differences between the two samples. The difference in carbon contents—the primary element in combustion analysis—is only 1%, which supports the reliability of using the reference data. Slightly higher differences are observed in hydrogen and oxygen, at 24.8% and 26.9%, respectively. However, the impact of the hydrogen difference is minimal due to its relatively low proportion in the fuel. Although oxygen shows a higher difference, its effect is offset by the close match in carbon content. The differences in nitrogen and sulfur can be neglected as their concentrations are low and their influence on the combustion process is insignificant.

Table 5. 13 Volatile gas composition for the reference fuel [32]

	Volatile gases	Percentage (%)
1	H_2	27
2	CO	24.01
3	CH_4	11.66
4	CO_2	32.12
5	C_2H_4	3.68
6	C_2H_6	1.53

Considering their small percentages and to simplify the simulation, C_2H_4 and C_2H_6 are not included in the analysis presented in this section.

The outlet temperature, CO_2 and CO mass fraction trends are summarized in Figure 5.7 and Figure 5.8. Figure 5.7 show the average values and Figure 5.8 show maximum values at the outlet. These results suggest that 60% excess air provides a higher temperature at the outlet with nearly zero CO mass fraction.

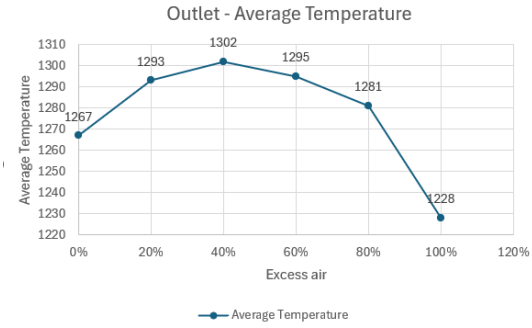

A

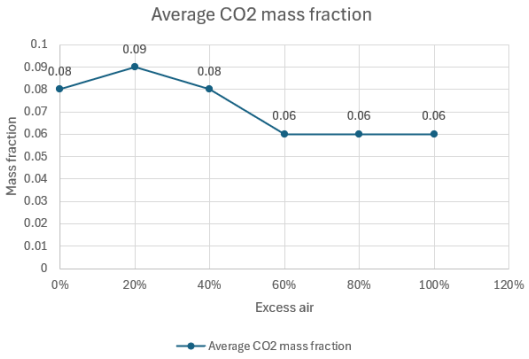

B

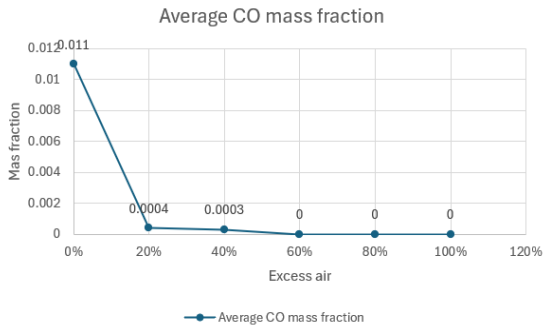

C

Figure 5. 7 Excess air versus temperature, CO2 and CO mass fraction- (A) Average Temperature (B) Maximum temperature (B)Average CO_2 (C)Average CO

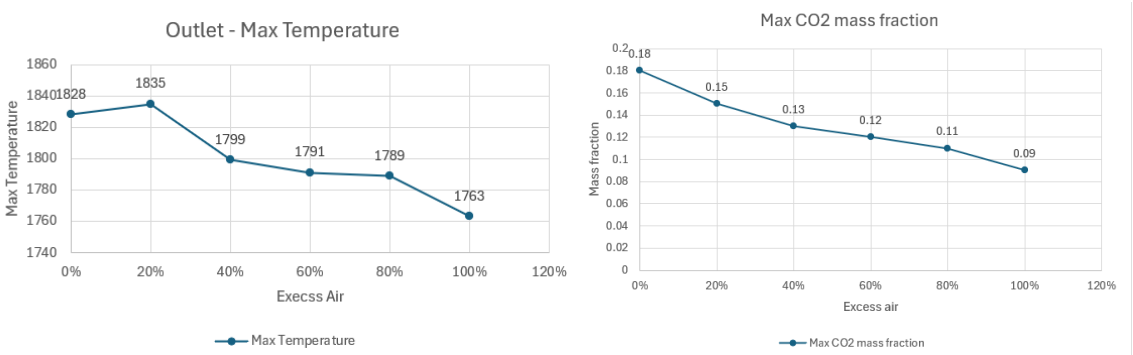

A B

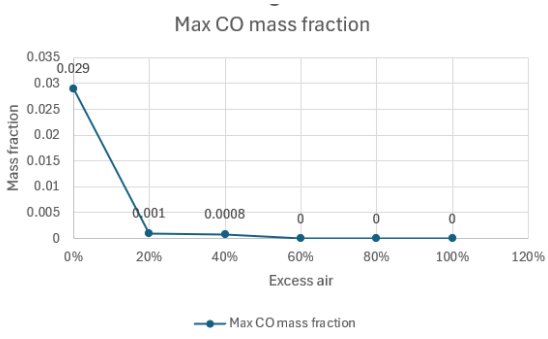

C

Figure 5. 8 Excess air versus temperature, CO2 and CO mass fraction- (A) Maximum temperature (B) Maximum CO_2 (C) Maximum CO

Temperature profiles, CO2 and CO mass fraction profile is presented for 60% excess air. The profile for the other excess air studies are presented at Appendix for reference.

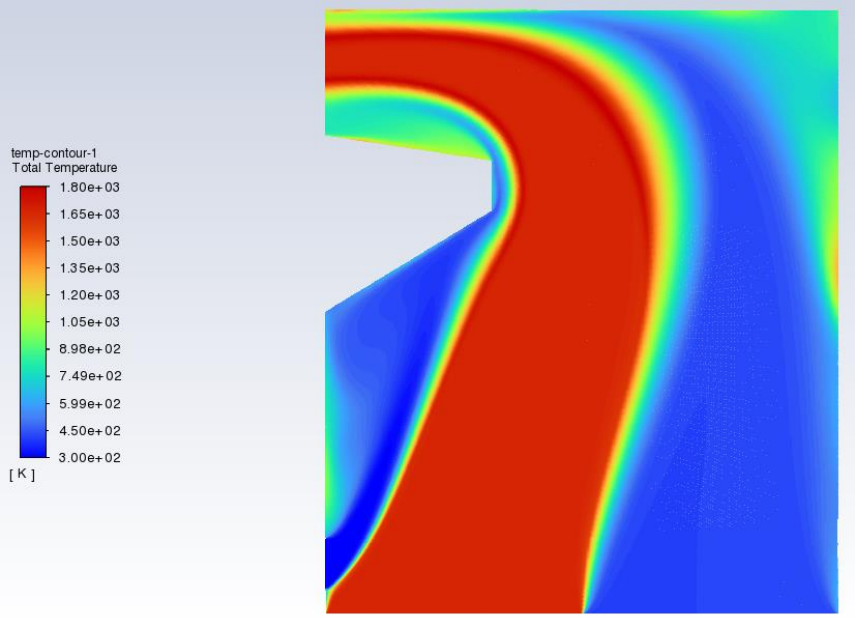

Figure 5. 9 Temperature profile for 60 % excess air

The simulation result showed in Figure 5.8 presents the total temperature distribution within a flow domain, involving gas phase combustion of the fuel. The contour plot, obtained from ANSYS Fluent, indicates a significant temperature rise in, reaching up to 1800 K, suggesting the presence of a combustion zone inside the furnace. As the flow moves through the curved region, a sharp temperature gradient forms, indicating rapid heat addition and possibly recirculation that enhances mixing and combustion. The result highlights the thermal behavior of the system, with the hottest region concentrated near the first half of the furnace where combustion of devolatilized gases occurred.

The simulation result shown in Figure 5.8 presents the total temperature distribution within the flow domain, involving gas-phase combustion of the fuel. The contour plot, obtained from ANSYS Fluent, indicates a significant temperature rise, reaching up to 1800 K, which suggests the presence of a combustion zone inside the furnace. As the flow moves through the curved region, a sharp temperature gradient develops, indicating rapid heat addition due to further combustion of unburned gases. The result highlights the system's behavior, with

the hottest region concentrated in the first half of the furnace, where the combustion of devolatilized gases occurs.

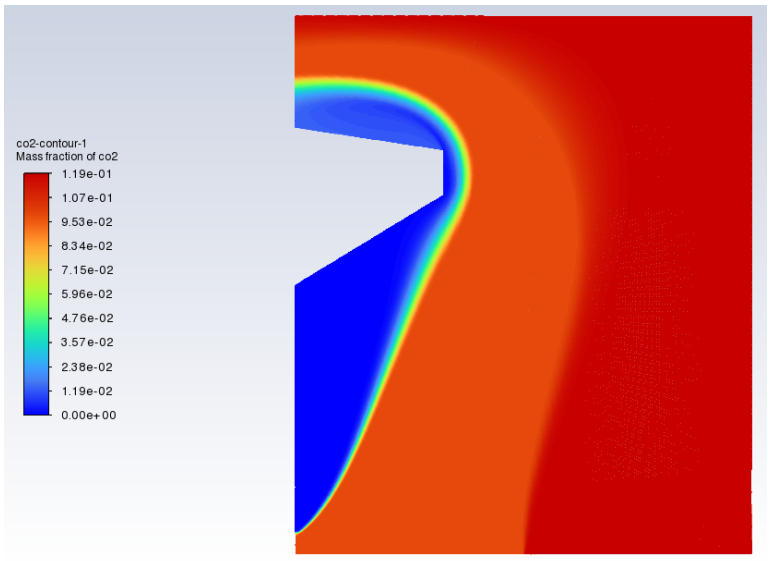

Figure 5. 10 CO2 mass fraction profile for 60 % excess air

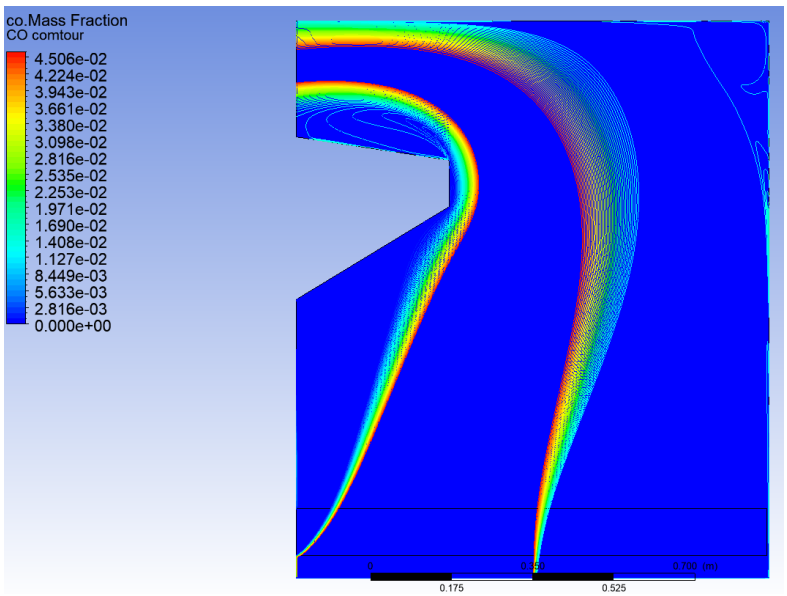

Figure 5. 11 CO mass fraction profile for 60 % excess air

5.4 Influence of Secondary Air Injection Position

To enhance mixing and complete combustion, secondary air was introduced at different positions along the combustion chamber walls. Three positions were tested: near the primary

combustion zone (Position A), opposite to the outlet (Position B), and closer to the outlet (Position C).

The reason for introducing secondary air and analyzing its effect at different positions is to ensure the combustion of any unburned fuel that may remain, even if the CO level appears sufficiently low with only primary air. In actual fuel combustion, the main products typically include CO, CO_2, and H_2O. However, a near-zero mass fraction of CO does not always guarantee complete combustion. Even with 60% excess air, the addition of secondary air can promote further combustion of residual fuel. In our simulation, the presence of H_2 at the outlet is observed, as shown in the figure below, which plots the mass fraction of H_2 (in ppm) against excess air. A small amount of unburned CH_4 is also detected at the outlet, although the quantity is minimal. Therefore, I believe adding secondary air and running the simulation is a reasonable approach. The results support this, as illustrated in the Figure 5.11.

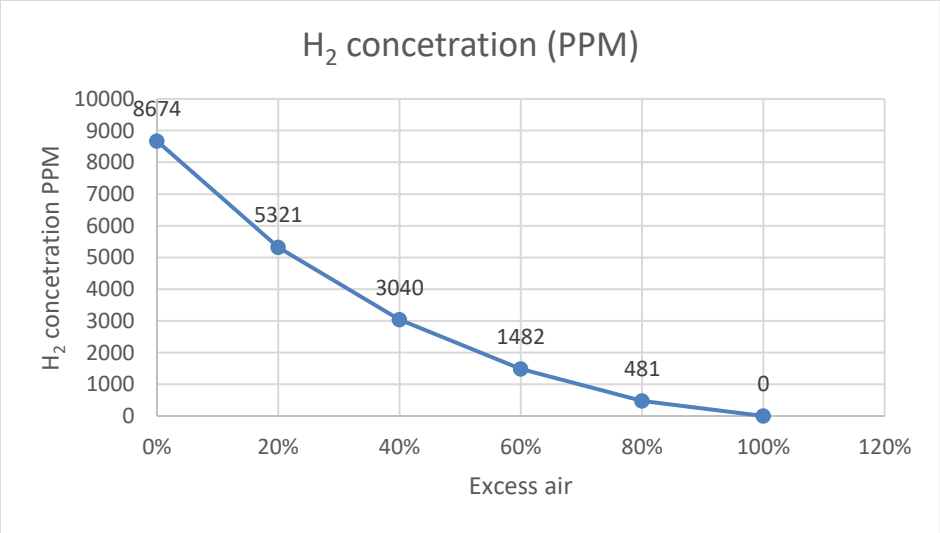

Figure 5. 12 Excess air versus H_2 concentration

In biomass combustion, the presence of molecular hydrogen (H_2) in the flue gas can be expected under certain conditions, especially in fuel-rich zones or where oxygen is locally limited. Incomplete combustion allows hydrogen released from volatiles or char to partially oxidize, resulting in detectable H_2[65]. Furthermore, during the pyrolysis phase of biomass combustion, significant amounts of H_2, CO, CH_4, and tars are produced; some of this H_2 can escape full oxidation if mixing is inadequate [26]. High temperature reactions, such as the water-gas shift and steam reforming (e.g., $C + H_2O \rightarrow CO + H_2$), can also contribute to H_2

formation[66]. Typically, increasing the excess air ratio reduces H_2 levels, as more oxygen facilitates complete combustion and promotes reactions like $H_2 + ½ O_2 \rightarrow H_2O$ and $CO + ½ O_2 \rightarrow CO_2$ [1].

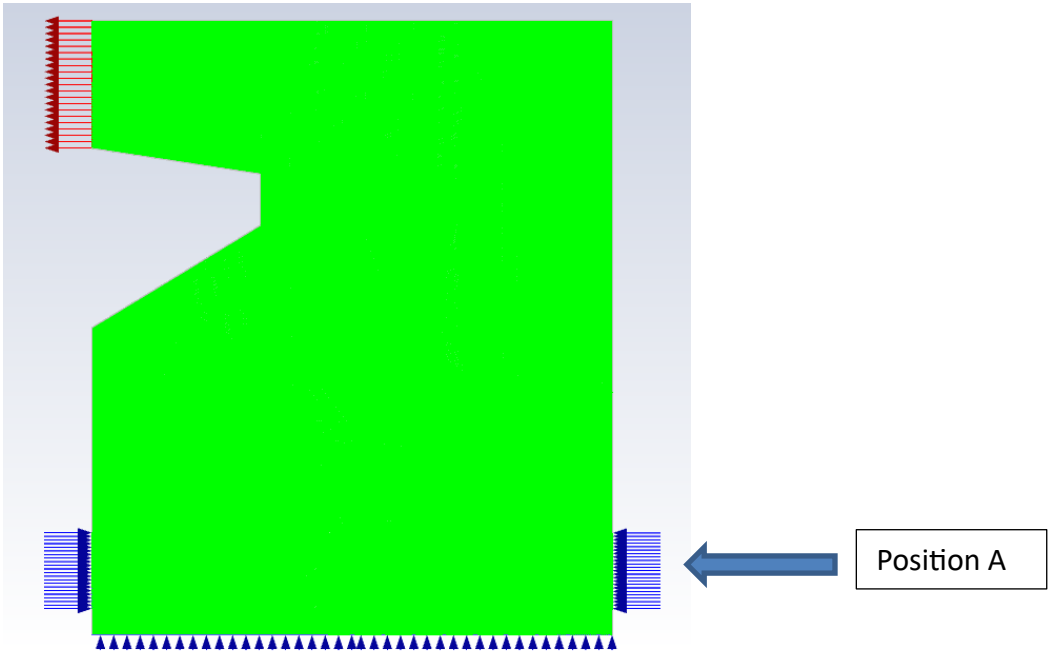

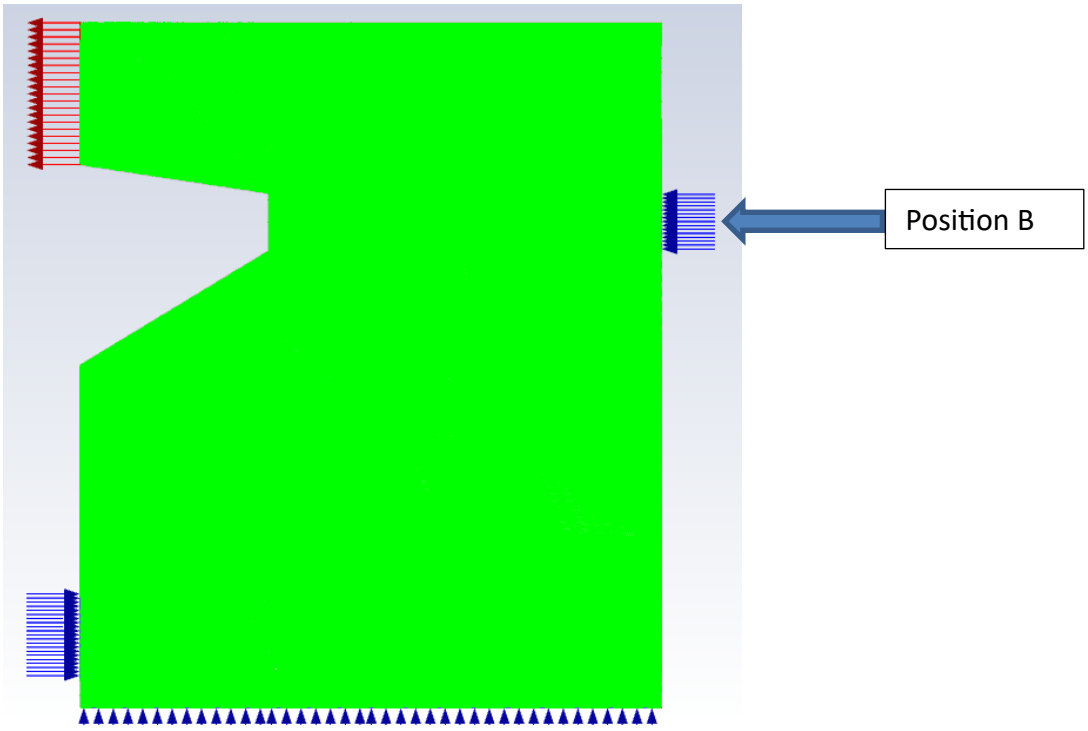

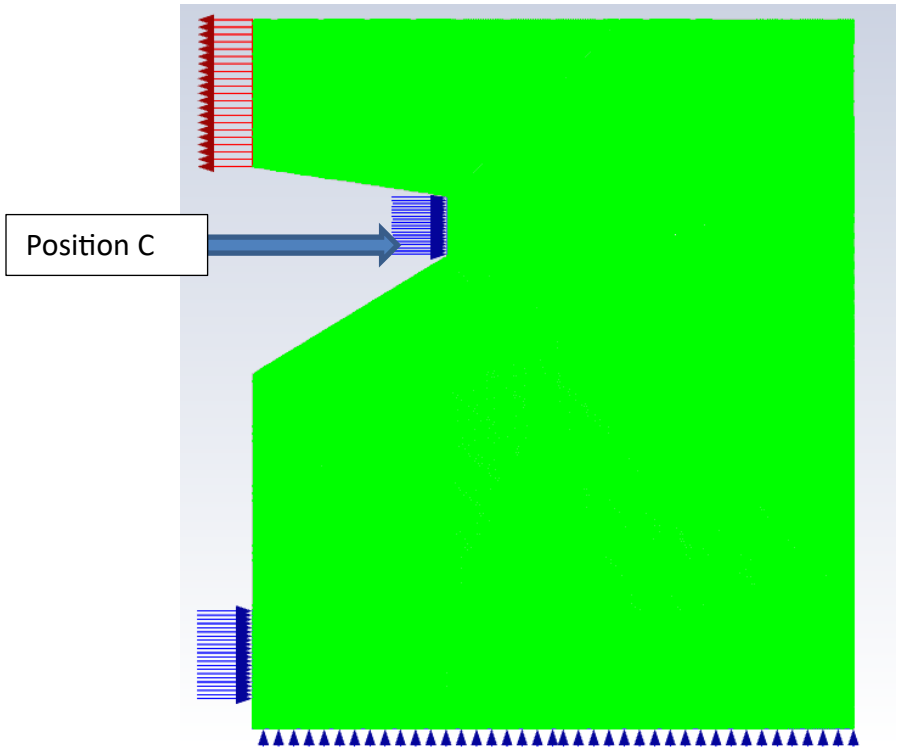

Figure 5. 13 Secondary air inlet positions

Table 5. 14 Summary of average and max value for temperature, CO2 mass fraction and CO mass fraction with 60 % excess air

	Temperature (k)		**CO2 - mass fraction**		**CO - mass fraction**	
	Average	**Max**	**Average**	**Max**	**Average**	**Max**
Secondary Air - Position A	1314	1781	0.069	0.109	~0	~0
Secondary Air - Position B	1319	1787	0.06	0.12	~0	~0
Secondary Air - Position C	1253	1785	0.06	0.16	~0	~0

A higher average and maximum outlet temperature is observed when secondary air is injected at Position B as presented in Table 5.12. No significant change is observed in the CO_2 and CO mass fractions, even when compared to the simulation without excess air, as shown in the Table 5.13. However, introducing secondary air significantly increases both the average and maximum outlet temperatures for Position A and Position B by 19 K and 24 K, respectively. In contrast, for Position C, the outlet temperature is lower than that of the case without secondary air, possibly due to a localized cooling effect caused by the proximity of the secondary air injection point to the outlet.

Table 5. 15 Average and max value for temperature, CO2 mass fraction and CO mass fraction without secondary air with 60 % excess air

	Temperature (k)		**CO2 - mass fraction**		**CO - mass fraction**	
	Average	**Max**	**Average**	**Max**	**Average**	**Max**
Without secondary air	1295	1791	0.06	0.12	0	0

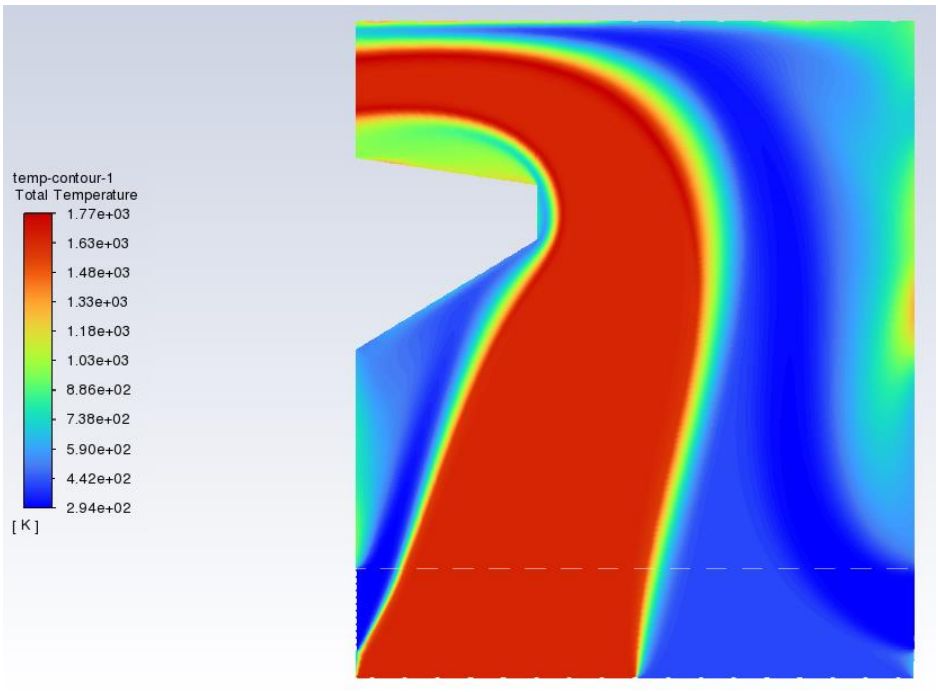

Figure 5. 14 Temperature profile for the secondary air combustion - Position A

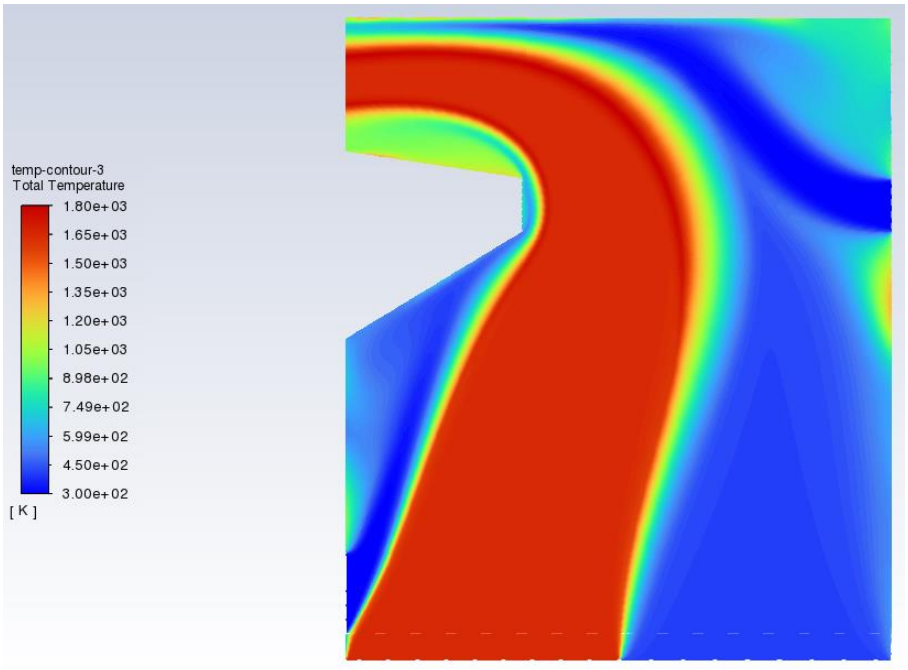

Figure 5. 15 Temperature profile for the secondary air combustion - Position B

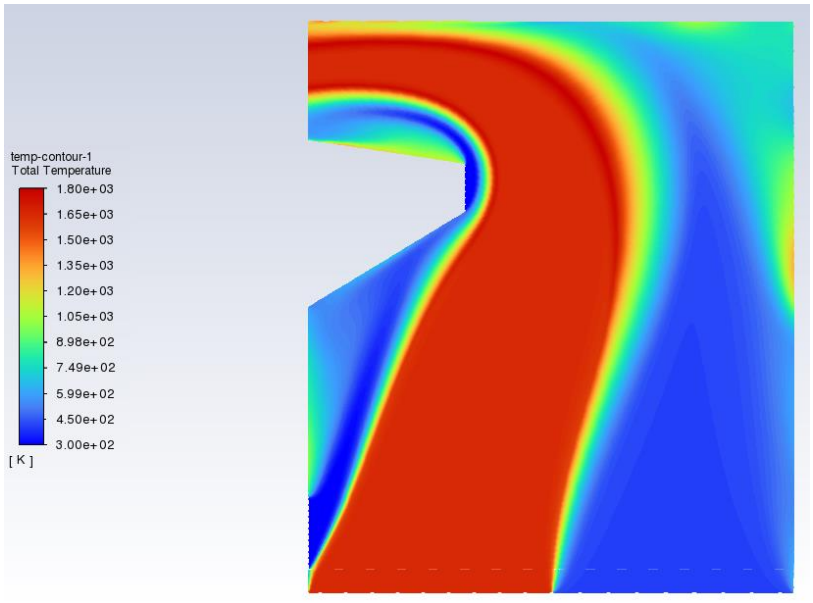

Figure 5. 16 Temperature profile for the secondary air combustion - Position C

5.5 Validation with rise husk experimental work

As part of the validation phase of this thesis, a published research paper was selected that presents a comprehensive experimental investigation on the combustion characteristics of various biomass fuels. The study evaluates and compares the combustion behavior of Nigerian coconut shell, rice husk, corn cobs, groundnut shell, and soda stooge from under controlled conditions[67]. Each fuel's performance is analyzed based on key parameters such as combustion efficiency, temperature, CO and NO_x mass fraction. The experimental was undergone in steel cylinder with 145 mm internal diameter and 2000mm height.

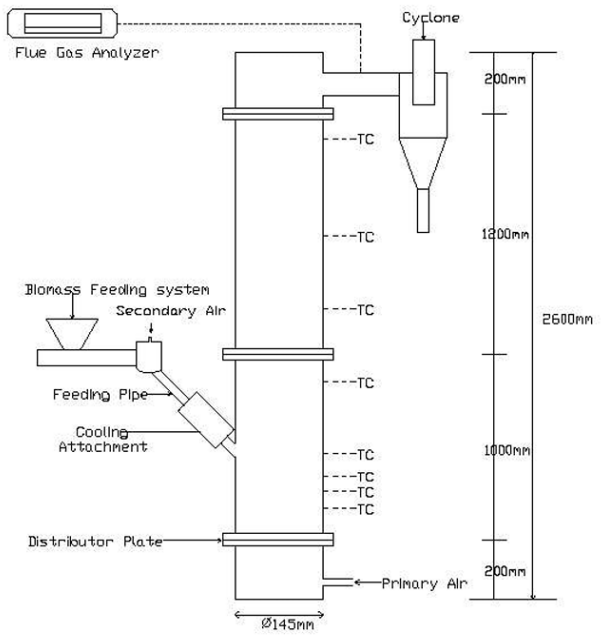

Figure 5. 17 Schematic diagram of the experimental setup [67]

For the purpose of this thesis, rice husk is selected as the primary biomass fuel of interest. The main reason for this approach is that I could not find any experimental work specifically on coffee husk combustion. As an alternative, I performed simulations using rice husk, a biomass fuel with similar physical structure and chemical properties, and for which experimental data is available. For validation, I followed the exact same simulation procedure using identical settings and kinetic parameters as I used in coffee husk case. A separate simulation was conducted using the properties of rice husk, and the results were compared with the corresponding experimental data.

The detailed experimental data provided in the referenced paper offers valuable insight into the combustion behavior of rice husk. This data serves as a reliable reference for validating the simulation model developed for the numerical analysis of coffee husk combustion. Specifically, the temperature of the flue gas at the outlet under varying excess air conditions was taken as a key comparison point between the experimental and numerical findings.

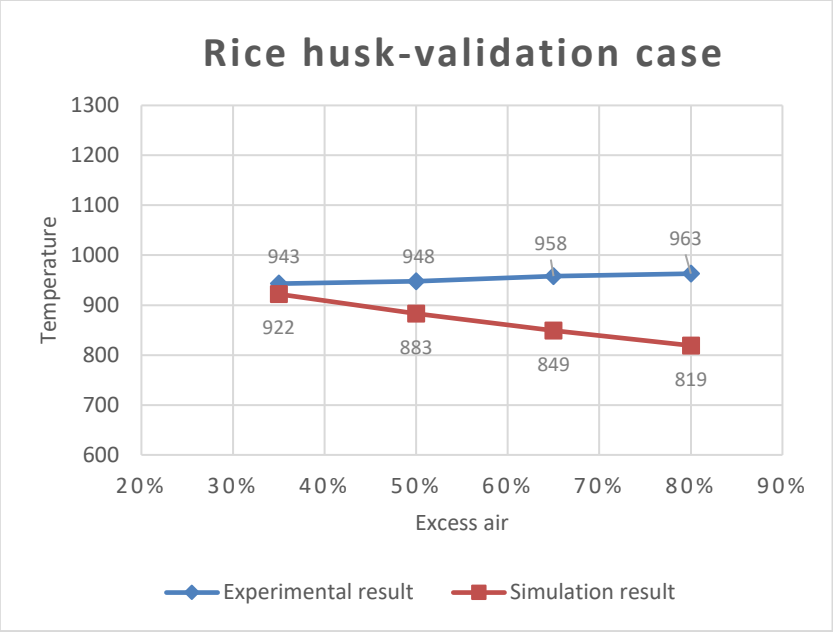

Figure 5. 18 Numerical and experimental results of rice husk combustion

The computed results show good agreement with the experimental data. The flue gas temperatures obtained from the numerical analysis were slightly lower than the experimental values. At an excess air level of 35%, only a 2.2% variation was observed, indicating a strong correlation between the two approaches. Although the variation increased with higher excess air levels, the difference remained within an acceptable range.

The focus of the validation was on comparing results under similar excess air conditions to those in my main simulation. While the coffee husk simulation covered a range of 0–100% excess air, the validation was carried out within the range of 35–80%. If the simulation were to be extended to excess air levels beyond 100%, additional model modification such as adjusting kinetic parameters might be required to maintain accuracy. But within the tested excess air range, the simulation results were found to be acceptable.

The primary reason for the lower flue gas temperatures in the numerical simulation is the absence of a heterogeneous reaction model. These reactions are exothermic in nature, and their exclusion led to a slight underestimation of the flue gas temperature in the numerical model compared to the experimental results.

Table 5. 16 Percentage variation between experimental and numerical results

	Excess air	Percentage variation (%)
1	35%	2.2
2	50%	6.9
3	65%	11.4
4	80%	15.0

The geometry and temperature profile generated for one of the excess air conditions in the rice husk furnace is presented Figure 5.18.

Validation error calculation

The comparison between my simulation results with the experimental work is further analyzed based on the calculated value of root mean square percentage error by equation 5.1 and 5.2.

$$\mathrm{MSE} = \frac{1}{\mathrm{n}} \sum_{\mathrm{i}=1}^{\mathrm{n}} (\mathrm{T_i} - \bar{T}_i)^2 \qquad 5.4$$

$$RMSPE = \sqrt{\frac{1}{n} \sum_{i=1}^{n} \left(\frac{T_i - \bar{T}_i}{T_i}\right)^2} \text{ X } 100\% \qquad 5.5$$

Table 5. 17 Root Mean square percentage error

Excess air	Experimental (k)	Simulation (k)	Error difference	square error
35%	943	922	21	0.001
50%	948	883	65	0.005
65%	958	849	109	0.013
80%	963	819	144	0.022
				0.041
			MSE	0.010
			RMSE	0.101

Two papers are used for comparing the acceptable error percentage. Both studies highlight that the percentage error between simulation results and experimental data remains within an acceptable range for biomass combustion modeling in their analysis. In the first study, the

relative error between simulation and experimental values was reported to stay within 10%, indicating good agreement [68]. Similarly, the second study validated its model using experiments in a cylindrical combustor with different biomass fuels, achieving relative errors below 13% in most cases. This level of accuracy is consistent with findings from recent research on similar topics, suggesting that simulation tools can reliably predict combustion behavior with errors typically under 10–13% [39]. The RMSE percentage error of the validation case is 10.1%, which is in acceptable range as discussed in the two papers.

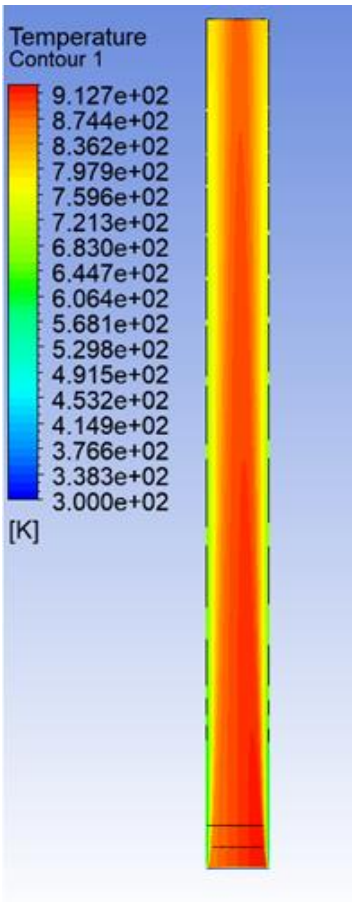

Figure 5. 19 Temperature profile of the validation case with rice husk combustion

Chapter Six
Conclusion and Recommendation

6.1 Conclusion

This study presented a numerical investigation of coffee husk combustion in a biomass furnace using ANSYS Fluent. The main focus was on designing a suitable combustion chamber and analyzing the effects of excess air, and secondary air inlet position on combustion performance and CO emissions. Coffee husk, being an abundant agricultural waste in coffee-producing countries like Ethiopia, showed good potential as a solid biomass fuel when proper furnace design and operating parameters are used.

The simulation results demonstrated that excess air plays a critical role in determining combustion efficiency and environmental impact. An excess air level of 60% provided an optimal balance between high outlet temperature and minimal carbon monoxide emissions. In addition, adjusting the position of the secondary air inlet significantly influenced the mixing and combustion of gases inside the furnace.

Additionally, the numerical model was validated using experimental data on rice husk combustion, selected for its similarity to coffee husk. Flue gas temperatures showed good agreement, with only a 2.2% variation at 35% excess air. The root mean square percentage error also calculated and found out 10.1 %, which is acceptable compared to other works done in this area. The results confirm the reliability of the model for predicting coffee husk combustion behavior.

Overall, the findings confirm that coffee husk can be effectively used in direct combustion systems and offers a sustainable energy solution when supported by proper design and parameter optimization.

6.2 Recommendation

While this simulation provided useful insights, further studies are recommended to improve and validate the results:

- Inclusion of particle tracking and solid-phase modeling would provide a more complete picture of combustion, particularly for moisture evaporation, volatile release, char burn-out, and ash formation.
- Investigation of NOx and particulate emissions should be considered to better understand the full environmental impact.
- Exploration of different furnace designs and air staging techniques may further enhance combustion efficiency and reduce emissions.

Reference

[1] Energy Institute -, "Statistical Review of World Energy (2024)." [Online]. Available: https://ourworldindata.org/energy-production-consumption

[2] A. W. Yalew, "The Ethiopian energy sector and its implications for the SDGs and modeling," Renewable and Sustainable Energy Transition, vol. 2, p. 100018, Aug. 2022, doi: 10.1016/j.rset.2022.100018.

[3] E. Danso-Boateng and O.-W. Achaw, "Bioenergy and biofuel production from biomass using thermochemical conversions technologies—a review," AIMSE, vol. 10, no. 4, pp. 585–647, 2022, doi: 10.3934/energy.2022030.

[4] Y. Wang and L. Yan, "CFD Studies on Biomass Thermochemical Conversion," *IJMS*, vol. 9, no. 6, pp. 1108–1130, Jun. 2008, doi: 10.3390/ijms9061108.

[5] M. Yang *et al.*, "CFD modeling of biomass combustion and gasification in fluidized bed reactors using a distribution kernel method," Combustion and Flame, vol. 236, p. 111744, Feb. 2022, doi: 10.1016/j.combustflame.2021.111744.

[6] A. Tefera, "Coffee Annual Report," United States Department of Agriculture - Foreign Agriculture Service, ET2023-0014, May 2023.

[7] S. Amertet, Y. Mitiku, and G. Belete, "Analysis of a Coffee Husk Fired Cogeneration Plant in South Western Ethiopia Coffee Processing Industries," Low Carbon Economy.

[8] P. S. Murthy, "Sustainable management of coffee industry by-products and value addition—A review," Resources, Conservation and Recycling, vol. 66, Sep. 2012.

[9] C. K. Law, Combustion physics, 1. paperback ed. Cambridge: Cambridge University Press, 2010.

[10] D. P. Maxwell, "Combustion of alternative and low-grade biomass fuels on small-scale systems: Potential and optimisation through pre-treatment".

[11] J. George and S. Sabapathi, "Cellulose nanocrystals: synthesis, functional properties, and applications," Nanotechnology Science and Applications, 2015.

[12] L. Hu, X. Fang, M. Du, F. Luo, and S. Guo, "Hemicellulose-Based Polymers Processing and Application," American Journal of Plant Sciences.

[13] P. McKendry, "Energy production from biomass (part 1): overview of biomass," Bioresource Technology, 2002.

[14] Z. Mahmood, M. Yameen, M. Jahangeer, M. Riaz, A. Ghaffar, and I. Javid, “Lignin as Natural Antioxidant Capacity,” in Lignin - Trends and Applications, Intech Open science, 2018, pp. 181–204.

[15] R. Shrestha, “Experimental Analysis and Modeling of Biomass Gasification using a Downdraft Gasifier.” Msc Thesis, Auburn University, 2014.

[16] M. Kamruzzaman, “Investigation of Physical and Thermo-Chemical Characteristics of Biomass Fuels from Local Agricultural Residues,” Msc Thesis, Islamic University of Technology, 2011.

[17] B. S. Alganash, “Numerical investigation of the combustion processes of various combustion regimes.” PhD Thesis, University of Glasgow, 2015.

[18] L. Zhang and P. Champagne, “Overview of recent advances in thermo-chemical conversion of biomass,” Energy Conversion and Management, 2010.

[19] “Bioenergy Project Development and Biomass Supply,” International Energy Agency (IEA), France, 2007. [Online]. Available: https://www.ieabioenergy.com/wp-content/uploads/2013/10/Good-Practice-Guideines-Bioenergy-Project-Development-and-Biomass-Supply.pdf>[accessed April, 2024]

[20] B. M. Jenkins, L. L. Baxter, T. R. M. Jr, and T. R. Miles, “Combustion properties of biomass,” 1998.

[21] L. Puri, Y. Hu, and G. Naterer, “Critical review of the role of ash content and composition in biomass pyrolysis,” Front. Fuels, vol. 2, p. 1378361, Mar. 2024, doi: 10.3389/ffuel.2024.1378361.

[22] P. McKendry, “Energy production from biomass (part 1): overview of biomass,” Bioresource Technology, 2002.

[23] K. L. Martinez-Mendoza *et al.*, “Thermochemical behavior of agricultural and industrial sugarcane residues for bioenergy applications,” Bioengineered, vol. 14, no. 1, p. 2283264, Dec. 2023, doi: 10.1080/21655979.2023.2283264.

[24] S. Van Loo and J. Koppejan, Eds., The handbook of biomass combustion and co-firing. London ; Sterling, VA: Earthscan, 2008.

[25] R. Saidur, “A review on biomass as a fuel for boilers,” Renewable and Sustainable Energy Reviews, 2011.

[26] P. McKendry, “Energy production from biomass (part 1): overview of biomass,” Bioresource Technology, vol. 83, no. 1, pp. 37–46, May 2002, doi: 10.1016/S0960-8524(01)00118-3.

[27] J. E. Leach, “Biomass for thermochemical conversion: targets and challenges,” Frontiers in Plant Science.

[28] G. T. Marangwanda, D. M. Madyira, and T. O. Babarinde, “Combustion models for biomass: A review,” Energy Reports, 2020.

[29] C. M. Galanakis, Ed., Handbook of coffee processing by-products: sustainable applications. London, United Kingdom: Academic Press, an inprint of Elsevier, 2017.

[30] K. Mutuku, “Characterization of Physical Properties of Biomass Waste Materials in Kenya for Gasification: Rice Husks and Coffee Husks,” vol. 7, no. 2, 2019.

[31] M. Saenger, E.-U. Hartge, J. Werther, T. Ogada, and Z. Siagi, “Combustion of coffee husks,” Renewable Energy, vol. 23, no. 1, pp. 103–121, May 2001, doi: 10.1016/S0960-1481(00)00106-3.

[32] A. Domínguez *et al.*, “Conventional and microwave induced pyrolysis of coffee hulls for the production of a hydrogen rich fuel gas,” Journal of Analytical and Applied Pyrolysis, vol. 79, no. 1–2, pp. 128–135, May 2007, doi: 10.1016/j.jaap.2006.08.003.

[33] N. Couto, V. Silva, E. Monteiro, P. S. D. Brito, and A. Rouboa, “Experimental and Numerical Analysis of Coffee Husks Biomass Gasification in a Fluidized Bed Reactor,” Energy Procedia, vol. 36, pp. 591–595, 2013, doi: 10.1016/j.egypro.2013.07.067.

[34] B. G. Miller and D. A. Tillman, Eds., Combustion engineering issues for solid fuel systems. Boston, MA: Academic Press, 2008.

[35] A. A. Bhuiyan and J. Naser, “CFD modelling of co-firing of biomass with coal under oxy-fuel combustion in a large scale power plant,” Fuel, vol. 159, pp. 150–168, Nov. 2015, doi: 10.1016/j.fuel.2015.06.058.

[36] D. O. Hall and PatriciaA. Moss, “Biomass for energy in developing countries,” GeoJournal, vol. 7, no. 1, 1983, doi: 10.1007/BF00191854.

[37] M. Balat and G. Ayar, “Biomass Energy in the World, Use of Biomass and Potential Trends,” *Energy Sources*, vol. 27, no. 10, pp. 931–940, Jul. 2005, doi: 10.1080/00908310490449045.

[38] J. Silva, J. Teixeira, S. Teixeira, S. Preziati, and J. Cassiano, “CFD Modeling of Combustion in Biomass Furnace,” Energy Procedia, vol. 120, pp. 665–672, Aug. 2017, doi: 10.1016/j.egypro.2017.07.179.

[39] Z. Zhang, F. He, Y. Zhang, X. Li, and Z. Gao, “Simulation of combustion process of a single biomass pellet based on heterogeneous-dimension discretization,” Journal of the Energy Institute, vol. 92, no. 3, pp. 630–639, Jun. 2019, doi: 10.1016/j.joei.2018.03.009.

[40] R. Scharler and I. Obernberger, “Numerical Modelling of Biomass Grate Furnaces,” 2000.

[41] S. K. Kær, “Numerical modelling of a straw-fired grate boiler,” *Fuel*, vol. 83, no. 9, pp. 1183–1190, Jun. 2004, doi: 10.1016/j.fuel.2003.12.003.

[42] C. Yin, L. Rosendahl, S. K. Kær, S. Clausen, S. L. Hvid, and T. Hille, “Mathematical Modeling and Experimental Study of Biomass Combustion in a Thermal 108 MW Grate-Fired Boiler,” *Energy Fuels*, vol. 22, no. 2, pp. 1380–1390, Mar. 2008, doi: 10.1021/ef700689r.

[43] J. Porteiro, J. Collazo, D. Patiño, E. Granada, J. C. Moran Gonzalez, and J. L. Míguez, “Numerical Modeling of a Biomass Pellet Domestic Boiler,” Energy Fuels, vol. 23, no. 2, pp. 1067–1075, Feb. 2009, doi: 10.1021/ef8008458.

[44] B. Rajh, C. Yin, N. Samec, M. Hriberšek, and F. Kokalj, “CFD modeling and experience of waste-to-energy plant burning waste wood,” 2013.

[45] S. Kar, “Straw combustion on slow-moving grates?a comparison of model predictions with experimental data,” Biomass and Bioenergy, vol. 28, no. 3, pp. 307–320, Mar. 2005, doi: 10.1016/j.biombioe.2004.08.017.

[46] C. K. Westbrook and F. L. Dryer, “Chemical kinetic modeling of hydrocarbon combustion,” Progress in Energy and Combustion Science, vol. 10, no. 1, pp. 1–57, Jan. 1984, doi: 10.1016/0360-1285(84)90118-7.

[47] G. Tufano, “Fully-Resolved Simulations of Ignition and Combustion of Single Coal Particles and Coal Particle Clouds,” PhD, University of Stuttgart, Germany, 2021.

[48] H. K. Versteeg and W. Malalasekera, An introduction to computational fluid dynamics: the finite volume method, 2nd ed. Harlow, England ; New York: Pearson Education Ltd, 2007.

[49] S. De, A. K. Agarwal, S. Chaudhuri, and S. Sen, Eds., Modeling and Simulation of Turbulent Combustion. in Energy, Environment, and Sustainability. Singapore: Springer Singapore, 2018. doi: 10.1007/978-981-10-7410-3.

[50] B. S. Alganash, "Numerical investigation of the combustion processes of various combus tion regimes," 2015.

[51] T. L. Bergman and F. P. Incropera, Eds., *Fundamentals of heat and mass transfer*, 7th ed. Hoboken, NJ: Wiley, 2011.

[52] M. F. Modest, *Radiative heat transfer*, 3d edition. New York: Academic Press, 2013.

[53] P. C. Corrêa, O. Resende, and D. M. Ribeiro, "DRYING CHARACTERISTICS AND KINETICS OF COFFEE BERRY," *RBPA*, vol. 8, no. 1, pp. 1–10, Jun. 2006, doi: 10.15871/1517-8595/rbpa.v8n1p1-10.

[54] A. Mujumdar, Handbook of industrial drying, Third. Taylor&Francis, 2006.

[55] M. Kutz, Ed., Handbook of farm, dairy, and food machinery engineering, Second edition. Amsterdam: Academic Press, 2013.

[56] Y. Cengel and M. Boles, Thermodynamics: An Engineering Approach, Fifth. McGraw-Hill, 2006.

[57] Y. Cengel and M. Boles, Thermodynamics: An Engineering Approach, Fifth. McGraw-Hill, 2006.

[58] W. N. Hern´andez-D´ıaz1 and F. J. Hern´andez-Campos1, "Coffee grain rotary drying optimization," Revista Mexicana de Ingenieria Quimica, 2013.

[59] Masitah, A.R.S, Mardiana I Ahmad, and Y.M. Yatim, "Heat Transfer and Effectiveness Analysis of a Cross-Flow Heat Exchanger for Potential Energy Recovery Applications in Hot-Humid Climate," Energy Research Journal, Apr. 2015.

[60] School of Mechanical and Electrical Engineering, Henan Institute of Science and Technology, Xinxiang 453003, China, F. Chengguo, F. Yipeng, T. Yishui, L. Mingchao, and Z. Zhengchuan, "Design of a 1 t/h Biomass Chain Boiler and ıts Fuel Adaptability Analysis," *JESTR*, vol. 13, no. 5, pp. 132–142, 2020, doi: 10.25103/jestr.135.17.

[61] A. S. Tariq, P. Reupke, and G. Sarwar, Biomass combustion systems: a guide for monitoring and efficient operation. Chatham Maritime, Kent, U.K.: Natural Resources Institute, 1994.

[62] R. Dahlquist, Technologies for converting Biomass to useful energy, vol. FOUR. CRC Press, 2013.

[63] T. Klason, Modelling of biomass combustion in furnaces. Lund: Lund University, 2006.

[64] "ANSYS meshing user guide." ANSYS Inc., Nov. 2010.

[65] P. Basu, Biomass gasification and pyrolysis: practical design and theory. Burlington, MA: Academic Press, 2010.

[66] T. Nussbaumer, "Combustion and Co-combustion of Biomass: Fundamentals, Technologies, and Primary Measures for Emission Reduction," Energy Fuels, vol. 17, no. 6, pp. 1510–1521, Nov. 2003, doi: 10.1021/ef030031q.

[67] J. O. Nordiana, O. Ighodalo, and O. Obodeh, "Experimental Study on Nigeria Biomass Combustion in a Fluidized Bed Combustor," vol. 2, no. 7, 2019.

[68] G. F. García Sánchez *et al.*, "Biomass Combustion Modeling Using OpenFOAM: Development of a Simple Computational Model and Study of the Combustion Performance of Lippia origanoides Bagasse," *Energies*, vol. 16, no. 6, p. 2932, Mar. 2023, doi: 10.3390/en16062932.

Appendix A. Simulation boundary conditions

Table A. 1 Mass fraction and mass flow rate used in the simulation – First fuel inlet section

First fuel inlet section

	Stochiometric		**1.2 times excess air**		**1.4 times excess air**		**1.6 times excess air**		**1.8 times excess air**		**2 times excess air**	
Gases	Mass flow kg/hr	Mass fraction	Mass flow kg/hr	Mass fraction	Mass flow kg/hr	Mass fraction	Mass flow kg/hr	Mass fraction	Mass flow kg/hr	Mass fraction	Mass flow kg/hr	Mass fraction
H2	2.65	0.03	2.65	0.03	2.65	0.03	2.65	0.02	2.65	0.02	2.65	0.02
CO	2.32	0.03	2.32	0.03	2.32	0.02	2.32	0.02	2.32	0.02	2.32	0.02
CO2	3.10	0.04	3.10	0.03	3.10	0.03	3.10	0.03	3.10	0.02	3.10	0.02
CH4	1.66	0.02	1.66	0.02	1.66	0.02	1.66	0.01	1.66	0.01	1.66	0.01
H2O	1.22	0.02	1.22	0.01	1.22	0.01	1.22	0.01	1.22	0.01	1.22	0.01
O2	15.19	0.20	18.25	0.20	21.28	0.21	24.26	0.21	27.36	0.21	30.38	0.21
N2	50.04	0.66	60.05	0.67	70.02	0.68	79.85	0.69	90.07	0.70	100.08	0.71
Total	76.18	1.00	89.25	1.00	102.24	1.00	115.06	1.00	128.38	1.00	141.41	1.00

Table A. 2 Mass fraction and mass flow rate used in the simulation – Second fuel inlet section

Second fuel inlet section												
	Stochiometric		**1.2 times excess air**		**1.4 times excess air**		**1.6 times excess air**		**1.8 times excess air**		**2 times excess air**	
	Mass flow kg/hr	Mass fraction	Mass flow kg/hr	Mass fraction	Mass flow kg/hr	Mass fraction	Mass flow kg/hr	Mass fraction	Mass flow kg/hr	Mass fraction	Mass flow kg/hr	Mass fraction
CO	1.33	0.0702	1.33	0.0599	1.33	0.0523	1.33	0.0463	1.33	0.0416	1.33	0.0378
CO2	1.33	0.0702	1.33	0.0599	1.33	0.0523	1.33	0.0463	1.33	0.0416	1.33	0.0378
O2	3.82	0.2011	4.57	0.2055	5.33	0.2090	6.08	0.2115	6.84	0.2137	7.60	0.2153
N2	12.49	0.6584	15.01	0.6748	17.50	0.6864	20.02	0.6959	22.50	0.7030	25.02	0.7092
Total	18.97	1	22.25	1	25.49	1	28.76	1	32.00	1	35.28	1

Table A. 3 Mass flow rate of air per section used in the simulation with Secondary air simulation

	Mass fraction	**Total air flow (kg/hr)**	**Primary air (kg/hr) – Section 1**	**Primary air (kg/hr)– Section 2**	**Primary air (kg/hr)– Section 3**	**Secondary air (kg/hr)**
O2	0.23	40.0	6.0	24.0	4.0	6.0
N2	0.77	133.9	20.1	80.4	13.4	20.1
	Total(kg/hr)	174.0	26.1	104.4	17.4	26.1

Table A. 4 Mass fraction and mass flow rate used in with secondary air simulation – *Section 1*

First fuel inlet section			
No	Gases	Mass flow kg/hr	Mass fraction
1	H2	2.65	0.023
2	CO	2.32	0.020
3	CO2	3.09	0.027
4	CH4	1.66	0.014
5	H2O	1.22	0.011
6	O2	24.01	0.208
7	N2	80.35	0.697
Total		115.31	

Table A. 5 Mass fraction and mass flow rate used in with secondary air simulation – Section 2

Second fuel inlet section			
No	Gases	Mass flow kg/s	Mass fraction
1	CO	1.33	0.066
2	CO2	1.33	0.066
3	O2	4.07	0.203
4	N2	13.36	0.665
Total		20.09	

Appendix B. Temperature, CO2 and CO mass fraction profile

Stoichiometric (0 % excess air)

Temperature profile

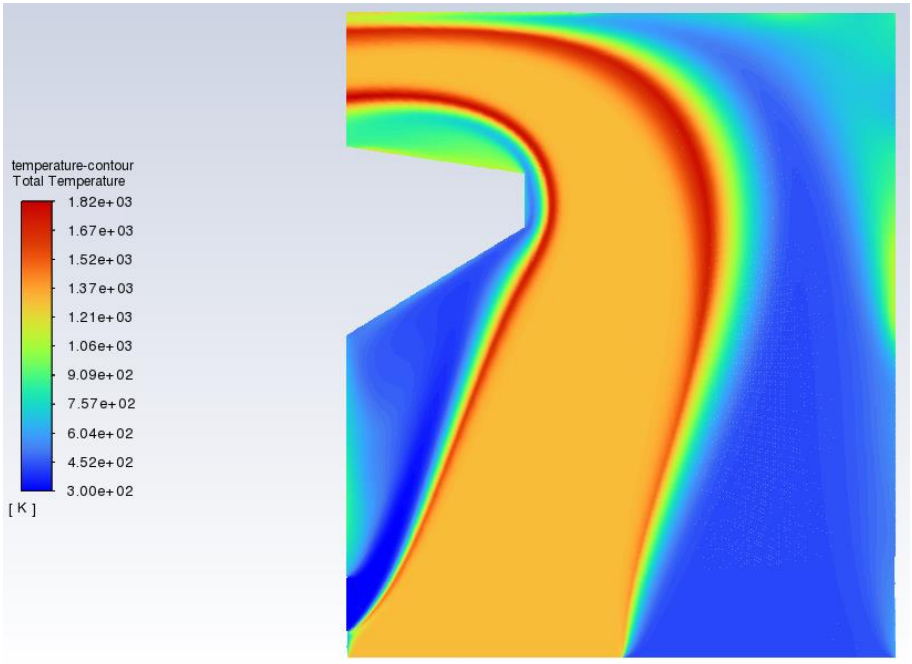

CO2 mass fraction

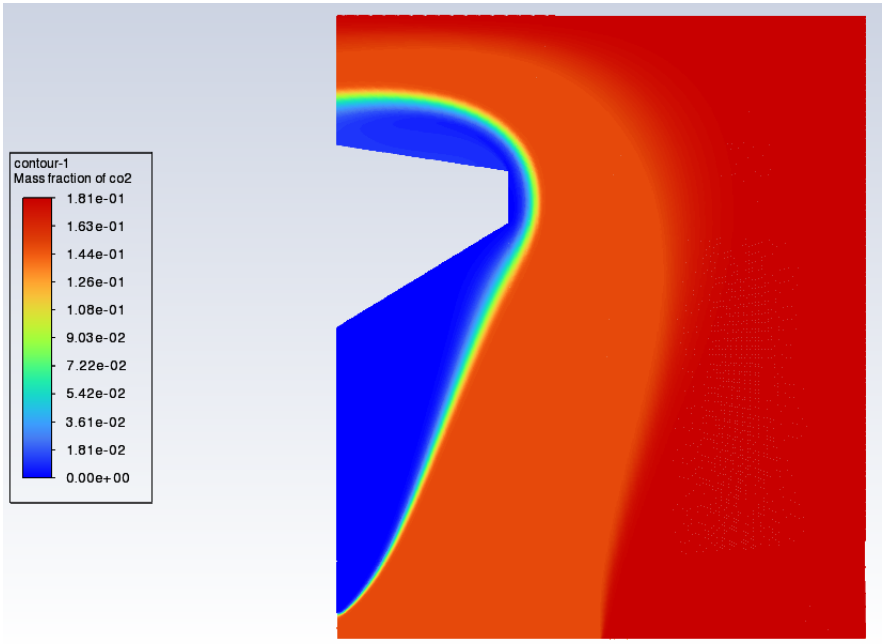

CO mass fraction

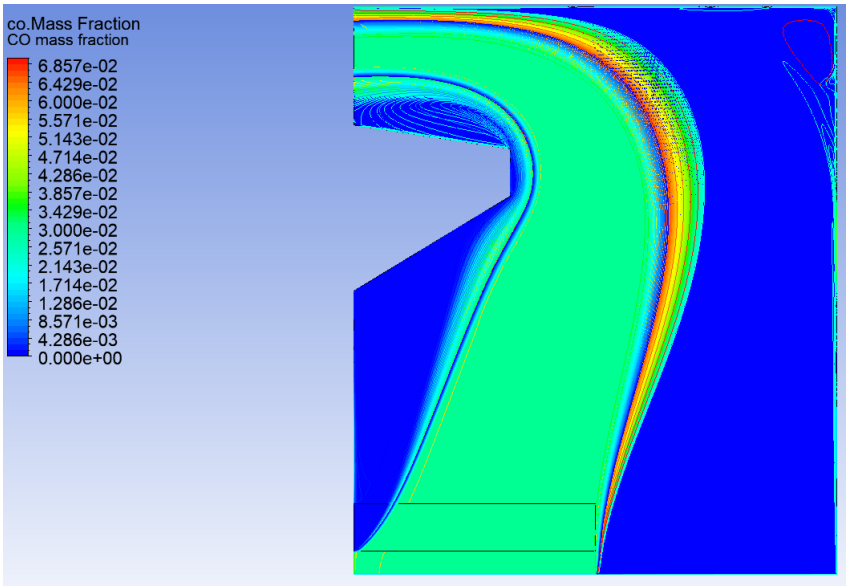

20% excess air

Temperature profile

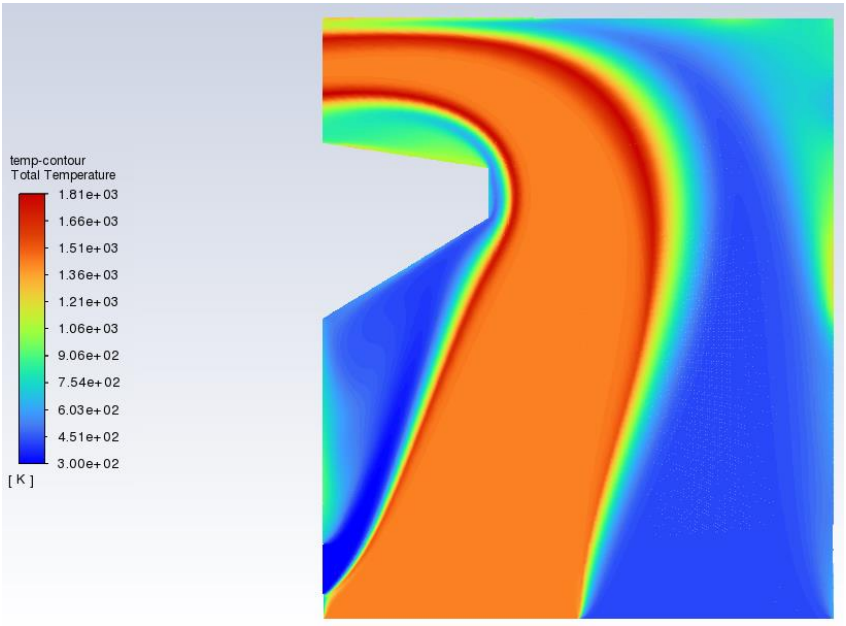

CO2 mass fraction

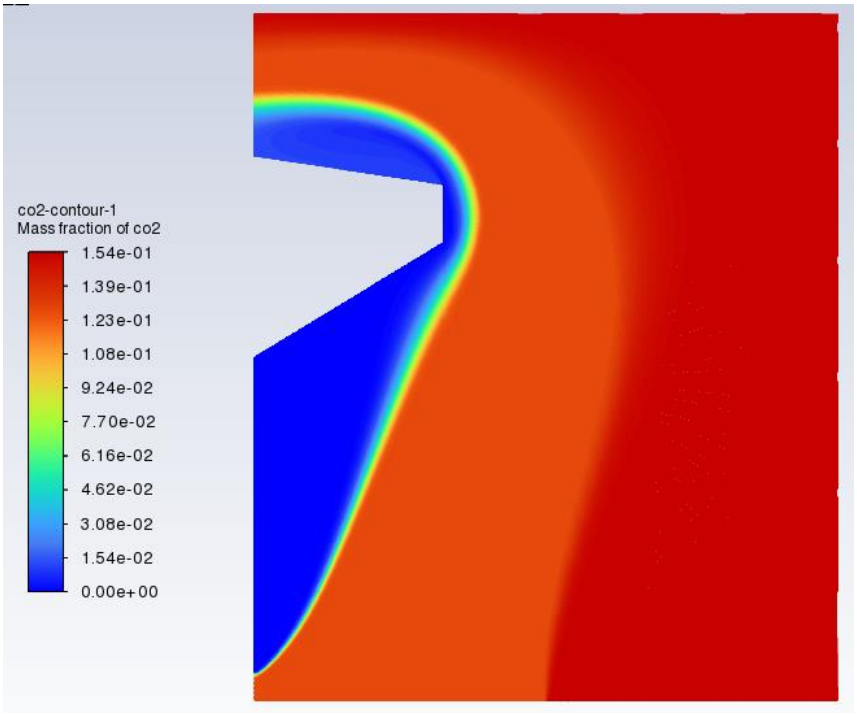

CO mass fraction

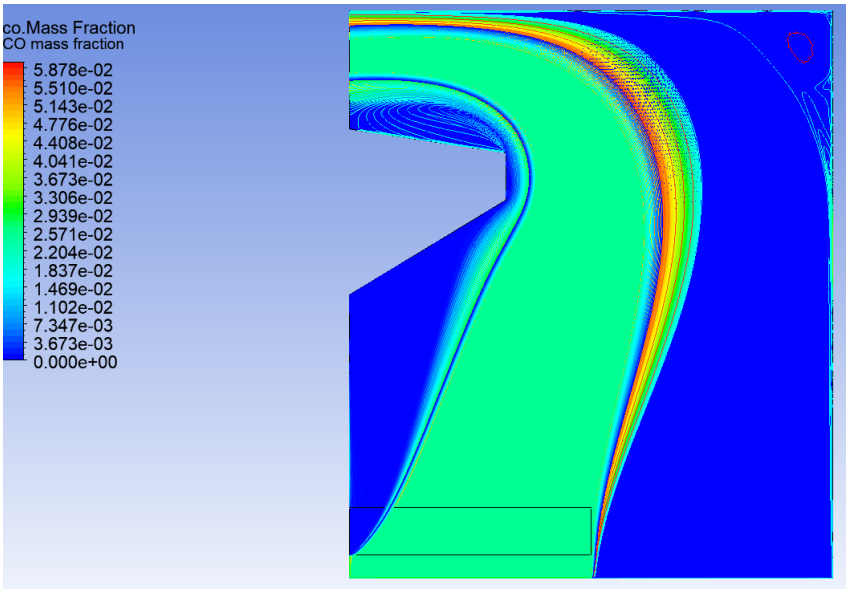

40% excess air

Temperature profile

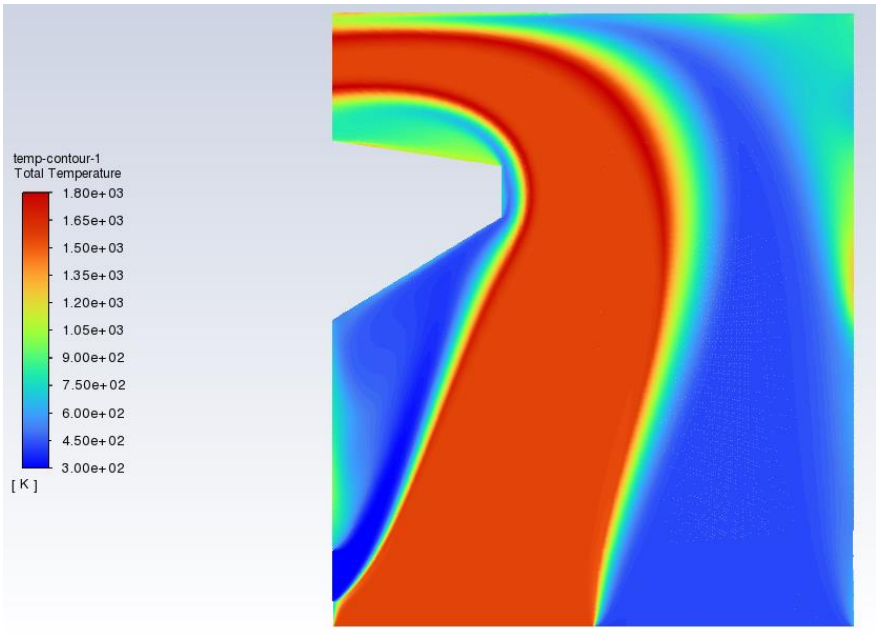

CO2 mass fraction

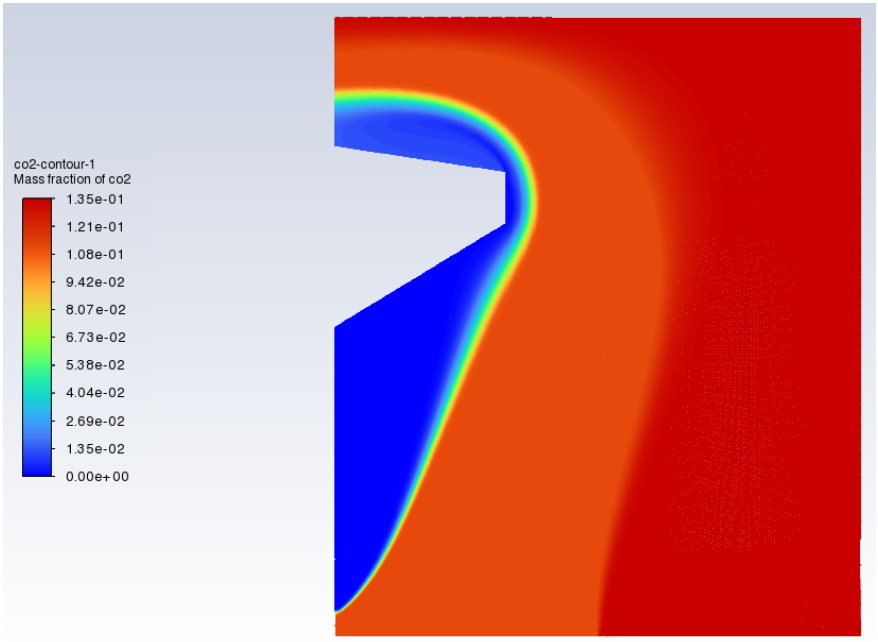

CO mass fraction

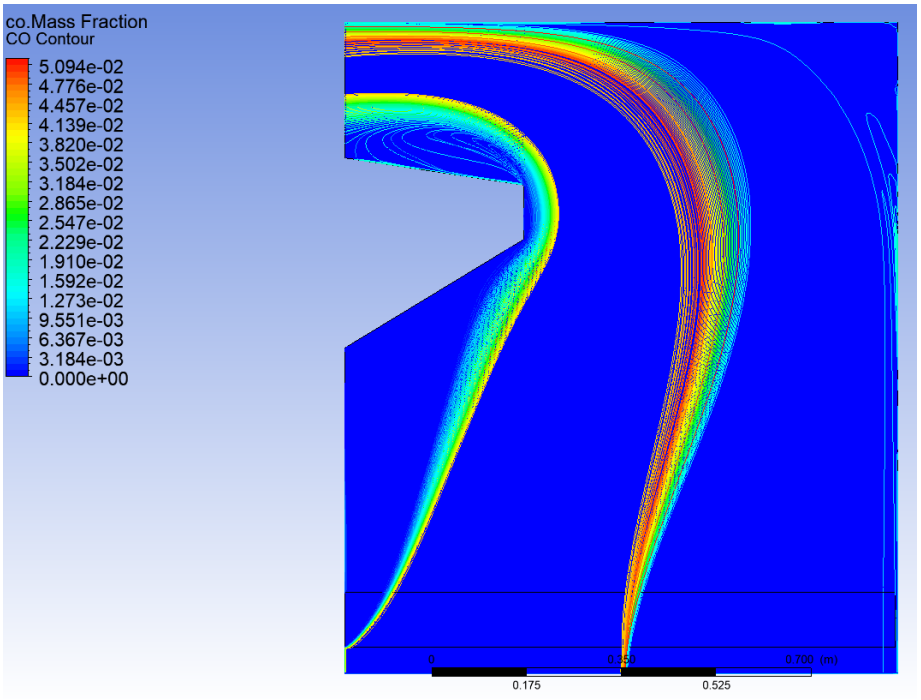

60% excess air

Temperature profile

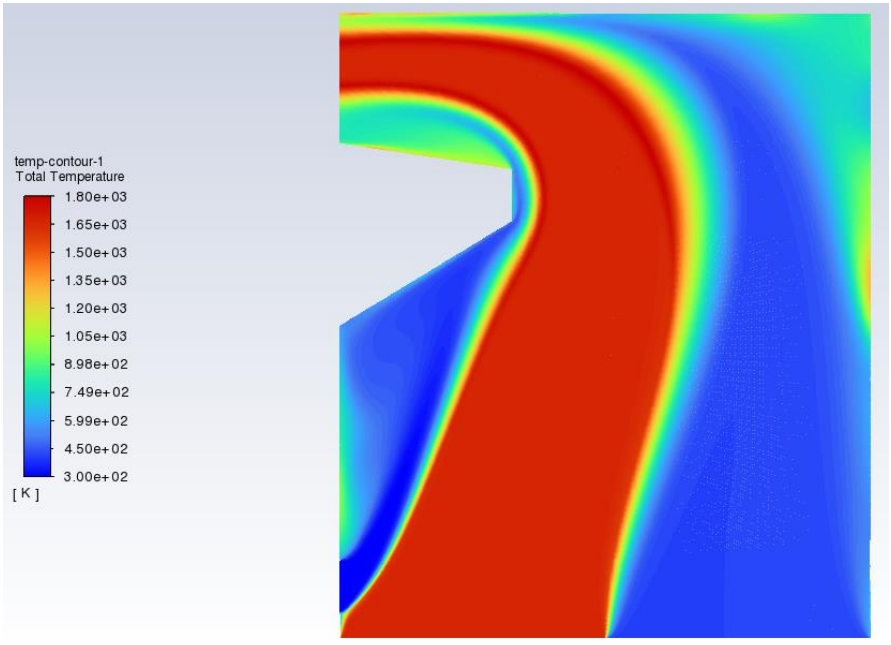

CO2 mass fraction

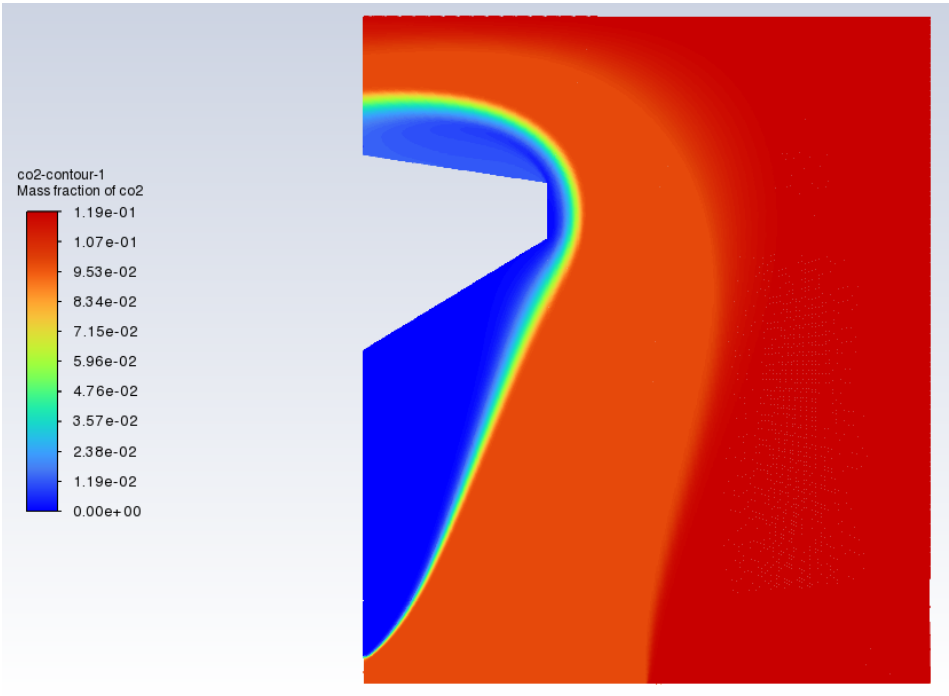

CO mass fraction

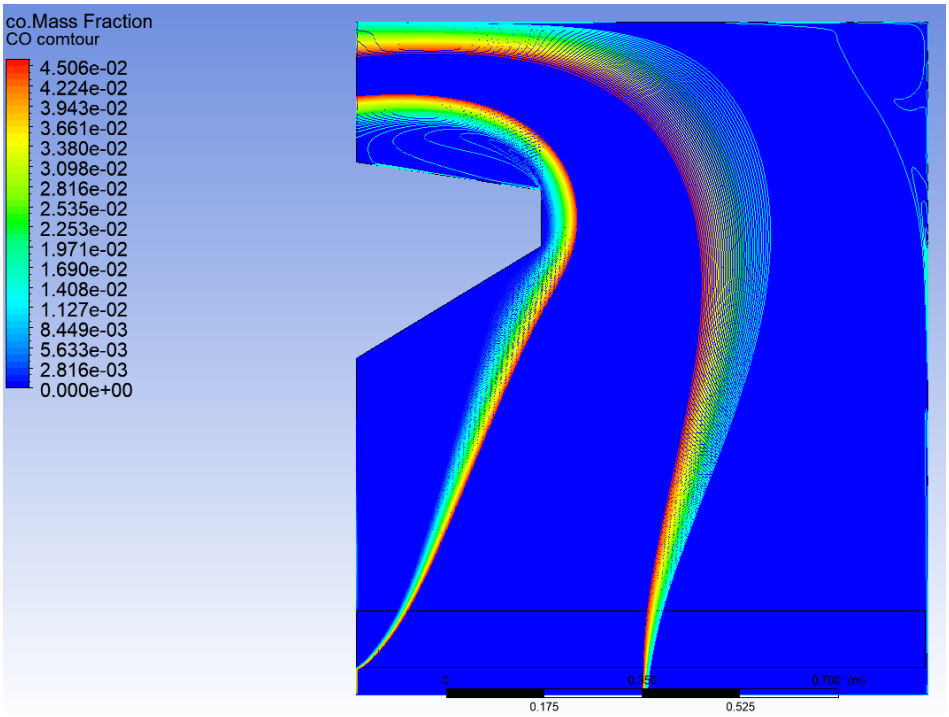

80% excess air

Temperature profile

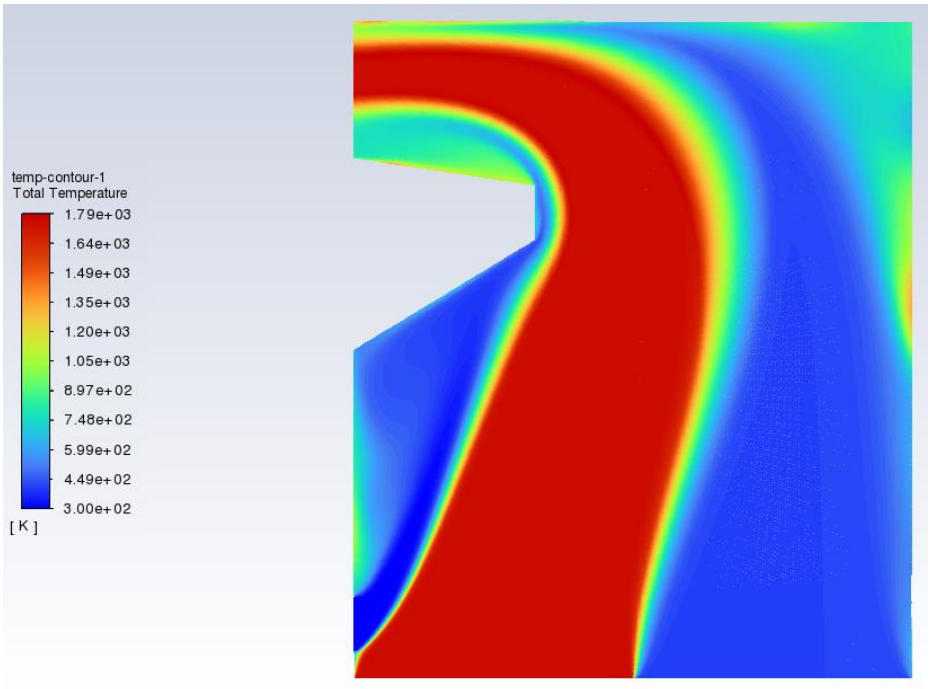

CO2 mass fraction

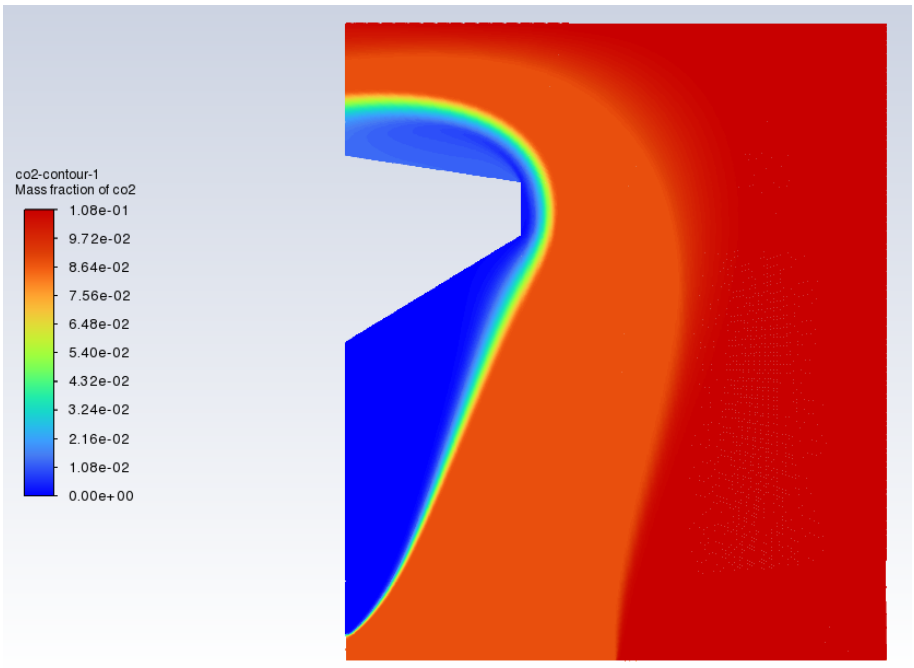

CO mass fraction

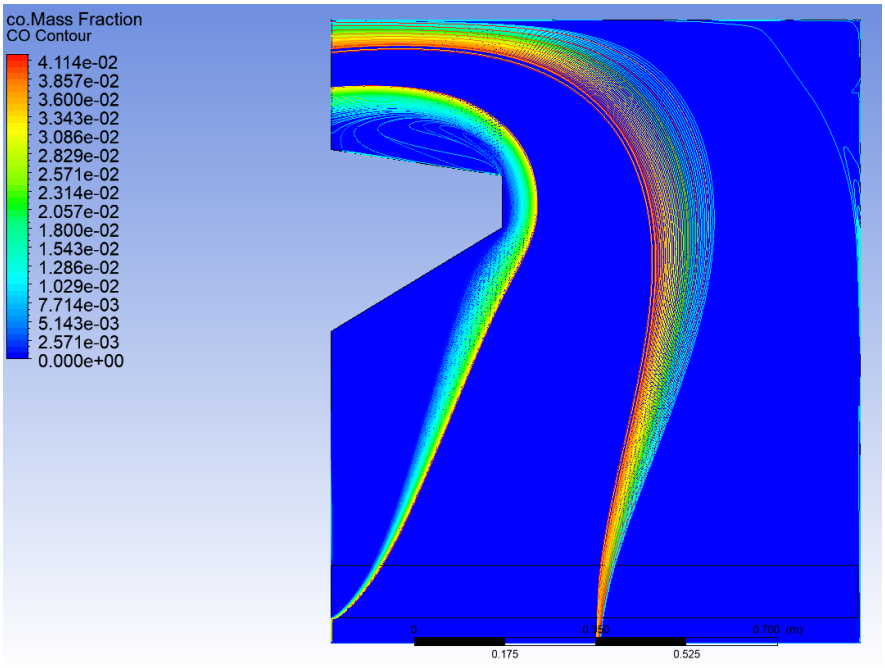

100% excess air

Temperature profile

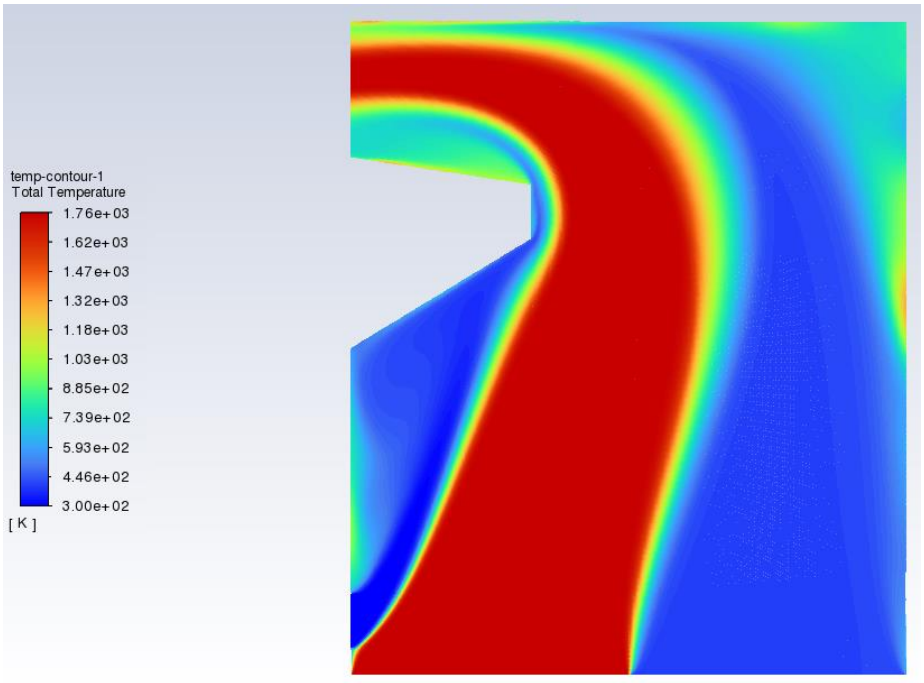

CO2 mass fraction

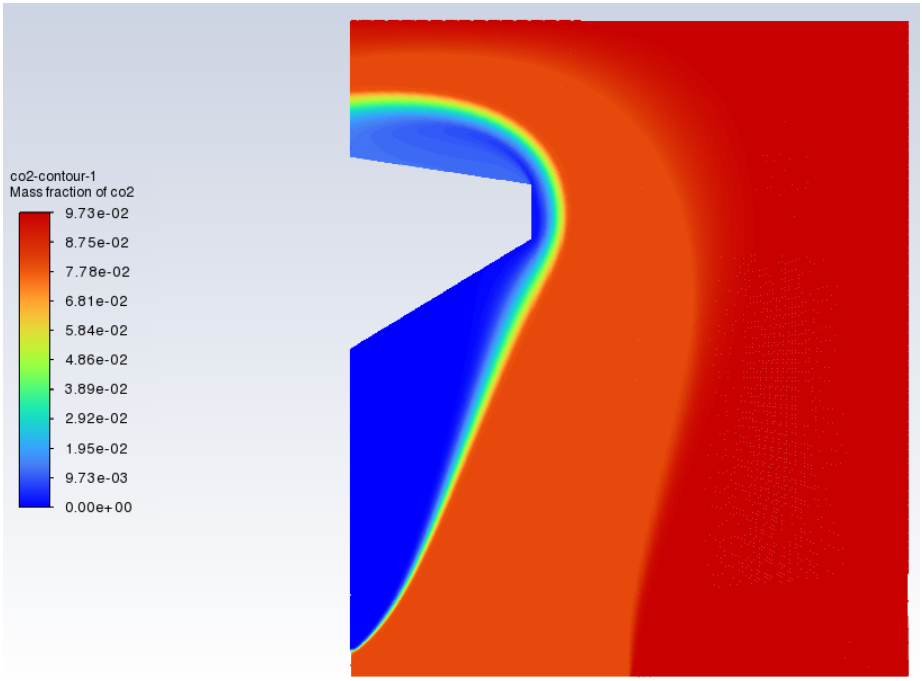

CO mass fraction